The Institute of Paper Chemistry

Appleton, Wisconsin

Doctor's Dissertation

An Investigation of the Effects of Fiber Cross Sectional Shape on the Resistance to the Flow of Fluids Through Fiber Mats

Richard Peter Labrecque

January, 1967

AN INVESTIGATION OF THE EFFECTS OF FIBER CROSS SECTIONAL SHAPE ON THE RESISTANCE TO THE FLOW OF FLUIDS THROUGH FIBER MATS

A thesis submitted by

Richard Peter Labrecque

B.S. (Ch. E.) 1962, University of Maine
M.S. 1964, Lawrence College

in partial fulfillment of the requirements
of The Institute of Paper Chemistry
for the degree of Doctor of Philosophy
from Lawrence University
Appleton, Wisconsin

January, 1967

TABLE OF CONTENTS

SUMMARY

The purpose of this study was to determine the effects of fiber cross-sectional shape on the resistance to the flow of fluids through fiber mats. In essence, such an investigation involved: (a) procuring synthetic fibers with the required cross-sectional shapes, (b) forming fiber mats through a constant-rate filtration technique, (c) determining their water permeability properties at various levels of compaction, and (d) measuring the exposed hydrodynamic surface area of the fibers within the mats.

Synthetic fibers were used in this study because of the easier definition of parameters such as specific surface area, cross-sectional shape and size, density, etc. Admittedly, the use of wood pulp would have been more directly relatable to the papermaking process; however, the added problems associated with its use would have seriously limited the scope of this investigation.

Because of the severe dependence of permeability properties on the surface area exposed to fluid flow within these porous media, a considerable amount of effort was expended in establishing a suitable method of evaluating the surface area. Initial attempts were centered around a dye adsorption technique. However, when this procedure was found to be unsuitable, a secondary approach, utilizing a light-scattering procedure, was developed. This procedure consisted of measuring the optical transmission and reflectance of the fiber mats at various porosities. A linear relationship between the specific scattering coefficient, calculated through the use of the transmittance and reflectance values, and the microscopically determined surface area of nylon 6 fibers was established at unit porosity. Reasonably good agreement was found between the surface areas experimentally determined through this technique and those calculated by means of a modified form of the statistically derived equations of Onogi and Sasaguri. In both procedures, contact

area values of no more than 16% of the total area were found for fiber mats composed of fibers which had aspect ratios as high as 4.69:1, at porosities as low as 0.5. In all determinations, linear relationships were found between the percentages contact area present in the fiber mats and the mat porosity.

The results of the permeability determinations were represented in terms of the Kozeny factor. Quadratic relationships between the Kozeny factor and the fiber cross-sectional aspect ratios were found. These relationships became more and more dependent upon fiber aspect ratio as the porosity was decreased. In the range of aspect ratios up to 3:1, there was very little effect of fiber cross-sectional shape on the resistance to the flow of fluids through fiber mats. However, beyond this ratio, the Kozeny factor was found to increase significantly. Whether or not this factor continues to increase at higher aspect ratios was not determinable during the course of this investigation.

INTRODUCTION

Because of the extreme complexity of porous media, it is virtually impossible to obtain an exact geometrical description of even an isotropic porous structure. Furthermore, if such a description were available, a complete delineation of the porous structure of a fiber mat would additionally require a knowledge of the distance from each randomly located point to a solid surface, the surface orientation, as well as the textural properties of the surface. In view of these considerations, it has generally been found to be more practical to describe the structure of porous media in terms of the flow of fluids through such systems. In theory, the differential equations describing the conservation of matter, momentum, and energy, are sufficient to predict all of the details of fluid flow motion through any confined space, regardless of its shape or complexity. However, even a casual inspection of the classical hydrodynamic texts (1), reveals that, excluding the case of relatively simple geometries, the solution of these equations is virtually impossible.

In view of these limitations, it has been necessary to revert to more phenomenological approaches for describing the flow of fluids through porous fiber mats. In this respect, a tenable, quantitative description of flow through porous media can be obtained through the use of Darcy's equation. For the case of steady-state, isothermal slow flow of an incompressible viscous fluid through a homogeneous undeformable porous medium in one direction, this equation may be written as

$$U = Q/A = K_o \Delta P/L \qquad (1)$$

where

$\underline{U}$ = superficial linear approach velocity

$\underline{Q}$ = volumetric rate of flow

$\underline{A}$ = cross-sectional area of the fiber mat

$\Delta\underline{P}$ = frictional pressure drop across the porous medium

$\underline{L}$ = thickness of the test specimen, and

$\underline{K}_o$ = a proportionality factor which is dependent on the properties of the porous medium and the permeating fluid

In the flow region where Darcy's equation is valid, the inertial effects are negligibly small and the frictional pressure drop may be considered to be entirely due to the viscous drag of the permeating fluid.

While Darcy's equation was derived from an empirical correlation of experimental data over a century ago, it has only been in recent years that attempts have been made to justify it theoretically. Through irreversible thermodynamic considerations, Mokadain (2) was able to derive a general equation for flow through porous media. However, in his treatment he assumed, for nebulous reasons, that the viscous terms could be omitted from the equation of motion. However, Darcy's equation was formulated to represent the viscous flow of fluids through porous media.

Another, but more realistic, attempt at arriving at the theoretical basis of Darcy's equation was made by Whitaker (3). In his treatment, he rigorously describes the flow of fluids through porous media in terms of the equations of continuity and motion, expressed on the basis of the microscopic dimensions of the system. He then contends that an averaging procedure can be used to convert these equations to the macroscopic dimensions of the system and subsequently arrives at the Darcy equation. Consequently, if his averaging procedure is

considered valid, it may be stated that Darcy's equation is a theoretically and experimentally valid law in the flow regime known as viscous or laminar flow.

As mentioned above, the proportionality factor, $\underline{K}_o$, includes the properties of the permeating fluid as well as the properties of the porous medium. Since it has been shown (4), experimentally and theoretically, that the fluid density is not a factor in the region of applicability of Equation (1), the effects of the fluid on $\underline{K}_o$ may be separated in the following manner, based on the known phenomenon of viscous flow,

$$K_o = K/\mu \qquad (2),$$

where $\underline{K}$ is the new permeability coefficient of the porous medium, and μ is the fluid viscosity. The permeability coefficient is then a function of only the structure of the porous medium and is not affected by the nature of the permeating fluid.

Combining Equations (1) and (2) results in the familiar form of Darcy's law,

$$U = K\Delta P/(\mu L) \qquad (3).$$

The separation of the permeability coefficient into the structural properties of porous media is considerably more difficult than separating the fluid properties from those of the solid phase. It is generally conceded that the permeability coefficient is dependent on at least two geometrical properties of the medium: void fraction or porosity and specific surface area.

Kozeny (5) developed a widely used theory, based on the hydraulic radius concept, to describe the flow of fluids through porous media. He noted the close similarity between Darcy's law and the generalized form of the Poiseuille

equation, for flow through capillaries, and related the permeability coefficient to the structural properties of the porous medium. Carman (6) later modified this concept in order to account for the tortuosity of the flow channels comprising the porous medium. Expressed on a volume basis, the Kozeny – Carman equation was then represented as

$$U = Q/A = \epsilon^3 \Delta P/[kS_v^2(1-\epsilon)^2 \mu L] \qquad (4),$$

where ϵ is the porosity or void fraction, S_v is the specific surface area, and k is the Kozeny factor.

By comparing this relationship with Darcy's law, it can be seen that the permeability coefficient is represented by

$$K = \epsilon^3/[kS_v^2(1-\epsilon)^2] \qquad (5).$$

Happel (7) recently proposed a free surface model for describing fluid flow through porous media. In his model each cylinder within a porous medium is considered to be surrounded by a concentric envelope of fluid with a free surface, constituting a unit cell. The cylinder is supposed to be moving in the direction perpendicular to its longitudinal axis at a uniform velocity in a stationary fluid. This is equivalent to the case of the cylinder being stationary with fluid flowing past it at a uniform velocity.

By assuming the boundary conditions of no slippage of the fluid at the surface of the cylinder and no shearing stress at the free surface, Happel was able to solve the equation of continuity and the creeping flow equations for two-dimensional flow. Without giving the details of his solution, Happel represented the drag force per unit length of cylinder as

$$F_d = 8\pi\mu U/\left[\ln\frac{1}{1-\epsilon} - \frac{1-(1-\epsilon)^2}{1+(1-\epsilon)^2}\right] \qquad (6),$$

where U is the fluid velocity, and F_d is the drag force.

The pressure drop across the assemblage of cylinders is represented as the drag force divided by the surface area of the cylinders,

$$\Delta P = 4L(1-\epsilon)F_d/(\pi d^2) \qquad (7),$$

where d is the diameter of the cylinders.

The permeability coefficient can therefore be given by

$$K = \mu LU/(\Delta P) = \left\{d^2/[32(1-\epsilon)]\right\} \left\{\ln[1/(1-\epsilon) - [1-(1-\epsilon)^2]/[1+(1-\epsilon)^2]\right\} \qquad (8).$$

Comparison of Equation (8) with Equation (5) reveals the theoretical basis for the inverse square dependence of K on the specific surface area, S_v, of the cylinders, since the specific surface for a cylinder is given by $4/d$.

By combining Equations (5) and (8), it is possible to express the Kozeny factor as

$$k = \frac{2\epsilon^2}{(1-\epsilon)\left\{\ln[1/(1-\epsilon)] - [1-(1-\epsilon)^2]/[1+(1-\epsilon)^2]\right\}} \qquad (9).$$

Equation (9) contains no empirical factors and, bearing in mind the assumption involved in the development of the model, is rigorously correct for flow perpendicular to an array of cylinders. This equation provides a theoretical basis for the variation of Kozeny factor with porosity, which has so often been found in the various experimental studies, especially for high porosities.

Upon checking the experimental values of k with Happel's prediction, it was found that the trends were similar, but there appeared to be some discrepancy in the absolute magnitudes. Earlier, Davis (8) developed the following empirical correlation to express the dependence of k on ϵ.

$$k = 3.5[\epsilon^3/(1-\epsilon)^{1/2}][1+57(1-\epsilon)^3] \qquad (10).$$

Carroll (9) later proposed a three-parameter correlation in order to overcome the shortcomings of the Davis relationship at the lower porosities. This correlation is

$$k = 5.0 + \exp[14(\epsilon - 0.8)] \qquad (11).$$

Figure 1 is a representation of these relationships plotted along with some of the experimental data which have been obtained in past investigations on circular glass and nylon fibers (10).

As can be seen from this figure, the Carroll correlation appears to fit the experimental data better than Davis' expression, at the lower porosities. However, it should be pointed out that, technically speaking, the entire Kozeny – Carman approach to flow through porous media is tenable only in the region where the Kozeny factor is practically constant. Such a region of constancy for fiber mats might be approximated in the porisity range from 0.6 to 0.8 (see Fig. 1), although Carroll's correlation indicates a continuous decrease of k with decreasing ϵ.

However, since it is entirely possible that the porosity function, based on cylindrical fibers, may change with fiber shape, its use for cellulosic, or noncircular, fibers may be of questionable value. Bliesner (11) obtained results which indicate that there is an effect of fiber cross-sectional shape when using wood fibers within porous media. In his study he used bleached sulfite pulp which was classified to remove the fines. Using fixed values of Kozeny factor, which were obtained by using circular fibers, he observed an apparent increase in the surface area exposed to fluid flow within a pulp fiber mat as the wet pressure applied to the mat was increased. It was hypothesized that this was due to a progressive collapse of the fibers as the wet pressure applied to the mat was increased. As the fibers collapsed, the fiber cross sections changed from more or less circular shapes into elliptical

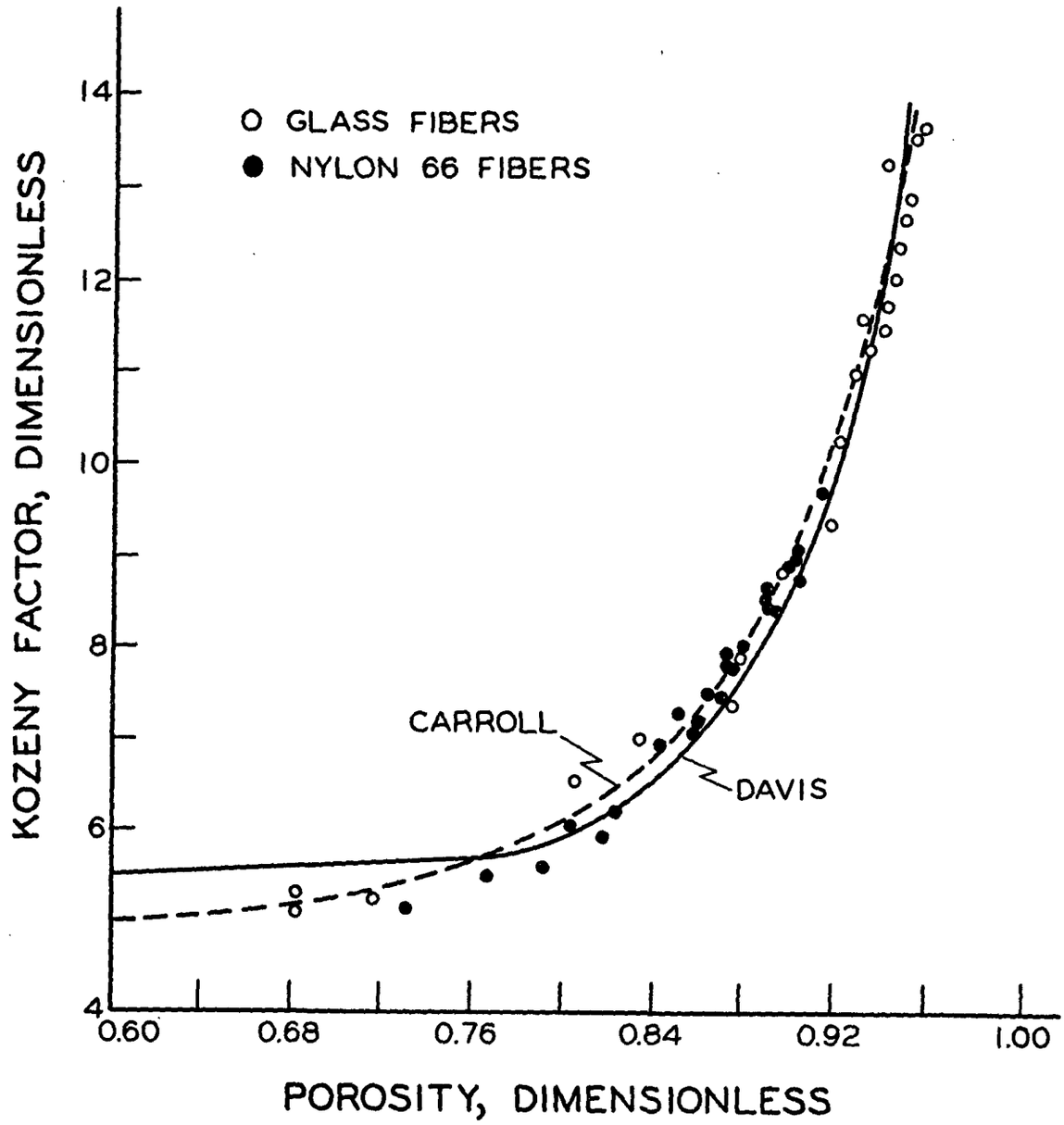

Figure 1. Kozeny Factor versus Porosity Data Obtained from Previous Investigations with Circular Fibers (10)

or ribbonlike shapes. It was contended that an array of such collapsed fibers would offer more resistance to fluid flow than an assemblage of circular cross-section cylinders, if compared at the same mat concentration.

As an exploratory investigation of this hypothesis, Bliesner measured the water-permeability properties of thick fiber mats formed with circular cross-section nylon fiber, flattened elliptical cross-section nylon, and dog-boned shaped cross-section orlon fibers. He used the equations derived by Onogi and Sasaguri (12) for statistically estimating the number of contact points in a fiber mat. Coupling these values with estimates of the contact area per contact point, based on measurements obtained from photomicrographs of the fiber cross section, he attempted to correct the value of specific surface area used in Equation (5) for that area which was in actual contact. Figure 2 is a representation of those determinations. The trends depicted in this figure are in qualitative agreement with Bliesner's proposed explanation for the increases he found in the calculated surface areas, when studying the permeability properties of thick mats of wood fibers. These findings are based on estimates of contact areas as high as 23% of the total area for orlon fiber beds, (4.14 aspect ratio), at 0.7 porosity. However, two conceptual errors, which affect the magnitudes of these values, were found in the original calculations of those data. The corrected equations and results of these determinations are included in the Discussion of Results section of this thesis.

The reader is referred to (11) for a more complete review of the literature pertaining to flow through porous media.

As an extension of Bliesner's exploratory study it was decided to expand the scope of the investigation, to cover a wider range of fiber aspect ratios.

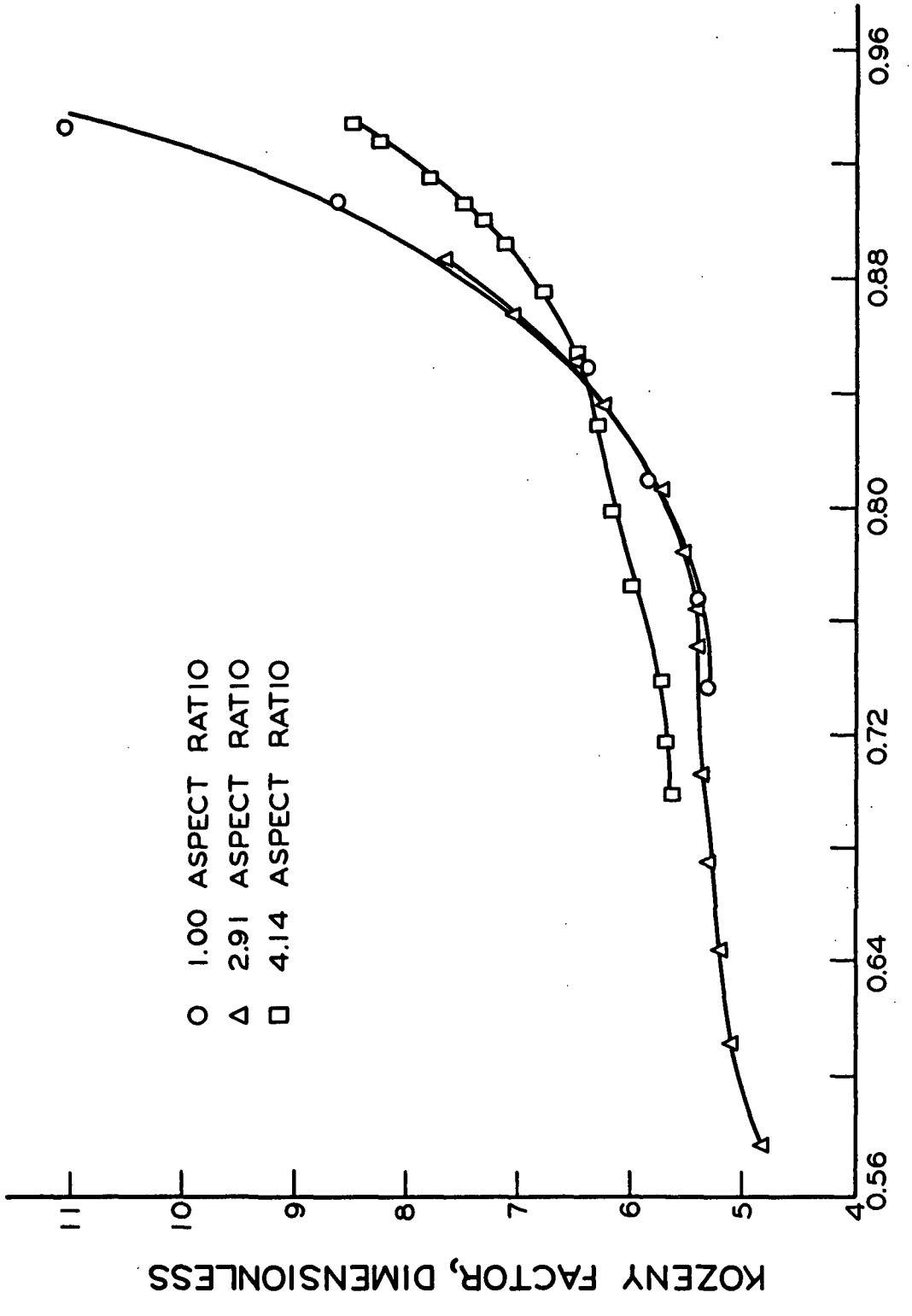

Figure 2. Kozeny Factor versus Porosity – Bliesner's (11) Original Data

Because of the severe dependence of permeability properties on the surface area exposed to fluid flow within these porous media, it was felt that an experimentally determined estimate of that quantity should be obtained for use in Equation (5).

The term "surface area" is quite ambiguous when applied to fiber mats since the value of the surface area obtained is usually a function of the type of experiment developed to determine it. Several such methods are available for determining the various surface areas. The gas adsorption method, the dye adsorption method, the silvering method, the microscopic method, and lastly the light-scattering technique are all methods which have been tried for measuring the surface area within fiber mats. In general, each of these methods gives a different value of surface area for the same sample.

In the present investigation, it was decided to use a light-scattering technique which was calibrated against the microscopic method of surface area determination. Arnold (13) has recently reviewed, in considerable detail, the literature pertaining to the light-scattering technique. This technique is based on the theory developed by Kubelka and Munk (14), as later modified by Van den Akker (15).

As early as 1940, Davis (16) suggested that the surface area of the particles in a sheet was proportional to the specific scattering coefficient. Parsons (17) experimentally found that the specific scattering coefficient, s, was linearly related to the external specific surface of a pulp when its surface area was determined by the silvering technique. Ratliff (18) and Leech (19) both encountered similar experimental evidence. Haselton (20) also found a linear relationship between s and the nitrogen adsorption surface area of pulp fibers.

However, some doubt was cast upon the linearity of this relationship by Ingmanson and Thode (21) and Swanson and Steber (22). In their experimental

procedures they varied the surface area of a pulp by beating it to various degrees. In doing so, they obtained nonlinear relationships of $\underline{s}$ versus specific surface. Conceivably, this nonlinearity could be due to the changes in fiber cross-sectional shape upon beating. On the other hand, such a phenomenon could be the result of fibrillation or fiber-to-fiber bonding present in such systems.

In short, the present study was an attempt to clarify the effects of fiber shape and fiber-to-fiber contact area on the permeability of fiber mats. As was mentioned earlier, this involved obtaining synthetic fibers of the correct cross-sectional shapes, measuring the permeability properties of fiber mats formed with each type of fiber, and determining the exposed surface area within the mats at the various levels of porosity.

EXPERIMENTAL PROCEDURES AND RESULTS

FIBER PREPARATION

The fibers used in this study were obtained as experimental samples from the American Enka Corporation. By varying the shape of the spinnerets, they were able to extrude continuous monofilaments of nylon 6 fiber in cross-sectional shapes ranging from circular to 4.69 quasielliptical aspect ratios. These undrawn fibers were received in continuous filament form, with no delustrant added, and of 7.3 denier. (A denier is the weight, in grams, of 9000 meters of monofilament fiber.) In order to increase the bending stiffness, and decrease the cross-sectional size of these fibers, the fibers were drawn before being cut. This was accomplished while using the apparatus depicted in Fig. 3. The fiber was fed through the nip formed when the loading wheel was placed against the face of the 7.5-cm. diameter rubber-faced pulley. The fiber then went over the reversing pulley, located 115 cm. away, and back to the 15-cm. diameter rubber-faced pulley, which was driven at the same angular speed as the 7.5-cm. pulley (11.7 r.p.m.). In this way a 200% elongation was effected, since there was no slippage of the fiber relative to either pulley. The fiber was then rewound onto squares of chipboard which were fastened to the faces of the octagonal wheel. This in turn, was driven at the same peripheral speed as the 15-cm. pulley. The lengths of representative samples of each type of fiber were measured and the samples dried at 50°C. for 12 hours. The fiber was then weighed and the denier of each sample calculated. The results of these determinations are reported in Table I.

After rewinding, the fibers were cut with a razor blade gang cutter, as described by Arnold (13). The results of length distribution determinations on samples of each of these fibers, are also reported in Table I.

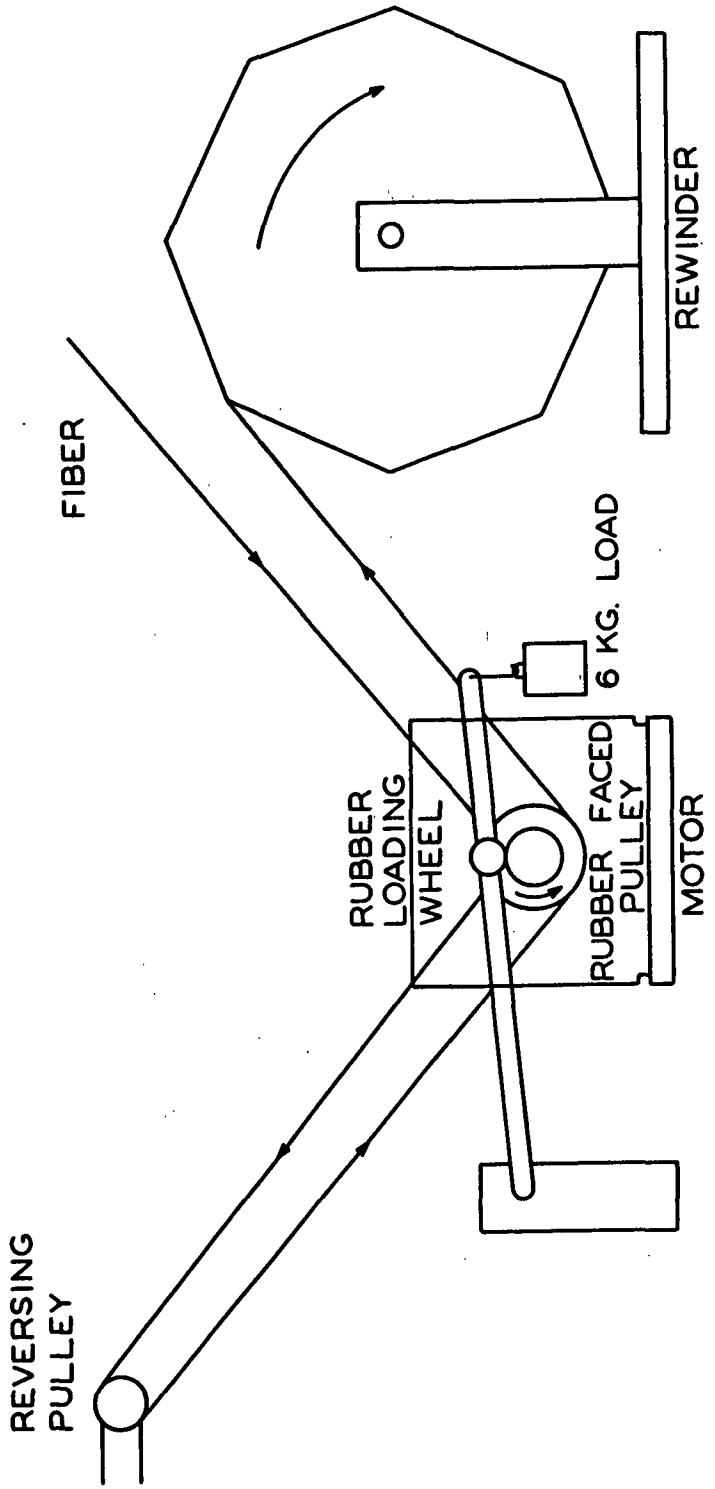

Figure 3. Fiber Stretching Apparatus

TABLE I

SUMMARY OF FIBER PROPERTIES

	Fiber Identification			
	Rx-1169	Rx-1167	Rx-1165	Rx-1164
Weighted average fiber length, μm.	3610	3790	3710	3800
Arithmetic average fiber length, μm.	3590	3770	3690	3790
Fiber width, μm.	25.3	39.0	50.6	53.3
Fiber thickness, μm.	25.3	14.8	12.2	11.4
Aspect ratio	1.00	2.64	4.12	4.69
Fiber perimeter, μm.	78.5	89.3	109	116
Fiber cross-sectional area, $(\mu m.)^2$	464	464	522	520
Density, g./cc.	1.200	1.191	1.242	1.186
Denier, g./9000 m.	3.8	3.8	3.8	3.8
Specific surface area, $cm.^2/cc.$	1535	1720	1860	1990

Samples of each type of fiber were then embedded in Epon 812 and microtomed cross sections of each obtained. Photomicrographs were taken of the cross sections and enlarged to a magnification of 950 diameters on film negative. Figure 4 is a representation of these photomicrographs at a magnification of 200 diameters. The width and thickness of each fiber were measured with a plastic ruler divided in millimeter divisions. The perimeters of the fiber cross sections were measured with the aid of a calibrated map reader and the cross-sectional areas measured with a planimeter. The aspect ratio of each fiber was then determined by dividing the fiber width by its thickness. The results of these determinations are also presented in Table I.

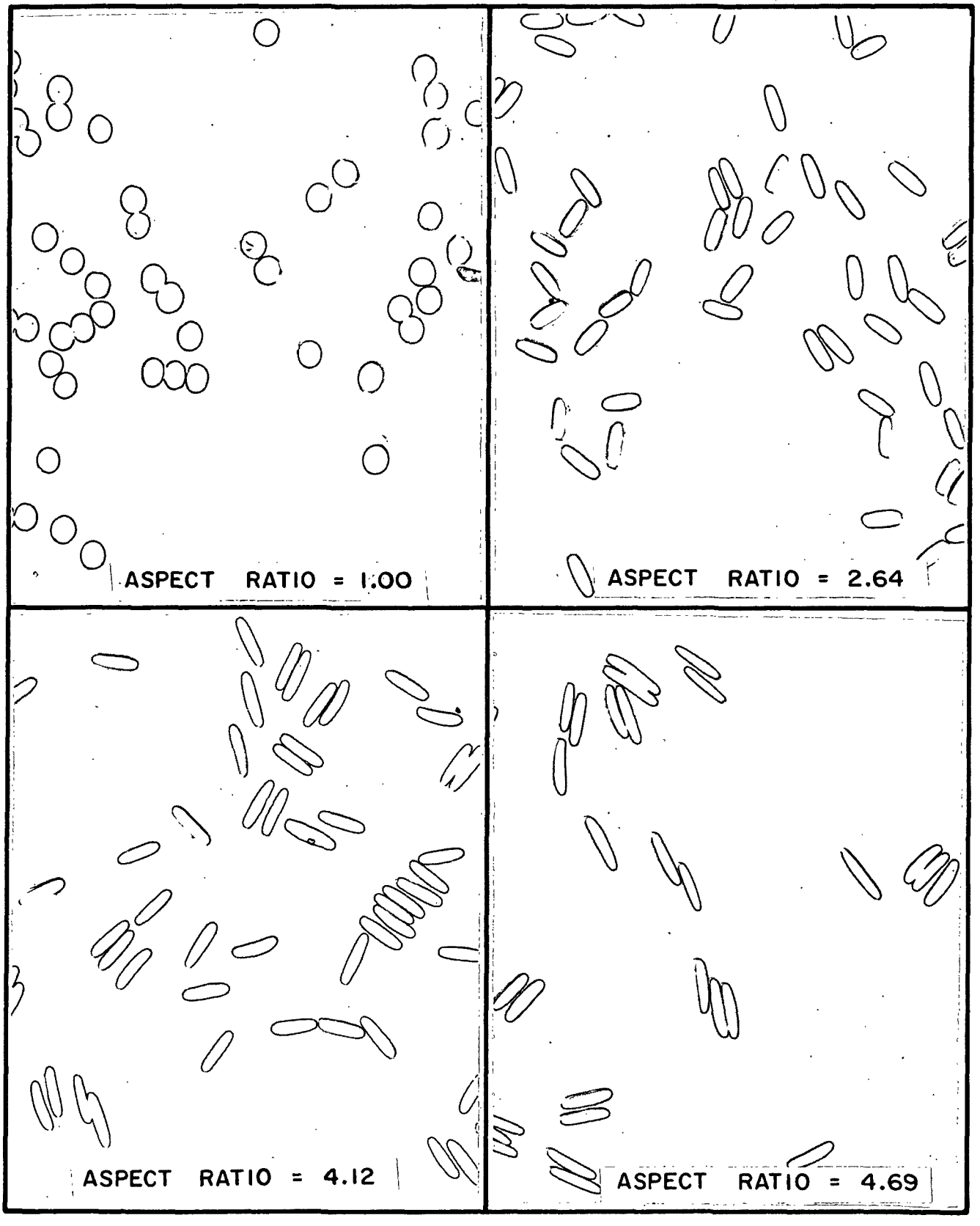

Figure 4. Cross-Sectional Shapes of Fibers used in this Study (Magnification ≅ 200 Diameters)

Since the fiber dimensions affecting the hydrodynamic properties of fiber mats are the swollen dimensions, it was decided to measure the aqueous swelling of the circular nylon 6 fibers used in this study. This was done by microscopically measuring the diameter of fibers, which had been presoaked for 24 hours, while they were immersed in water and comparing these measurements to those obtained when the fibers were immersed in a nonswelling fluid of 1.520 refractive index. After measuring 100 fibers in both fluids, a 4.3% diameter swelling was found for this fiber.

The moduli of elasticity of samples of each fiber were determined while using the Institute Individual Fiber Tensile Apparatus, as described by Hardacker (23). Samples of fiber were mounted in the 2-mm. span of the instrument, and load-elongation curves obtained for each. By measuring the initial slopes of these curves, as well as the cross-sectional areas of the fibers, it was possible to calculate the modulus of elasticity, in the axial direction, for each fiber. It was found that the individual values varied between 246,000 g./cm.^{2} for fibers with an aspect ratio of 2.64:1 and 290,000 g./cm.^{2} for the circular fibers. The average modulus for all four fiber samples was 273,000 g./cm.^{2}.

PERMEABILITY MEASUREMENTS

Early attempts at forming fiber mats with existing filtration apparatus revealed that more than 80% of the fibers were curled enough to form circles or even double circles. Apparently, this was due to some stress relaxation within the fibers as they were added to the water, since they were quite straight before being added to the system. In order to correct this problem, a low-temperature alcohol-forming process was incorporated into the system. By dispersing the fibers in absolute ethyl alcohol, at -50 to -60°C., it was possible to prevent fiber curvature, as long as the temperature was not allowed to rise above -15°C.

At these temperatures, nylon 6 became very stiff and even the high shear forces found in the British disintegrator did not cause bending of these minute fibers. However, there was a possibility that subjecting these cold fibers to such high shear forces might cause rupturing or breaking of the fibers. This was checked, through microscopic examinations at a magnification of 1000 diameters, and it was found that no discernible fiber damage had occurred.

In view of the safety hazards associated with using large volumes of ethanol, it was decided to design the flow system so that water permeability, rather than alcohol permeability, could be used to measure the hydrodynamic properties of the fiber mats. Figure 5 is a schematic of the flow system used in this study. In the forming process the alcohol was first filtered into a five-gallon glass carboy and deaerated for one hour at room temperature. It was then carefully added to the slurry tank, the refrigeration unit activated, and the alcohol cooled to -25°C. A two-liter sample of this alcohol was then added to the British disintegrator and further cooled, indirectly with dry ice, to -60°C. A four-gram sample of fiber was then added to the British disintegrator and the mixture disintegrated for 225 counts. After disintegration, the mixture was again deaerated for one half hour at -50°C.

Through manipulation of the proper valves, the forming tube was filled by flowing cold alcohol from the slurry tank up through the septum. This was necessary in order to force any entrapped air below the septum out of the system. The forming tube was the same as that described by Ingmanson (24) and the septum assembly was similar to that used by Bliesner (11) for couching thick mats, except that this one was only 2.993 inches inside diameter.

The pump was started and the flow rate adjusted by controlling the bypass valve and the variable speed pump drive. After temperature equilibrium had

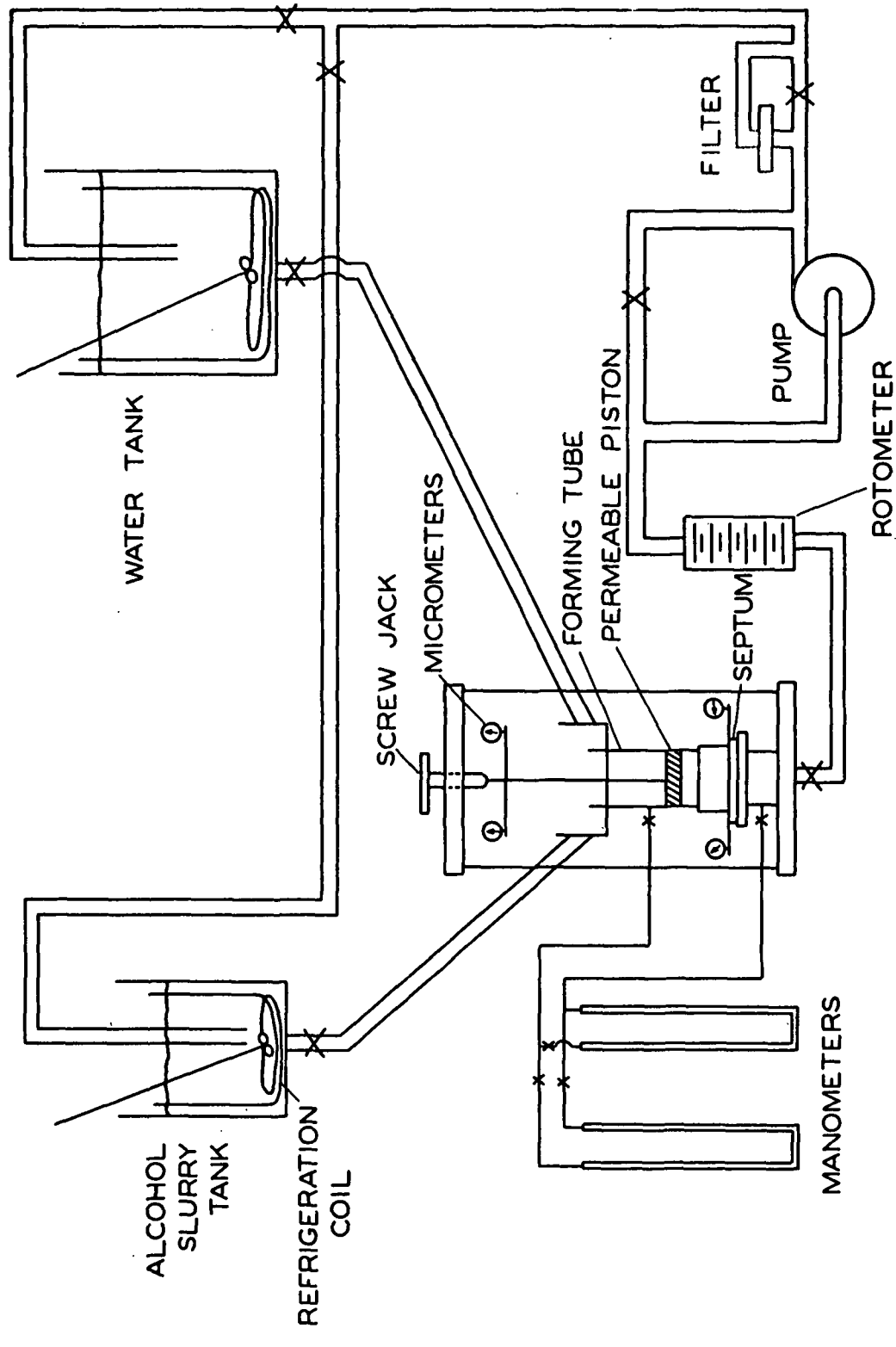

Figure 5. Permeability Apparatus

been attained (-20 to -30°C.), a 400-ml. sample of cold disintegrated fiber suspension was added to the slurry tank and mildly agitated. The suspension was then allowed to flow through the forming tube, where the fibers were filtered out, and the alcohol recirculated to the slurry tank. The flow rate was adjusted so that the fibers were deposited in the mat with their major cross-sectional, as well as longitudinal, axes in the horizontal, or X-Y, plane of the mat. This process was continued, at a constant flow rate, until the slurry consistency had dropped below approximately 0.001%. At this time, another 400-ml. sample of the disintegrated fiber suspension wad added to the slurry tank. At no time was the slurry tank consistency allowed to become greater than 0.008%.

After a sufficiently thick fiber mat had been formed, a permeable brass piston, which was covered with 100-mesh brass wire, was placed on top of the fiber mat. Flow from the slurry tank was then stopped and 2 liters of freshly deaerated, cold (-30 to -40°F.) ethanol was passed through the fiber mat to assure that no air was present in the alcohol remaining in the bed. This alcohol was then itself flushed out of the bed with distilled water, which had been filtered through a number HAWP 14200 Millipore filter, deaerated, and cooled to +5°C.

The manometer lines, connected to the water/chlorobenzene manometer, were then carefully flushed out with room temperature deaerated water in order to insure that no alcohol was present in the system. The entire apparatus was subsequently allowed to warm to room temperature and the permeability measurements initiated.

During the permeability measurements, deaerated, filtered, distilled water, at an accurately known temperature (approximately 25°C.), was passed through the

fiber bed at carefully controlled flow rates. The pressure drop across the bed was measured, at each flow rate, with the aid of a water/chlorobenzene manometer. The bed was then compressed by the permeable piston and its thickness at each given compression measured with the four dial micrometers mounted on the apparatus. Two of these micrometers were connected directly to the permeable piston shaft, and the other two were mounted on the septum itself. In this way, any movement of the septum due to the compressive forces of the piston, was easily detected and the necessary corrections effected.

After each compression, the flow rate and pressure drop data were collected. This process was repeated until the desired range of porosities had been covered. In all cases, the porosity was approached from a higher to a lower porosity, and the flow rates were approached from the lower to the higher values.

It should be pointed out that the flow rates used during the permeability determinations were adjusted so that the range of applicability of Darcy's law was not exceeded. That is, the flow rate was low enough to insure that linear relationships between flow rate and the resulting pressure drop were maintained throughout the experiments.

It should also be made clear that the maximum flow rate was adjusted so that the pressure drop resulting at that flow rate was always less than 3% of the load required to compress the mat to the porosity at which the data were obtained. This was necessary in order to ensure that no significant porosity gradient, from the top face of the mat to the septum, was established.

In order to account for the portion of the pressure drop across the bed that was due to the wire septum and piston, the pressure drop across these components was measured in the absence of any fiber mat. This was done by

assembling the apparatus, as usual, and clamping the permeable piston so that it was a fixed distance above the septum. Filtered, distilled, and deaerated water was then passed through the apparatus and the pressure drop noted. At the highest superficial approach velocities used in the flow determinations (0.31 cm./sec.), the pressure drop across these components was found to be negligibly small and no correction was needed.

In calculating the results of these flow measurements, the flow rate – pressure drop data were treated in a linear regression analysis in order to obtain the best values of the slopes of each set of flow data. These slopes were then used to calculate the permeability coefficients according to Equation (3). These results were then used to calculate the $\underline{\underline{k}}\underline{S}_{\underline{v}}^2$ relationships described in Equation (5). (The computer program which was used in these calculations is given in Appendix I.)

These $\underline{\underline{k}}\underline{S}_{\underline{v}}^2$ versus porosity relationships were, in turn, used in a computerized polynomial curve-fitting program, IBM Program Number 1620-7.0.002, and the most suitable mathematical relationships describing their behavior obtained. This served primarily as a data averaging procedure. Equations of the form,

$$kS_v^2 = a + b\epsilon + c\epsilon^2 + d\epsilon^3 \qquad (12)$$

were obtained over the porosity range from 0.5 to 0.84. The values of the various coefficients for each fiber, are represented in Table II. Figure 6 represents these same relationships in graphical form.

TABLE II

COEFFICIENTS FOR EQUATION (12)

Fiber Aspect Ratio	$\underline{a} \times 10^{-7}$	$\underline{b} \times 10^{-7}$	$\underline{c} \times 10^{-8}$	$\underline{d} \times 10^{-7}$
1.00	-1.48	3.67	–	–
2.64	2.64	-16.30	3.30	-1.76
4.12	-6.07	1.37	0.26	–
4.69	-1.73	7.38	-0.22	–

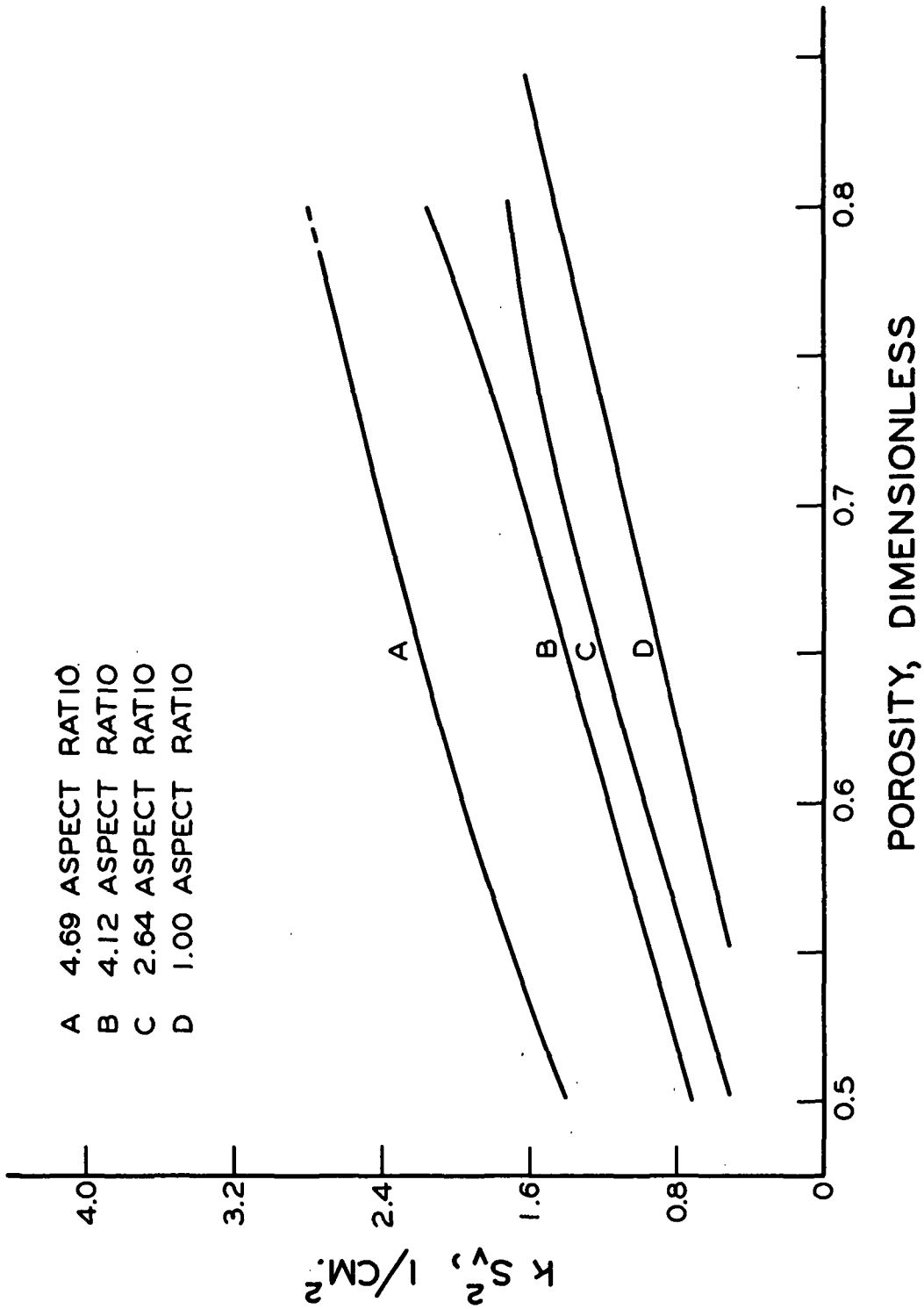

Figure 6. Kozeny Factor Times the Square of Specific Surface Area versus Porosity

The linearity of the relationship found for the mats composed of circular fibers was somewhat disturbing. If these $k\bar{S}_v^2$ values, obtained for circular fibers, are divided by a constant value of $\bar{S}_v^2$, as is generally done for systems in which there is point contact between fibers, a linear relationship of Kozeny factor versus porosity will result, over the porosity range from 0.6 to 0.85. Comparing this to the results obtained by Ingmanson and Andrews (10) on the water permeability of fiber mats composed of circular-cross-section nylon 66 fibers (see Fig. 1), indicates that, possibly, the assumption of point contact over this range of porosities was incorrect. Such a problem could conceivably arise if the fibers used in this study were appreciably softer or more deformable than those used in previous studies. In an attempt to determine if this premise was correct, the following experiment was performed.

The lateral deformability of individual circular fibers was measured while using the Institute Compacted Fiber Dimension Apparatus (CFDA), as described by Hardacker and Van den Akker (25). This was done by placing single circular fibers between the sapphire plates of the CFDA, measuring the unloaded diameter, adding a constant load, and then measuring the increase in fiber width.

By repeating these measurements on representative samples of both nylon 6 fiber and conventionally used nylon 66, of the same diameter, it was found that this nylon 6 was at least 2.5 times more deformable. That is, for the same loading, nylon 66 showed an 18% increase in diameter as compared to the 50% increase found for nylon 6. Such a high relative deformability could conceivably account for the results noted above.

SURFACE AREA DETERMINATION

As was mentioned earlier, it is necessary to correct the value of specific surface area, used in the calculation of Kozeny factor, for the area in fiber-

to-fiber contact, since this area will not be contributing to the frictional drag force experienced by the flowing fluid. Admittedly, this area may still affect the "form" drag at the fiber intersection. However, "contact area" shall be used here to represent that part of the fiber surface area which is not contributing to the frictional flow resistance, as measured in the permeability determinations. Therefore, the most suitable method of measuring this variable should utilize the same flow system as was used during the permeability determinations. In this way the system would be in the same state of dynamic equilibrium and the quantity determined would relate more directly to the actual "hydrodynamic" area. In this respect, an attempt was made to develop a dye adsorption technique which could be incorporated into the permeability system.

In essence, a dye adsorption method of estimating surface area involves adsorbing a monolayer of dye molecules onto the fiber surface, measuring the amount of dye adsorbed, and calculating the dyed surface area from the molecular dimensions of the dye molecule. Several dyes were tried for this purpose, but unfortunately all the commercially available dyes tried were found to penetrate into the fiber to such an extent that the area measured was the total area (surface area plus internal area) and not just the external surface area. According to Chipalkatti, et al. (26), swollen nylon fibers have pore sizes of approximately 6 A. diameter, which could very well account for the above problem.

Attempts were then made to use nonswelling fluids from which to dye nylon. It was expected that this would decrease the amount of dye penetration into the fiber, and consequently would result in a more accurate measure of the surface area. Once again, this technique failed to give the desired results, primarily because no good system could be found for dyeing the nylon.

A summary of the dyes investigated for this purpose, as well as some of the solvents used, is included in Appendix II.

A light-scattering method of measuring surface area was then tried and found to be quite satisfactory. However, unlike the dye adsorption procedure, this technique consists of nondynamic determinations on dry fiber beds. Early measurements were made according to the procedure developed by Arnold (13). In essence, this procedure consisted of measuring the reflectances of fiber mats, at various levels of compaction, when they were backed by a black body, and again when they were backed by a white body of unknown reflectance.

The fiber beds used for these determinations were formed in the same manner as those used for the hydrodynamic measurements. The only modification was that after the final displacement of absolute ethanol, the water in the forming tube was drained to approximately 1.0 cm. above the upper face of the fiber mat. The discharge valve below the septum was closed and the upper section of the forming tube carefully removed without disturbing the septum assembly. A sealing brass piston fitted with a rubber O-ring was then inserted into the septum assembly so that no water could drain from the fiber mat. After proper sealing, the septum assembly, along with the saturated fiber mat, was carefully removed, in such a manner that no water could drain from the assembly. (This can be accomplished if the assembly is not tilted during the removal, since the surface tension of the water is great enough to prevent appreciable flow of water out of the equipment.) The entire assembly was then quickly frozen by immersion in a bath of dry ice and ethanol. The frozen fiber mat was then removed from the septum and freeze dried until the vapor pressure of the system fell below 20 microns of mercury.

Freeze drying was necessary in order to prevent the surface tension forces associated with drying from a liquid from causing disruption of the fiber mat. Normal drying was also found to cause some degree of fiber-to-fiber bonding with these fibers.

The dry fiber mats were then cut to 2.00 inches diameter with the aid of a carefully machined die. These samples were then placed in a slightly modified version of Arnold's sample holder and the necessary light-scattering measurements obtained.

The major sample holder modifications were that the front cover glass was tempered and cut to 2.5 inches diameter instead of 3.0 inches and the backing glass was 0.25-inch thick instead of 0.12 inch.

Problems were encountered while trying to calibrate the reflectance of the white-bodied background when it was in the sample holder. In order for the calibration to be valid, it was felt necessary to make all the measurements as a function of glass plate separation in the sample holder. Arnold neglected this point in his calibration. He assumed that the reflectance value obtained when the sample was placed on the G.E. Brightness Tester could be used in the calculation of the data obtained from the General Electric Recording Spectrophotometer (GERS). Reference to Fig. 7 will illustrate why such a procedure is unsuitable in this system. The details of the apparatus have been omitted for the sake of simplicity. A monochromatic, collimated light beam illuminated both the magnesium carbonate reference and the fiber pad. [See (27) for a more thorough discussion of the mechanics of operation of the GERS.] When the fiber pad was fully extended, such as when the back glass was at Position a, the light reflected from the back glass subtended a solid angle α into the integrating cavity. As the sample was compressed to Position b, the solid angle became

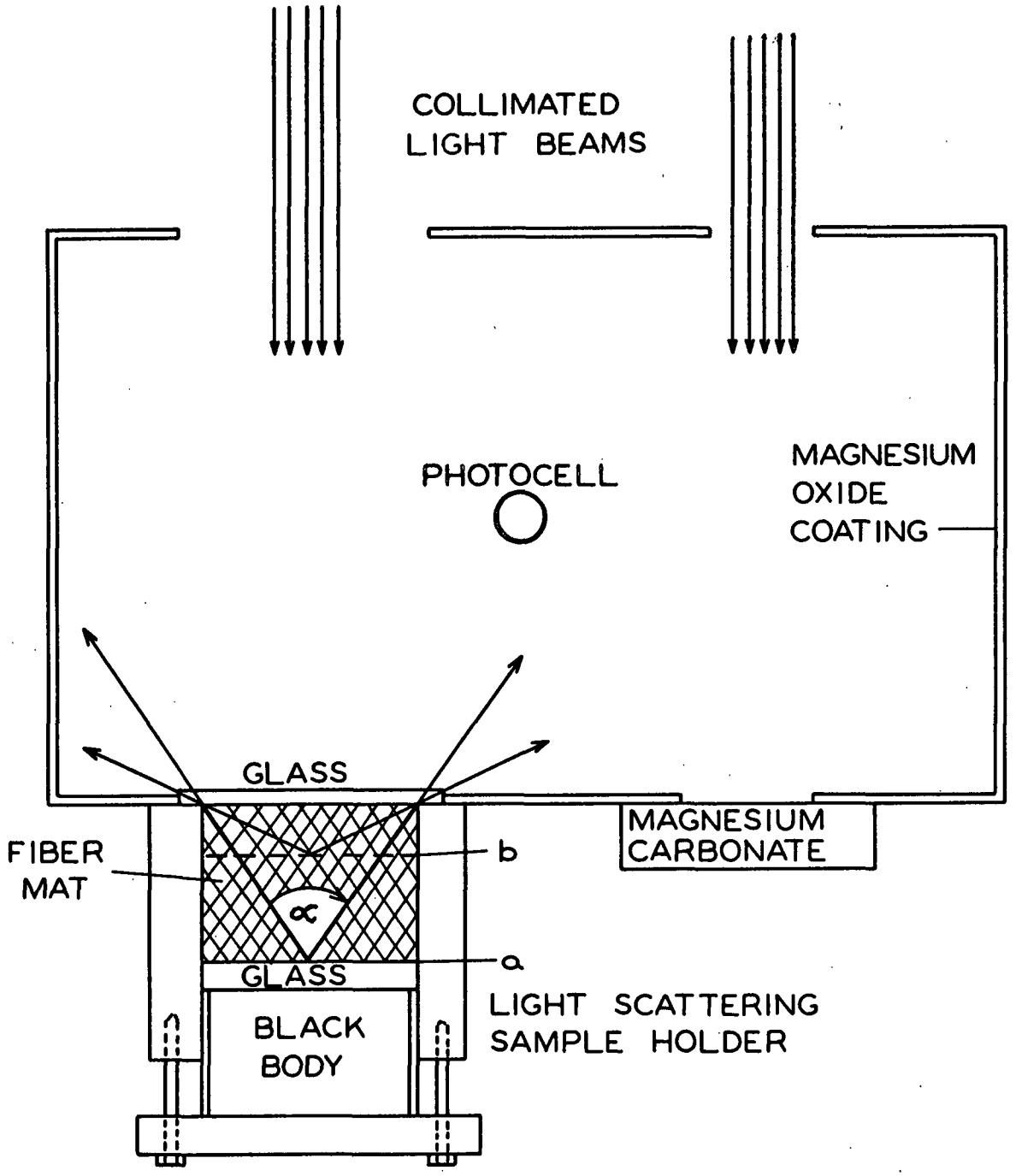

Figure 7. Top View of GERS Modified Integrating Cavity

significantly larger than α and thereby increased the amount of reflected light sensed by the phototube, which was located at the base of the integrating cavity. This in turn altered the value of reflectance measured by the instruments. Consequently, calibration measurements, which were obtained at one given distance of separation between the glass plates were not applicable to other separation distances.

However, it should be pointed out that although Arnold's calibration procedure was in error, and consequently the absolute magnitudes of his results were probably wrong, the trends found in his relationships were most likely still quite valid.

Because of calibration problems, it was decided not to measure the reflectance of the fiber mat when it was backed by a white background. Instead, a technique involving the use of the optical transmittance of the pad was developed. In this procedure, the fiber pad, 2.00 inches in diameter, was placed in the light-scattering sample holder. The back half of the holder, i.e., the movable 0.25-inch thick plate glass piston, was placed on top of the fiber pad and the plate separation fixed by tightening the various nuts. The thickness of the pad was then measured with a micrometer. The holder assembly was then placed in the rear sample port of the modified integrating cavity of the GERS. The only significant modification on this integrating cavity was that both the front and rear sample port openings had been enlarged to 2.5 inches diameter. This was necessary in order to move the sample closer to the plane of the cavity and consequently reduce any dissymmetry problems which might have been affecting the system. This also provided a method of aligning the sample, relative to the light source, since the front glass was also cut to 2.5 inches diameter.

A slightly oval collimated light beam (10 by 13 mm. at the entrance port), of 650 millimicrons wavelength, alternately illuminated the fiber pad and the

magnesium carbonate standard. A black cloth was then draped over the entire integrating cavity and sample, and the reflectance reading obtained from the instrument. The sample assembly was then removed from the rear sample port and the sample port covered by a large (3-inch diameter) block of magnesium oxide. The sample holder assembly was placed in the front sample port of the integrating cavity and the light beam allowed to pass through the fiber pad and into the integrating cavity. In both determinations, the front of the sample was facing the inside of the integrating cavity. The black cloth was again placed over the apparatus and the value of the optical transmittance of the pad obtained. The sample holder assembly was removed from the apparatus and the pad compressed to a lower porosity by tightening the nuts on the holder. The pad thickness was again measured and the reflectance ($\underline{R}_o$) and transmittance ($\underline{T}$) values again obtained.

This procedure was repeated, over the desired porosity range, on freeze-dried fiber beds composed of fibers of each aspect ratio.

The backing reflectance and the effects of the sample holder on the optical values obtained were calibrated in the following manner. Six sheets of 25-pound glassine which had been cut to 2.00 inches diameter were placed in the light-scattering sample holder. Three of these sheets were glued very lightly at the edge of the holder. The remaining three pieces were glued in the same way to the inside of the back glass plate. The sample holder was then assembled with a given distance of separation between the two glass plates. The necessary optical measurements, $\underline{R}_o$ and $\underline{T}$, were obtained as described above. The spacing of the glass plates was decreased and the necessary data again collected.

After repeating these measurements over the range of separations needed, the glassine paper samples were removed from the holder. Care was exercised

to insure that the orientation of each sample with respect to the light source was the same as in the light-scattering determinations. The six glassine samples were placed together and their composite optical transmission and reflectance values measured in the conventional manner (28) on the GERS. This GERS was equipped with a slightly modified integrating cavity which allowed measurements of total optical transmission. The values of $\underline{T}$ and $\underline{R}_o$ so obtained were used as the correct values. The ratios of these values to the ones obtained when the glassine samples were in the light-scattering sample holder were used as the correction factors at each fiber mat thickness. The various values of $\underline{T}$ and $\underline{R}_o$ obtained for each fiber mat at each mat thickness were multiplied by their respective correction ratios, $\gamma_{\underline{T}}$ or $\gamma_{\underline{R}_o}$. These correction ratios varied linearly from 1.28 at 0.25-inch plate separation to 1.25 at 0.04-inch separation for $\underline{R}_o$ and from 1.29 to 1.10 over the same separations for $\underline{T}$.

The resulting values were also multiplied by 0.98 in order to correct for the imperfect reflectance of the optical standard used as the reference in the above determinations. In equation form, these calculations can be represented as

$$R_o' = 0.98\ \gamma_{R_o}\ R_o \tag{13}$$

and

$$T' = 0.98\ \gamma_T\ T \tag{14}$$

where the primes indicate the corrected values. These values were then used to determine the scattering power ($\underline{sW}$), according to the method developed by The Institute of Paper Chemistry, Physics Department (29). The scattering power was then divided by the basis weight, in grams per square centimeter, to obtain the corresponding value of specific scattering coefficient, $\underline{s}$. Figure 8 is a plot of the specific scattering coefficients versus porosity for the various aspect ratio fibers.

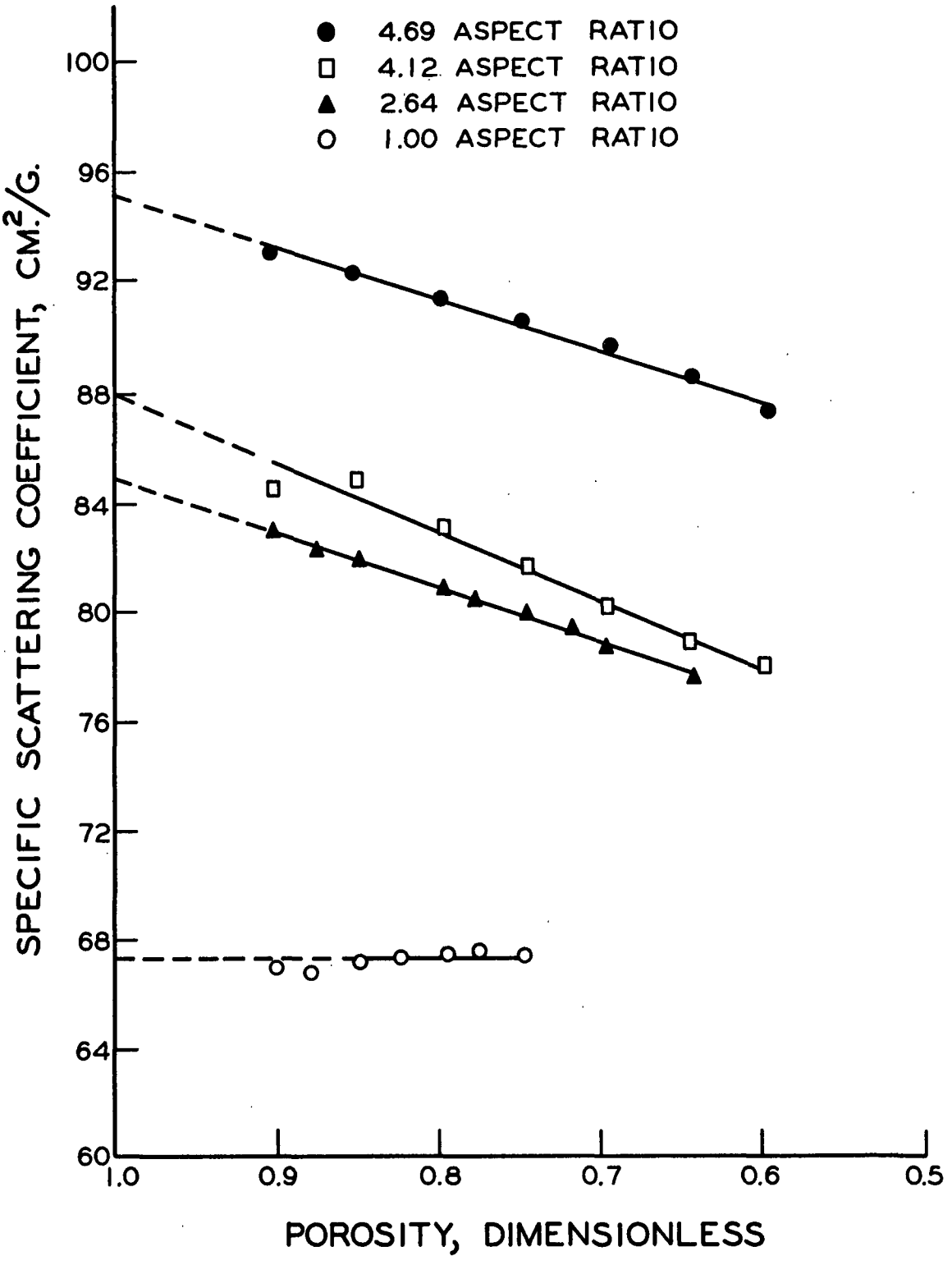

Figure 8. Variation of Specific Scattering Coefficient with Porosity

Quite surprisingly, (see optical data in Table VII, Appendix IV), it was noted that as a fiber mat was compressed to lower porosities, there was a reduction in the optical transmission of the structure. Theoretically, the reverse should have happened since the contact area within the bed was increased upon compaction. As the area available to scattering light was reduced, more light should have been transmitted through the sheet. A possible explanation for this phenomenon is as follows. As the fiber mat was compressed, more fibers were brought into optical contact with the glass plates confining the mat. This could result in more light entering the inside of those fibers. Unless this light struck the inner fiber wall at an angle above the critical angle, it would simply be reflected inside the fiber. Since nylon 6 does absorb some light, the amount of light lost to optical absorption would be increased by virtue of the fact that the light rays must travel through more solid nylon due to the multiple reflections. This, in turn, would be manifested as an increase in optical absorption and, concurrently, as a decrease in optical transmission of the fiber mat as a whole.

Nevertheless, the change in surface area within these fiber mats should still be directly relatable to the values of specific scattering coefficients obtained.

The horizontal light-scattering relationship, which was found for fiber mats composed of circular cross section fibers, is in good agreement with the contention that point contact existed at the fiber intersections within such fiber networks. Apparently, as the fiber mats were compressed to lower porosities, the number of contact points increased but the contact area remained the same due to the point contact at the fiber crossings. However, as will be seen in a later section (see Fig. 18), the hydrodynamic measurements

on fiber mats composed of these fibers indicated that the contact area does increase at porosities below 0.72. The absence of this decrease in scattering coefficient in this porosity region may well be explained on the basis of the higher modulus of elasticity of the dry fibers as compared to the fully saturated fibers. The wet fiber would naturally be more deformable and consequently even circular fibers would exhibit contact area in this porosity range. Had it been possible to go to lower porosities, the light-scattering coefficients would most probably have been found to decrease. However, the range of porosities covered in these determinations was limited by the loads required to obtain the needed mat concentrations. Compression to a porosity 0.02 unit below those shown in Fig. 8 very often resulted in breakage of the glass plates of the sample holder. Future work in this area should certainly allow for the use of higher compressive loads in these determinations.

The relationships obtained with the noncircular cross-section fibers were quite encouraging. Extrapolation of these very nearly linear curves to unit porosity, at which point it was assumed that the specific surface area was that area obtained through microscopic examination of the fibers, resulted in the relationship shown in Fig. 9. Since theory dictates that, for homogeneous fibers, at zero specific surface the specific scattering coefficient should be zero, the curve was drawn through the origin.

The low value of specific scattering obtained for the circular-cross-section fibers, as compared to the higher aspect ratio fibers, is in general agreement with the discussion presented by Arnold (13). He indicated that as the cross-sectional shape of fibers was changed from circular to ribbonlike, it could be expected that the value of the scattering coefficient would be significantly increased. Such a finding is also in good agreement with the nonlinear

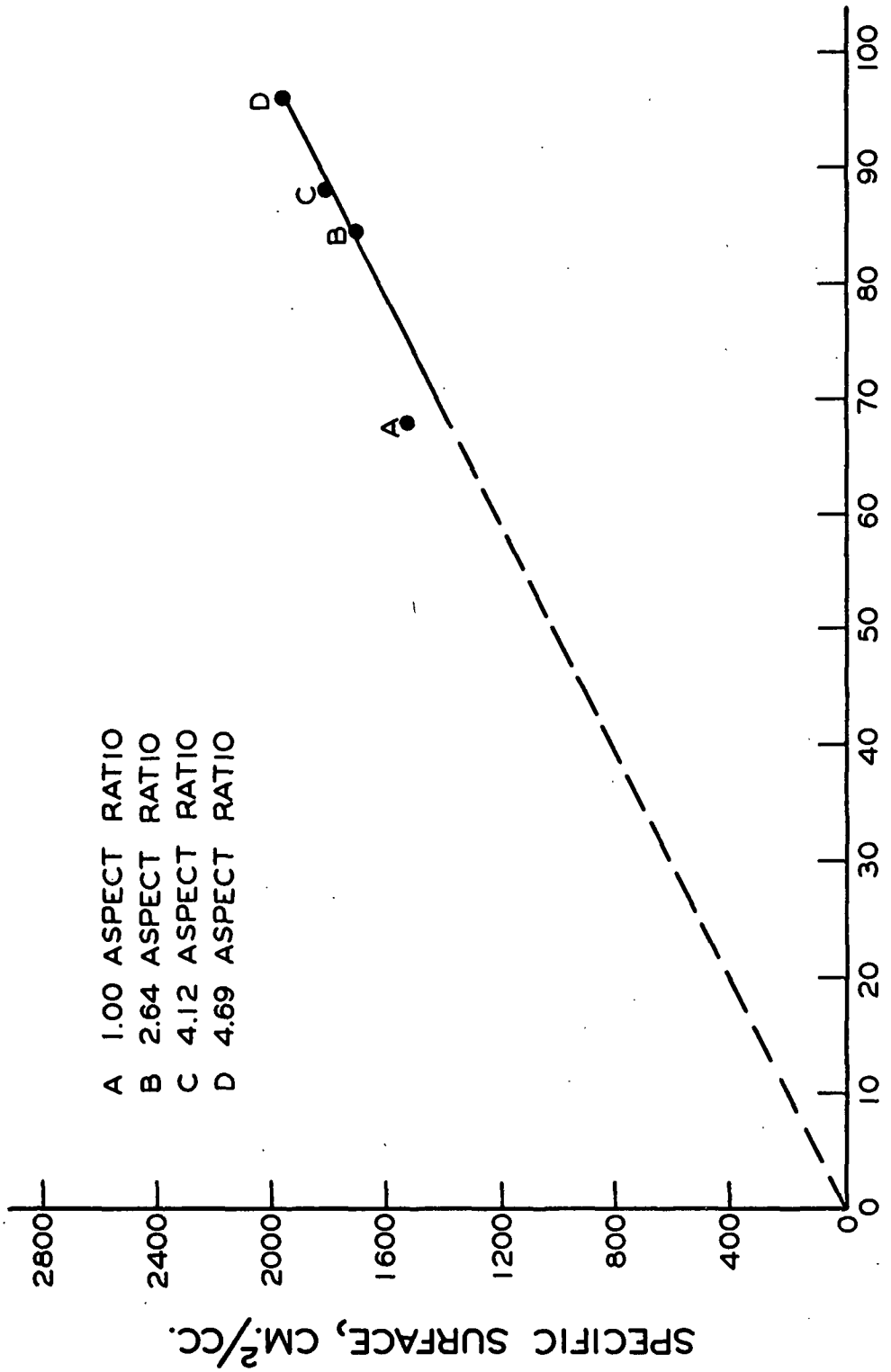

Figure 9. Variation of Specific Surface with Specific Scattering at Unit Porosity

relationships found by Ingmanson and Thode (21) and Swanson and Steber (22), while working with beaten wood pulps.

The relationship shown in Fig. 9 can be represented mathematically

$$S_v = 20.9\ s \tag{15}$$

whereas those of Fig. 8 can be depicted as

$$s = \alpha - \beta\ (1-\epsilon) \tag{16}$$

where α and β are the unit porosity intercepts, and slopes of the $\underline{s} - \epsilon$ relationships, respectively. The α values were found to be 67.8, 84.8, 88.0, and 95.1, whereas the β values were 0.0, 21.1, 24.8, and 18.2 for the 1.00, 2.64, 4.12, and 4.69 aspect ratio fibers, respectively.

A combination of these two relationships results in the following expression for describing the dependence of specific surface area on porosity, over the porosity range from 0.6 to 1.0,

$$S_v = 20.9\ [\alpha - \beta(1-\epsilon)] \tag{17}$$

The values of $\underline{S_v}$, calculated according to Equation (17), were then used in Equation (5) to calculate the values of Kozeny factor, over the porosity range in question. Table III is a summary of the results so calculated. Figure 10 represents the relationships obtained from these calculations. Figure 11 is a representation of the same values of $\underline{k}$ plotted as a function of the aspect ratio of the fibers. It should be pointed out that the values calculated at porosities below 0.6 were obtained by assuming that the $\underline{s} - \epsilon$ relationships, given by Equation (16), were unchanged at the lower porosities. Based on an examination of Fig. 8, such an extrapolation is probably not seriously in error.

TABLE III

KOZENY FACTOR CALCULATIONS
BASED ON LIGHT-SCATTERING SURFACE AREA ESTIMATES

Porosity	Specific Contact Area, $cm.^2/cc.$	Percent Contact Area	Specific Surface Area, $cm.^2/cc.$	Kozeny Factor
1.0 Aspect Ratio				
0.84	0	0	1535	6.78
0.82	0	0	1535	6.50
0.80	0	0	1535	6.20
0.78	0	0	1535	5.86
0.76	0	0	1535	5.57
0.72	0	0	1535	4.93
0.64	0	0	1535	3.69
0.60	0	0	1535	3.10
2.64 Aspect Ratio				
0.80	28	1.6	1692	6.08
0.76	45	2.6	1675	5.78
0.72	62	3.6	1658	5.35
0.70	71	4.1	1649	5.12
0.66	89	5.2	1631	4.58
0.58	124	7.2	1596	3.47
0.50	160	9.3	1560	2.34
4.12 Aspect Ratio				
0.80	126	6.8	1734	7.15
0.76	144	7.7	1716	6.48
0.70	178	9.6	1682	5.65
0.66	198	10.6	1662	5.14
0.62	219	11.8	1641	4.57
0.58	240	12.9	1620	4.04
0.50	281	15.1	1579	2.97
4.69 Aspect Ratio				
0.78	86	4.3	1906	7.47
0.74	98	4.9	1892	7.12
0.70	124	6.2	1876	6.77
0.66	139	7.0	1861	6.35
0.62	145	7.3	1845	5.92
0.58	160	8.0	1830	5.43
0.54	175	8.8	1815	4.92
0.50	190	9.6	1800	4.38

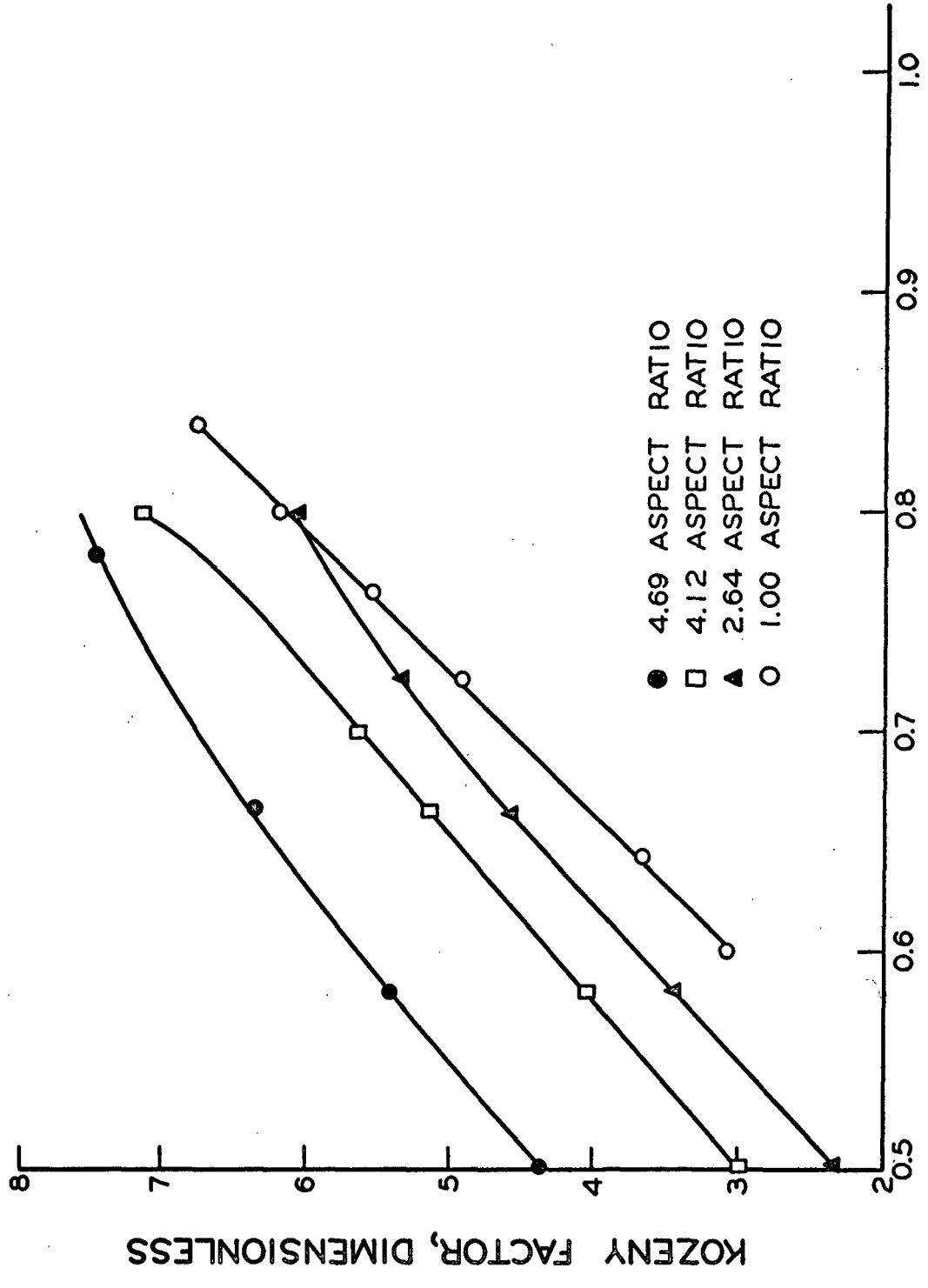

Figure 10. Kozeny Factor versus Porosity – Based on Light-Scattering Surface Area Estimate

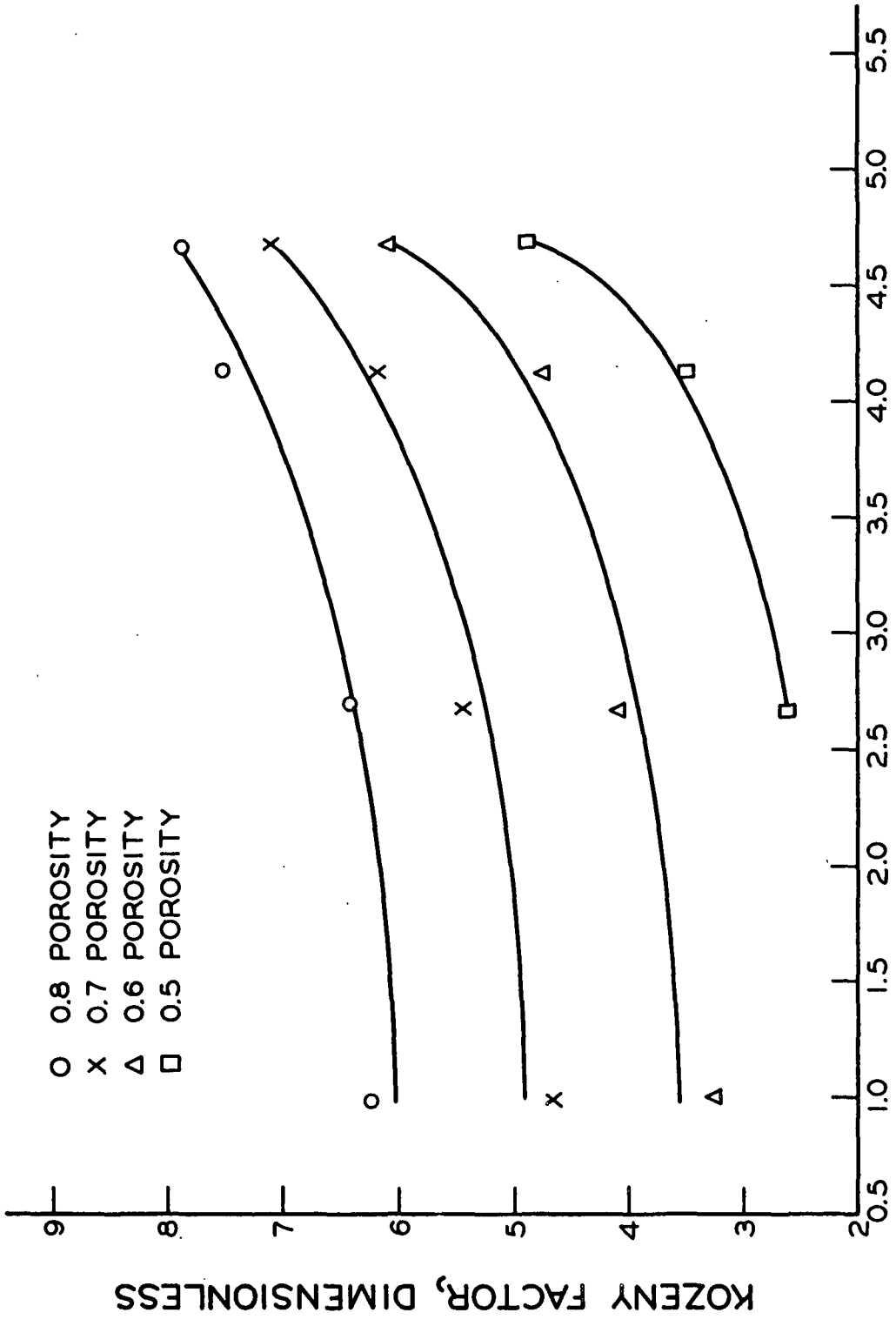

Figure 11. Kozeny Factor versus Aspect Ratio – Based on Light-Scattering Surface Area Correction

Discussion of the trends found in these figures will be reserved for a later section.

It is felt that since the light-scattering determinations have been completed on dry fiber mats and the hydrodynamic measurements carried out on fully saturated mats, some correction should be applied to the data to relate the two systems.

This was believed to be necessary primarily because of the differences in fiber deformability and flexibility encountered when comparing dry fiber mats to wet fiber mats. Simply by virtue of the fact that wet nylon fibers have appreciably lower moduli of elasticity, 1/4 to 1/3 that of dry nylon (30), it can be expected that the fibers will deform more at the points of contact for given loads, and consequently will exhibit higher values of contact area per contact point. By the same reasoning, it can be expected that the fibers will bend more easily due to their greater flexibility. This greater flexibility will result in more contact points and, concurrently, greater amounts of contact area.

In this respect, it was decided to measure the fiber mat compressibilities of mats which were fully saturated with water and again of freeze-dried mats. It is contended that the compressibility responses in both states is a function of the contact area in the beds and that the ratio of the slopes of the compressibility curves can be used to relate the light-scattering surface area to the hydrodynamic area.

Partial justification of this contention can be obtained by examining the following arguments.

A simplified form of the "compressibility equation" can be written as

$$c = M P_L^N \qquad (18)$$

where c is the fiber mat concentration, M and N are experimentally determined constants, and P_L is the compressive load applied to the fiber mat.

The compressibility constant, N, is a measure of the response of a fiber mat to the addition of a compressive load, P_L. It should therefore be intuitively expected that its value will be affected by such factors as fiber flexibility and interfiber frictional forces. Such interfiber frictional forces should certainly be altered by changes in the contact area between fibers within the porous media. Therefore, since differences in fiber deformability, such as those which exist between wet and dry fibers, will be manifested as differences in contact area within such fiber mats, it should be expected that the compressibility response, N, will similarly be affected. Consequently, measurements of N for both wet and dry fiber mats should provide some measure of the differences in contact area present in both systems.

For lack of a better method, it is now assumed that N is linearly related to the contact area present in the fiber mats and that the ratio of the dry compressibility slope, N_o, to the slopes of completely saturated fiber mats, N_w can be used to correct the response of the $s - \epsilon$ relationships of Fig. 8, which were obtained when using dry fiber mats.

The fiber beds used in the wet compression studies were formed in the same manner as the light-scattering beds. The beds were quickly frozen, as before, but were not freeze dried. Each frozen bed was then placed in the compressibility apparatus, which is described by Wilder (31), and the assembly filled with distilled water. After the mats had thawed and warmed to room temperature, the compressibility response of each was measured in the conventional manner (31).

In the dry compressibility determination, a freeze-dried fiber mat was used. There was no water present in the apparatus during the measurements. It was

noted after the mat had dried that its diameter had been significantly decreased due to the deswelling of the fibers. Initially, it was thought that this would cause problems in comparing the compressibility responses of the dry sample to the wet sample, since the dry compressibility would effectively be in a laterally unconstrained condition. However, a review of the work done by Chang (32) revealed that no more than a 5% increase in the slope of the compressibility curves could be expected upon going from a confined to an unconfined compressibility study.

Figure 12 is a representation of the data obtained from this compressibility study. The slopes of the compressibility response, N, obtained from each of the saturated fiber mats was found to be 0.12, whereas that obtained from the dry mat was 0.169. The ratio of these slopes (1.41) was used to correct the slopes of specific scattering coefficient versus porosity relationships shown in Fig. 8. The values of s, obtained from these new curves, were then used in Equation (15) to calculate S_V at each porosity. In mathematical terminology, these calculations can be represented as

$$S_V = 20.9\ [\alpha-(N_o/N_w)\ \beta\ (1-\epsilon)] \qquad (19).$$

The values of S_V, calculated according to Equation (19), were then used in Equation (5) to calculate the values of Kozeny factor over the porosity range in question. Table IV is a summary of the results so calculated. Figure 13 is a representation of the relationships obtained, between the Kozeny factor and aspect ratio, from these calculations.

At this point it should be pointed out that the trends found through the use of this procedure are, practically speaking, identical to those found when the data were calculated without the compressibility ratio correction (see Fig. 11).

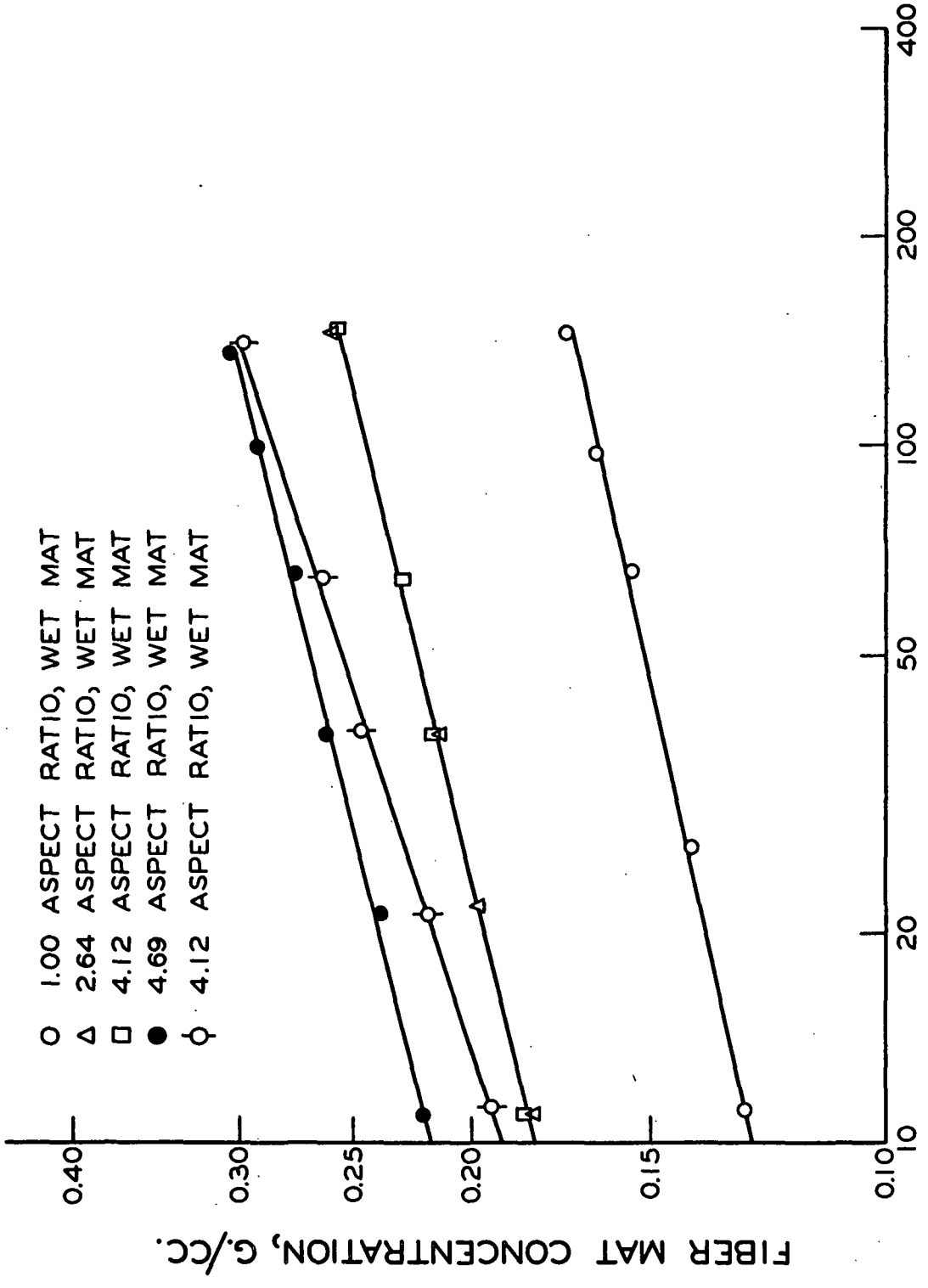

Figure 12. Fiber Mat Compressibility Determinations

TABLE IV

KOZENY FACTOR CALCULATIONS
BASED ON LIGHT-SCATTERING TECHNIQUE WITH
FIBER MAT COMPRESSIBILITY CORRECTION

Porosity	Specific Contact Area, $cm.^2/cc.$	Percent Contact Area, $cm.^2/cc.$	Specific Surface Area, $cm.^2/cc.$	Kozeny Factor
1.0 Aspect Ratio				
0.84	0	0	1535	6.78
0.82	0	0	1535	6.50
0.80	0	0	1535	6.20
0.78	0	0	1535	5.86
0.76	0	0	1535	5.57
0.72	0	0	1535	4.93
0.64	0	0	1535	3.69
0.60	0	0	1535	3.10
2.64 Aspect Ratio				
0.80	70	4.07	1650	6.39
0.76	95	5.52	1625	6.14
0.72	118	6.87	1602	5.72
0.70	130	7.56	1590	5.50
0.66	155	9.02	1565	4.98
0.62	180	10.5	1540	4.42
0.58	205	11.9	1515	3.83
0.50	255	14.8	1465	2.65
4.12 Aspect Ratio				
0.80	167	8.9	1693	7.51
0.76	196	10.5	1664	6.87
0.72	225	12.1	1635	6.36
0.70	239	12.8	1621	6.08
0.66	268	14.3	1592	5.59
0.62	298	15.9	1562	5.03
0.58	307	16.4	1533	4.46
0.54	356	19.0	1504	3.98
0.50	385	20.6	1475	3.41
4.69 Aspect Ratio				
0.78	118	5.93	1872	7.73
0.74	138	6.95	1852	7.43
0.70	160	8.05	1830	7.10
0.66	180	9.05	1810	6.72
0.62	200	10.0	1790	6.38
0.58	225	11.3	1765	5.85
0.54	245	12.3	1745	5.32
0.50	270	13.6	1720	4.81

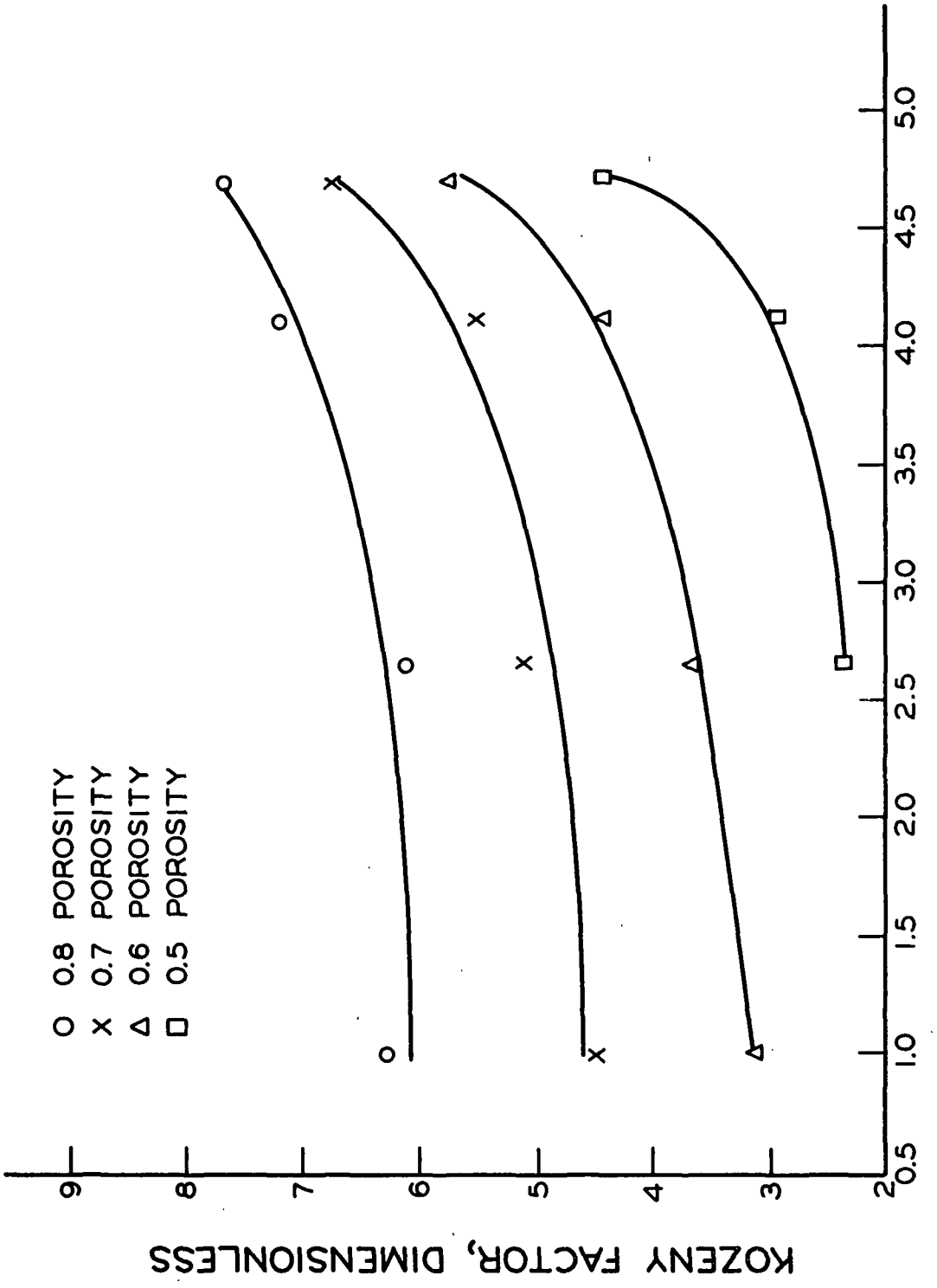

Figure 13. Kozeny Factor versus Aspect Ratio – Based on Light-Scattering Surface Area Estimate with Fiber Mat Compressibility Correction

In most cases, the correction appears only to affect the magnitude of the Kozeny factor by approximately 6-8%.

More complete discussions of these results will be presented in a later section.

DISCUSSION OF RESULTS

In the previous section, the experimental results of this study were reported and brief comments were made about the validity of each of these. In this section, more thorough discussions about the applicability of these findings are presented. Some speculation is advanced concerning the effects of higher aspect ratio fibers on the permeability properties of thick fiber mats. There are also included some comments about the applicability of using the Kozeny factor found for circular fibers when investigating the hydrodynamic properties of wood fiber mats.

SURFACE AREA DETERMINATIONS

EXPERIMENTAL SURFACE AREA ESTIMATES

At the start of work in the area of light scattering, it was expected that as the porosity of a fiber mat was increased to sufficiently high values, the scattering coefficient would reach a constant value. Unfortunately such a situation was not found in this study. Close examination of Fig. 8 revealed that the data did exhibit slight trends in this direction. However, in view of the uncertainty of these trends, it was decided to use a linear extrapolation to unit porosity in calibrating the technique. At unit porosity it was assumed that the specific surface area of the fibers within a mat was that area determined through microscopic examination of the individual fiber cross sections.

Obviously, such a procedure was not completely valid. In fact, the slight error introduced through its use may have caused some of the scatter found in Fig. 9. In determining the values represented on this curve, linear extrapolations to unit porosity were used for all fiber samples. However, the curve for the circular fibers was horizontal and consequently was not subject to the extrapolation error associated with the curves of the noncircular-cross-section fibers. As a result, the value obtained for the circular fibers is in disagreement with the

others. Whether or not its value is more correct than the values found for the other fibers is not presently ascertainable since alternate arguments can be advanced to explain the discrepancies. As was mentioned in an earlier section, Arnold (13) observed very similar trends upon changing his fiber cross-sectional shape from circular to dog-boned shaped. He then attributed this to a change in the inherent light-scattering behavior of fiber mats composed of fibers with different cross-sectional shapes. Unfortunately, he presented no theoretical basis for this speculation.

In relating the surface areas found through light-scattering measurements to the hydrodynamic surface areas in the permeability determinations, an attempt was made to use a correction factor, which utilized the compressibility response of wet and dry fiber mats. This was considered necessary because of the differences in contact areas which were expected to exist within wet and dry fiber mats. However, in view of the uncertainty associated with the scientific validity of the assumptions involved in that procedure, it is felt that, despite the small magnitude of that correction (6-8% of the Kozeny factor), further discussion of the effects of fiber shape on Kozeny factor should be based on the more technically sound estimate of surface area obtained from the light-scattering procedure without any correction. If, in the future, more fundamental reasons are uncovered, which support the fiber mat compressibility correction, the discussions, based on the uncorrected light-scattering procedure, will be easily adaptable to the corrected results since the trends found through the use of either procedure are very nearly the same. It is questionable whether the slightly lower values of Kozeny factor, which were calculated from the uncorrected procedure, are significantly different from those obtained by using the correction.

STATISTICAL ESTIMATE OF SURFACE AREA

In an attempt to check the validity of the above experimental surface area determinations, a statistically based estimate of those values has been obtained. As was mentioned earlier, Bliesner (11) tried to arrive at such an estimate by using the equation developed by Onogi and Sasaguri (12). Unfortunately, he made the faulty assumption that the number of contact points in a fiber bed was independent of fiber shape. However, upon rederiving this equation, with consideration of the effect of fiber shape, a distinctly different relationship resulted.

Onogi and Sasaguri represented the apparent density of a fibrous bed as:

$$\rho_b = c = N_x N_y N_z \int_0^\infty \lambda(\ell) \int_0^\infty \psi(A_F) A_F \ell \rho_F d(A_F) d(\ell) \qquad (20)$$

where ρ_b is the bed density, N_x, N_y, N_z are the number of fiber segments in the X, Y, and Z directions, respectively, $\lambda(\ell)$ and $\psi(A_F)$ are the frequency probabilities used to represent the distribution of ℓ and A_F, respectively, ℓ is the segment length, ρ_F is the fiber density, A_F is the fiber cross-sectional area, and c is the fiber mat concentration.

A solution can be obtained, for the idealized case in which all the segments lie in the plane of the sheet, if a frequency probability for ℓ can be assumed such that

$$\lambda(\ell) = \delta(\ell - \ell_o) \qquad (21),$$

where $\delta(\ell - \ell_o)$ is the Dirac delta function. This, in effect, assumes that all the segments in the fibrous bed have a uniform length, ℓ_o.

Making a similar assumption for the frequency probability of the cross-sectional area and reducing N_x, N_y, and N_z to

$$N_x = N_y = \pi/(2\ell_o) \qquad (22)$$

$$N_z = 1/t \tag{23}$$

where t is the fiber thickness, results in the following expression for the bed density:

$$c = (\pi^2/4)\ (A_F \rho_F / \ell_o t) \tag{24}.$$

Bliesner (11) made the error of representing N_z for all fibers as the reciprocal of the equivalent fiber diameter, instead of the fiber thickness. He defined his equivalent fiber diameter as the diameter of a fiber with the same cross-sectional area as the fiber in question.

Following through Bliesner's derivation, with this modification, results in the following expression for N_c, the number of contact points,

$$N_c = 4\ W_1^2\ t/(\pi^2 \rho_F^{\ 2} A_F^{\ 2}\ A\ L) \tag{25},$$

where W_1 is the weight of fibers in the bed, A is the cross-sectional area of the bed, and L is the bed thickness.

It can easily be shown (33) that, for a bed in which the fibers are randomly oriented in the X-Y plane, the average area of contact for each contact point, A_c, is given by

$$A_c = (\pi/2)\ w^2 \tag{26},$$

where w is the fiber width. However, closer examination of the fiber cross sections, see Fig. 4, reveals that not all of the projected fiber width will be in contact at each contact point. Therefore, Equation (26) should be multiplied by the square of the fraction of the fiber width which is in contact. Equation (26) then becomes,

$$A_c = (\pi/2)\ w^2\ F^2 \tag{27},$$

where F is the fraction of the fiber width which is in actual contact.

Measurements on the cross sections of the fibers used in this study revealed that this F factor had the following values: 0.550 for 1.00 aspect ratio fibers, 0.635 for 2.64 aspect ratio fibers, 0.810 for 4.12 aspect ratio fibers, and 0.840 for 4.69 aspect ratio fibers.

Bliesner had neglected to account for this factor in his calculations. Recalculation of his data with the following expression for total contact area, A_{Tc},

$$A_{Tc} = (2\ W_1^2\ t\ w^2\ F^2)/(\pi \rho_F^2 A_F^2\ A\ L) \tag{28}$$

and with values of F equal to 0.756 and 0.742 for his flattened nylon and orlon, respectively, resulted in the relationships of Kozeny factor versus porosity shown in Fig. 14. (It should be made clear that there are two contact points per fiber crossing and that the total contact area is the number of contact points times the area per contact point.)

Even casual observation of these results, in comparison to those previously presented by Bliesner (see Fig. 2), reveals the extreme sensitivity of the calculated values of Kozeny factor, with respect to surface area estimates. The two errors, in surface area estimates, found in Bliesner's calculations resulted in estimates of Kozeny factor which were exorbitantly high, even at porosities above 0.7. Examination of Fig. 14 reveals that at 0.7 porosity there is only a 10% increase in Kozeny factor upon going from circular fibers to 4.1:1 aspect ratio fibers, whereas the results of Fig. 2 indicate about a 70% increase for the same change. The use of such an erroneous value of k, in determining the surface area within a fiber mat composed of such high aspect ratio fibers, results in a calculated value of surface area which is approximately 20% lower than the correct value.

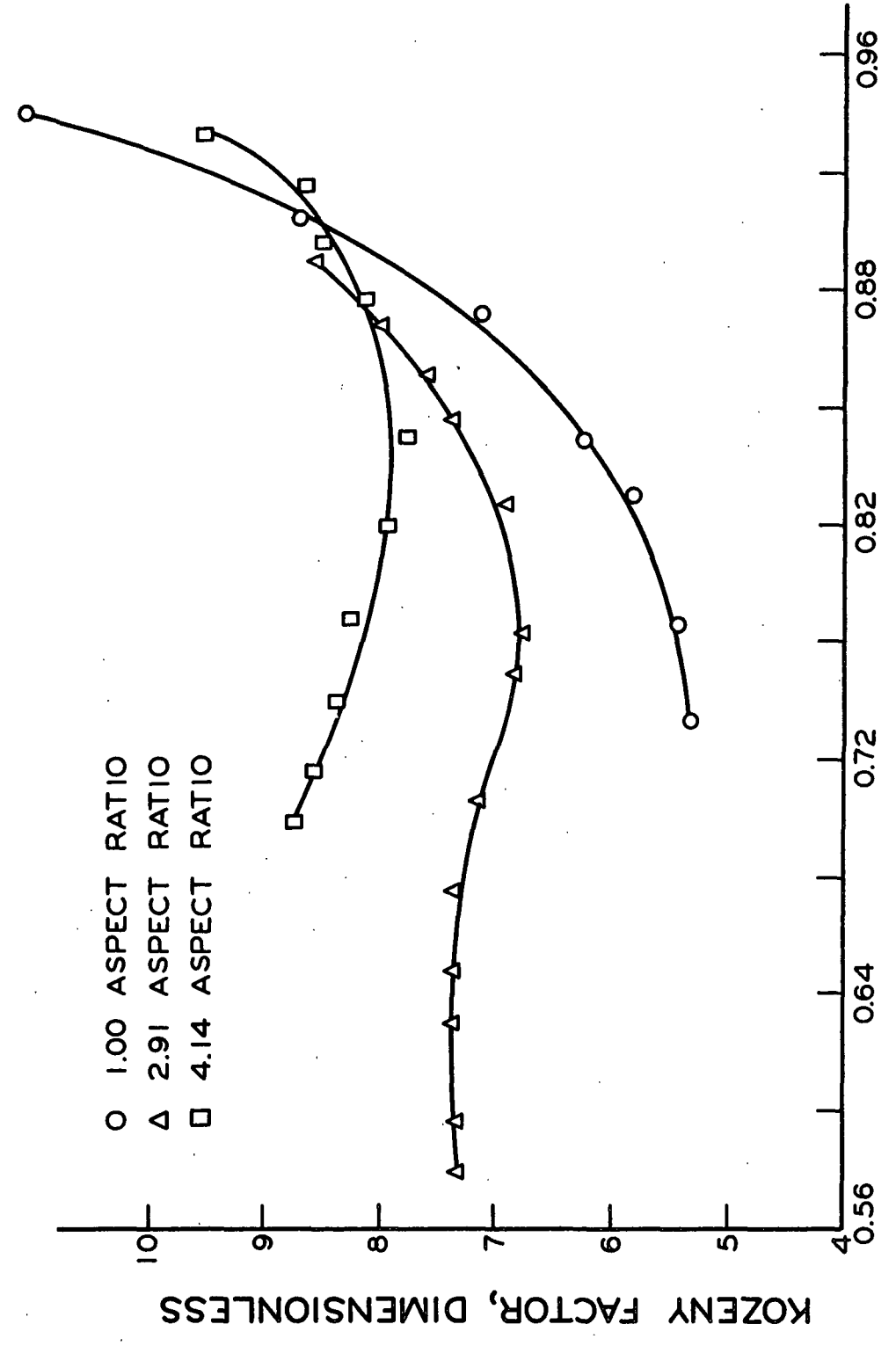

Figure 14. Bliesner's (11) Data Recalculated According to Equation (28)

Table V is a summary of the results of the data of this study calculated according to Equations (3), (5), and (28). Figure 15 is a representation of the Kozeny factors obtained through these calculations plotted as a function of porosity. Once again the problem of fiber deformability, for circular fibers, is evident at the lower porosities. In the above calculations the assumption, of constant contact area per contact point was made and, evidently, it was not a truly valid one. If a correction could have been applied to the contact area values at lower porosities, the curves would have been in better agreement with past work on circular fibers. In order for such a correction to be effected, a rather thorough knowledge of the compressibility response of fiber beds composed of each type of fiber would be required. The load per unit contact area could then be calculated if some knowledge of the deformability of each individual fiber at the various loads could be obtained. Obviously, such an undertaking would require a very large amount of time and expense and probably would not contribute significantly to resolving the main question of this study.

At this point, it should be pointed out that small errors in the contact area estimates can result in significant errors in the calculated Kozeny factor because of the inverse square dependence of $\underline{k}$ on $\underline{S_v}$ [see Equation (5)]. For example, an error of 3.0% contact area, at 0.68 porosity for circular fibers, results in a 7.3% error in the calculated value of Kozeny factor.

Figure 16 is a representation of Kozeny factor versus aspect ratio, as calculated while using the Onogi and Sasaguri relationships for correcting the contact area. One of the curves obtained from Bliesner's data at 0.8 porosity has been included for comparative purposes. The agreement of the two independent researches is remarkedly good in view of the fact that the experimental materials and equipment were entirely different.

TABLE V

KOZENY FACTOR CALCULATIONS
BASED ON THE ONOGI AND SASAGURI EQUATION

Porosity	Specific Contact Area, $cm.^2/cc.$	Percent Contact Area	Specific Surface Area, $cm.^2/cc.$	Kozeny Factor
1.00 Aspect Ratio				
0.84	00	0.0	1535	6.79
0.82	00	0.0	1535	6.49
0.80	00	0.0	1535	6.18
0.78	23	1.5	1512	6.03
0.76	25	1.6	1510	5.74
0.72	28	1.8	1507	5.12
0.68	32	2.1	1503	4.82
0.64	36	2.3	1499	3.88
0.60	40	2.6	1495	3.29
2.64 Aspect Ratio				
0.81	47	2.7	1673	6.33
0.80	50	2.9	1670	6.24
0.76	60	3.5	1660	5.88
0.72	70	4.1	1650	5.40
0.70	75	4.4	1645	5.13
0.66	85	4.9	1635	4.57
0.62	95	5.5	1625	3.98
0.58	105	6.1	1615	3.38
0.50	125	7.3	1595	2.24
4.12 Aspect Ratio				
0.80	106	5.7	1754	6.97
0.76	128	6.9	1732	6.33
0.72	148	7.9	1712	5.78
0.70	160	8.6	1700	5.53
0.66	181	9.8	1679	5.04
0.62	202	10.9	1658	4.48
0.58	222	11.9	1638	3.95
0.50	265	14.3	1595	2.92
4.69 Aspect Ratio				
0.78	138	6.9	1852	7.92
0.74	163	8.2	1827	7.66
0.70	188	9.4	1802	7.32
0.66	213	10.7	1777	6.98
0.62	239	12.0	1751	6.58
0.58	263	13.2	1727	6.13
0.54	288	14.5	1702	5.59
0.50	313	15.7	1677	5.06

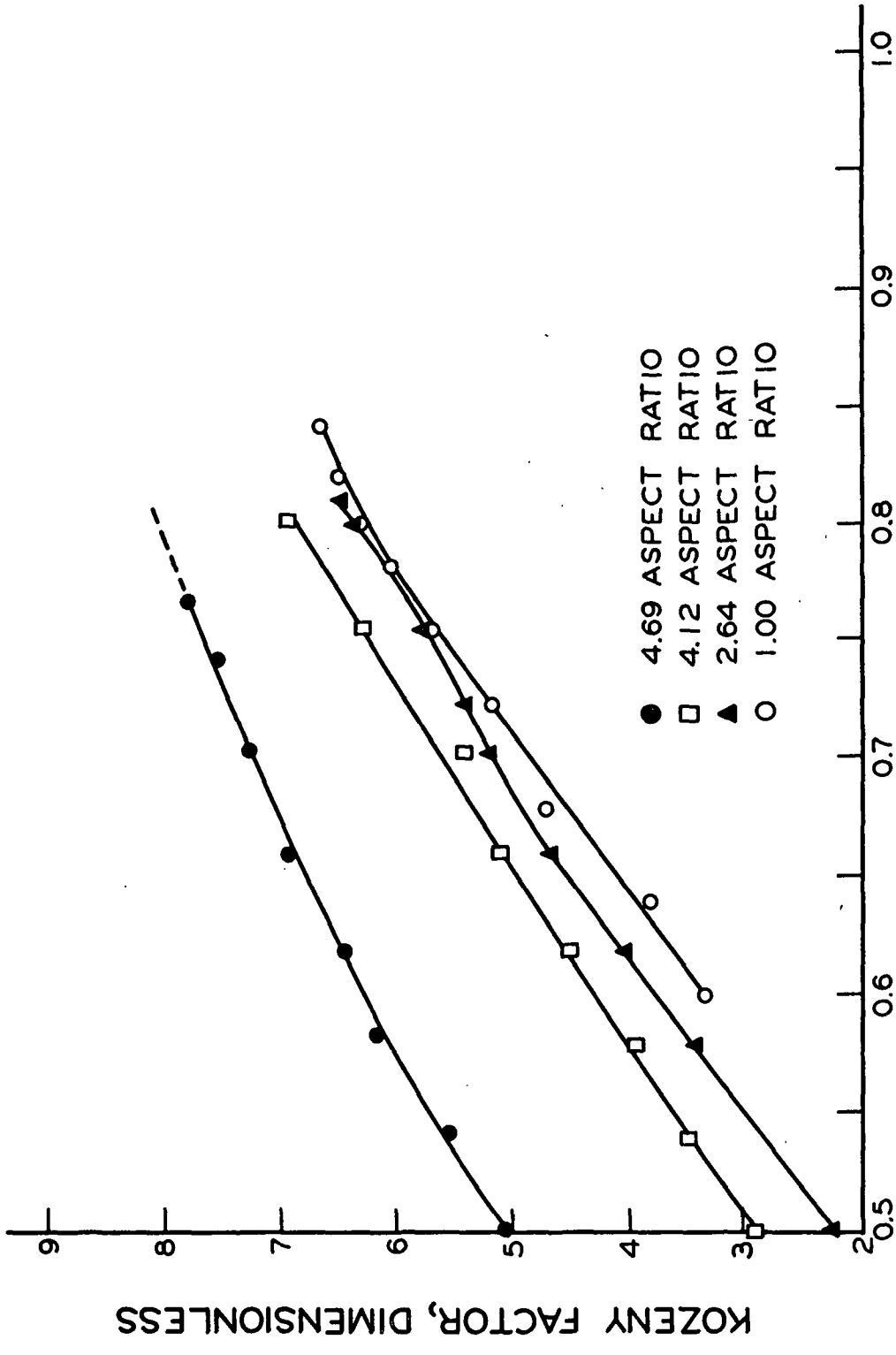

Figure 15. Kozeny Factor versus Porosity – Based on Equation of Onogi and Sasaguri (12)

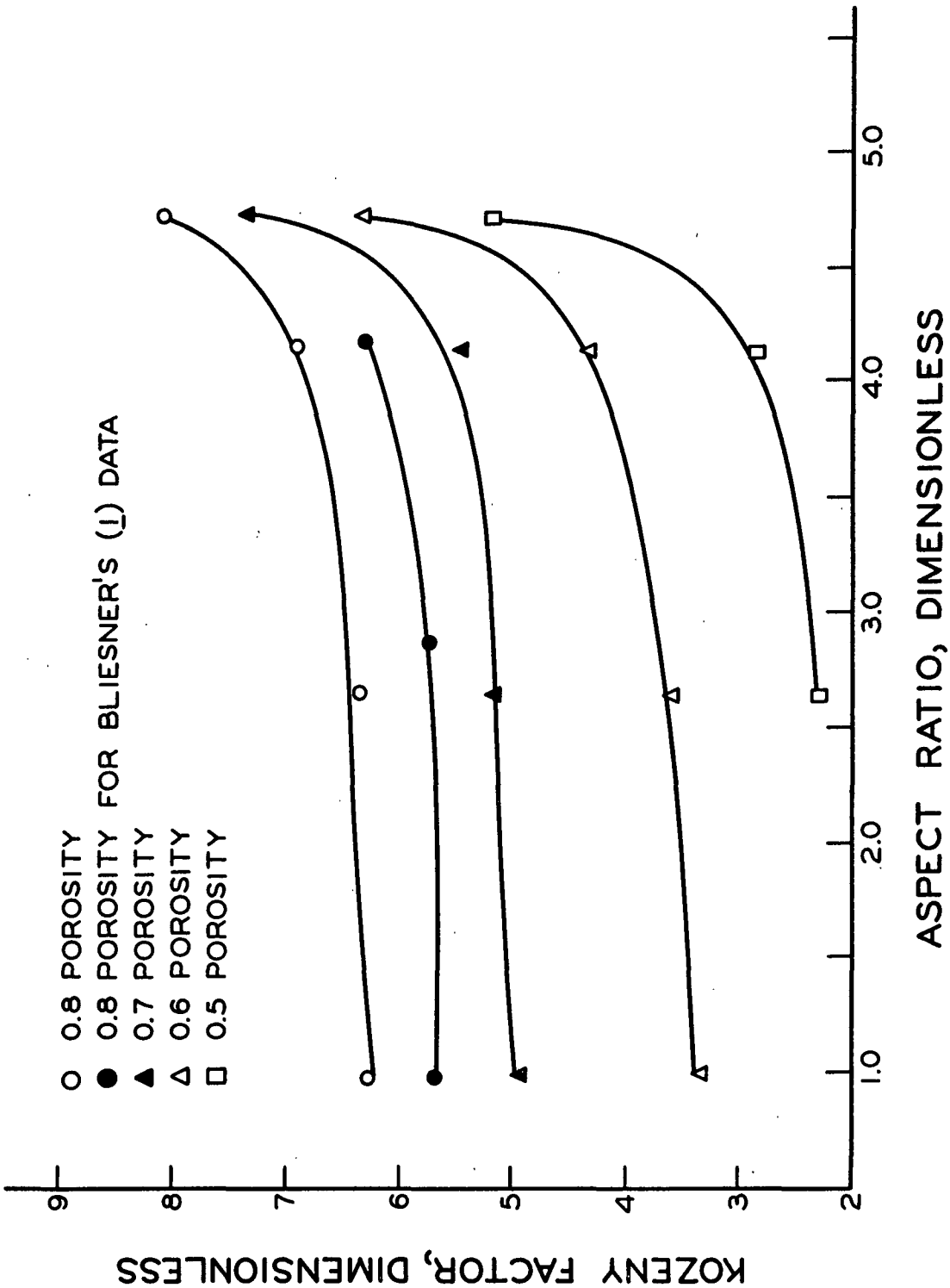

Figure 16. Kozeny Factor versus Aspect Ratio – Based on Equation of Onogi and Sasaguri (12)

The close similarity between the results depicted in Fig. 11, which are based on the light-scattering estimates of surface area, and those of Fig. 16 is quite encouraging. Such close agreement in the general trends, as well as in the relative magnitude, was not expected in view of the assumptions involved in both methods of surface area estimation. Nevertheless, this agreement does provide excellent support for the reliability of the light-scattering technique as a tool for surface area determination.

Figure 17 is a representation of the percentages contact area present at various porosities, for the data obtained experimentally, as well as that calculated according to the equation of Onogi and Sasaguri. The agreement between the two sets of data is quite good. Both methods of contact area estimation produce linear relationships with porosity, over the porosity range from 0.8 to 0.5, and in most cases, the differences in absolute magnitudes between the two estimates is less than 5% contact area. Conceivably, some of this discrepancy can be attributed to inherent structural differences within fiber mats composed of the various aspect ratio fibers. In using the Onogi and Sasaguri relationship, the tacit assumption of uniformity of fiber mat structure for all fiber mats was made. Minor departures from this assumption could quite logically explain the above discrepancies.

The fact that the trend of contact area with increasing aspect ratio at a given porosity does not increase continuously is not surprising in light of the relationship represented by Equation (25). This equation indicates that as the fiber thickness decreases, as in the case of higher aspect ratio fibers, there are fewer contact points within the fiber mat. Unless the contact area per contact point increases by a proportionate amount, or greater, there will be a decrease in overall contact area within the mats upon increasing the fiber

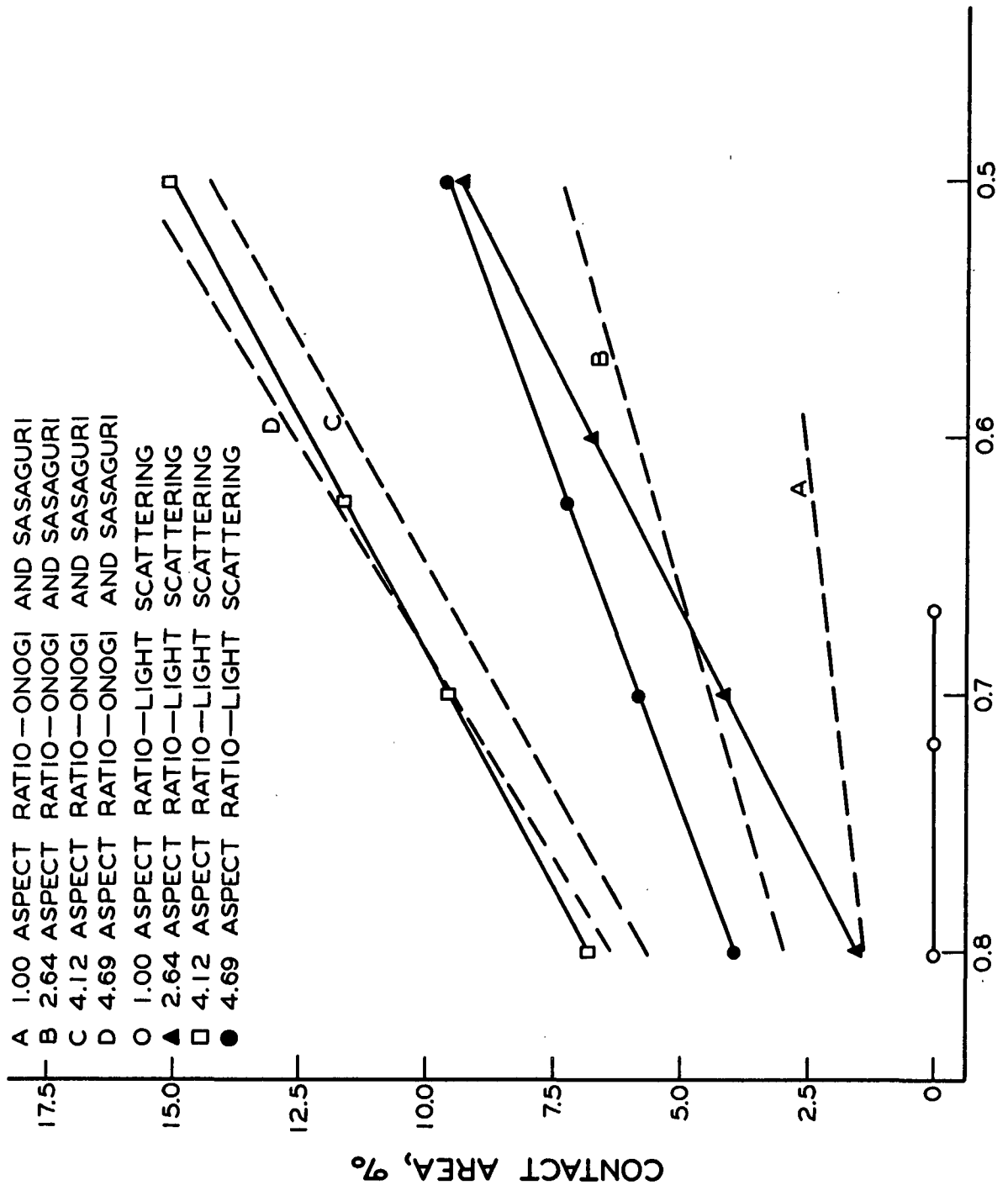

Figure 17. Percent Contact Area versus Porosity

aspect ratios. Evidently, this is what has occurred upon going from the 4.12 to the 4.69 aspect ratio fibers, when using the light-scattering method of surface area estimation. This effect was not detected when using the statistical equations, because of a possible overestimation of the $\underline{F}$ factor.

In any event, it is interesting to note that, even at porosities as low as 0.5, the amount of contact area is still quite low (less than 16%) for fiber mats composed of fibers with aspect ratios as high as 4.69:1. Original estimates, based on Bliesner's form of the Onogi and Sasaguri relationships, ranged as high as 38% contact area at 0.5 porosity for 4.14:1 aspect ratio fibers. Admittedly, contact areas as high as these might possibly occur in cellulose fiber mats because of the greater deformability of such fibers and also because of fibrillation and fiber-to-fiber bonding present in such systems. However, studies utilizing synthetic fibers, such as these, should not be as seriously handicapped by contact area problems as was originally believed.

HYDRODYNAMIC RESULTS

The permeability measurements on fiber beds composed of circular-cross-section nylon 6 fibers yielded results which were slightly dissimilar to previous work in this area. The Kozeny factor-porosity relationships above zero porosity were in agreement with past work; however, upon going to lower porosities, some discrepancies became apparent. The most probable explanation for these discrepancies is, as was mentioned earlier, that these fibers deformed more than conventionally used fibers and consequently resulted in significantly large contact areas within the fiber mats. By using the accepted Kozeny factor values, determined through air and water permeability measurements on nylon 66 fiber mats, it was possible to calculate the contact areas needed to bring the above data into agreement with past work. Figure 18 is a representation of these results. The sharp increase in

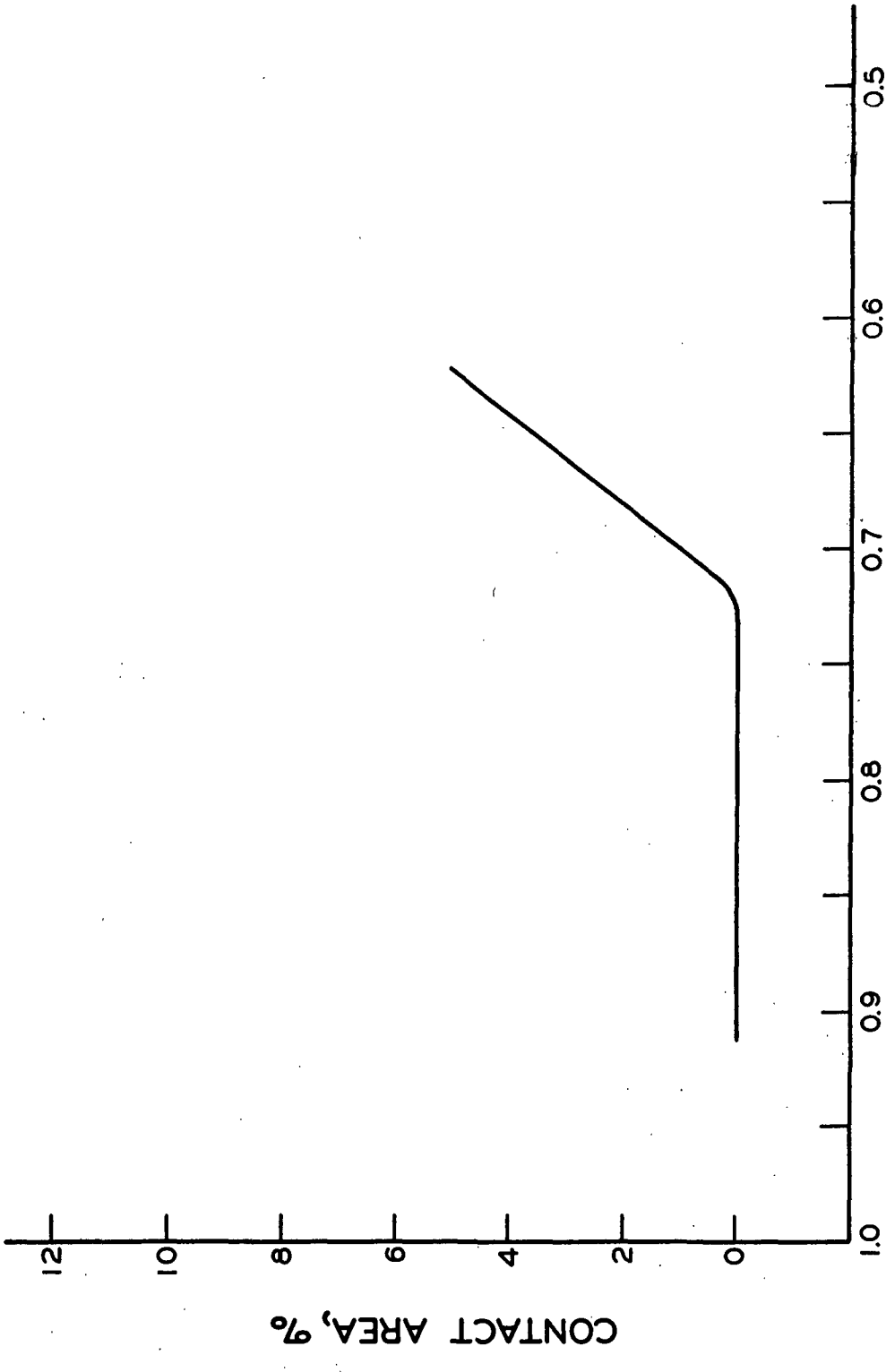

Figure 18. Percent Contact Area Needed to Bring the Circular Fiber Data of this Study into Agreement with Past Work on Circular Fibers (10)

the percentage contact area at 0.72 porosity was probably due to the collapse of the fibers when a given critical load was reached. Indications that this might occur were obtained when trying to measure the contact area of individual fiber crossings, while using the CFDA. Each crossing was microscopically examined as the load on the crossings was gradually increased. As soon as optical contact was observed, no more load was added. Within three minutes of this time, the crossing area increased from approximately 10% contact area to 90% contact area. This was most probably a result of severe creep behavior within the fibers, and could well have accounted for the above anomalous behavior. However, it should be pointed out that the relationship shown here most probably slightly over-estimates the effect of fiber deformability.

The effects of fiber cross-sectional shape on the resistance to the flow of fluids through fiber mats, as represented by the Kozeny factor-aspect ratio relationships, are in good agreement with the initial hypothesis of this study. As the fiber aspect ratio was increased, there was found a slight increase in the resistance to fluid flow through fiber mats. This effect becomes much more pronounced at aspect ratios above 3.0:1.0. However, the relationships depicted in Fig. 11 are difficult to rationalize if the concepts of pore shape factor and tortuosity are employed. Arguments incorporating these concepts generally lead to predictions of linear variations of Kozeny factor with aspect ratio. In the region of aspect ratios less than 3.0:1, such linear relationships might be made to apply to the data, but even then, only as first approximations.

Examination of a unit volume of fiber mat (see Fig. 19) may illustrate how such a nonlinear relationship could occur. By definition, the porosity of a fiber bed is given as the fraction of a volume element which is not occupied by fibers, or more concisely, the void fraction. In Fig. 19, abcd is the cross section of a

volume element of unit depth, and a'b'c'd' is the cross section of a fiber within that volume element. According to the above definition, the porosity can be represented as

$$\epsilon = 1-a'b'/ab \qquad (29).$$

Therefore, if the fiber aspect ratio is doubled by reducing b' by one half, at constant a', b will have to decrease to half of its original value if a constant porosity is to be maintained. Since b is directly proportional to the cross-sectional size of the lateral flow channels, it should be expected that the resistance to flow will be increased due to the smaller size of the channels. As the fiber thickness is further reduced, i.e., the aspect ratio increased, the flow channels will continue to decrease in size and the resistance will be further increased.

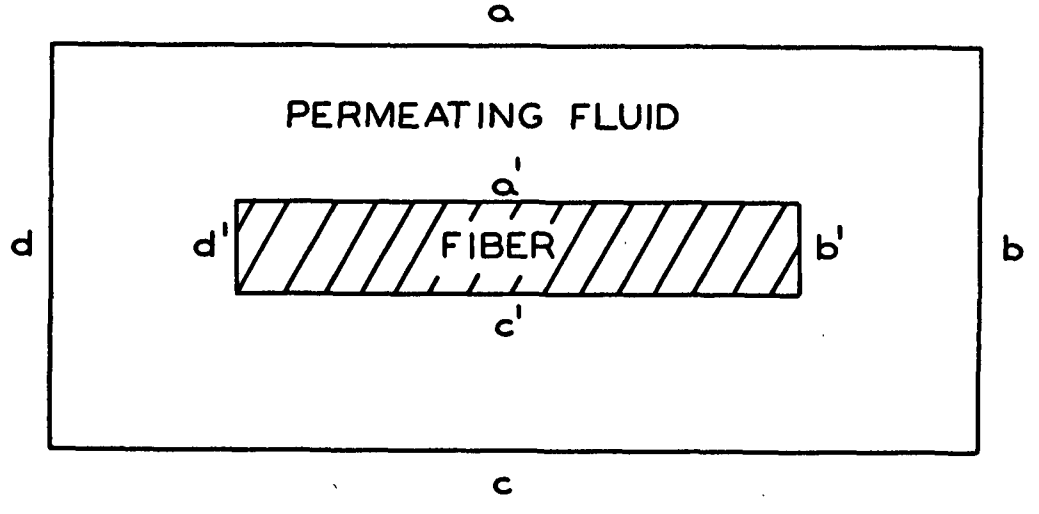

Figure 19. Volume Element of a Fiber Mat

This process is analogous to flow between two parallel flat plates where the solution of the creeping flow equations for such a system has been given by Pao (34) as

$$\Delta P = 12\mu Q L_1 / b^3 \qquad (30)$$

where Q is the volumetric flow rate per unit width of the plates, L_1 is the length of the plates, and b is the distance of separation between the plates. It can be seen from this relationship that the flow resistance is proportional to the cube of the distance of plate separation.

At this point, it might be contended that the Kozeny factor should similarly be a cubic function of the distance of plate separation. However, reference to Equation (5) reveals that the Kozeny factor is also a function of the inverse square of the specific surface. It can be shown that the specific surface is almost doubled each time the fiber aspect ratio is doubled if the fiber width is maintained constant. (The specific surface is defined as the fiber perimeter divided by the fiber cross-sectional area.) Consequently, as the fiber aspect ratio is increased, the distance of plate or fiber separation will be decreased with the resulting cubical increase in flow resistance. At the same time, the specific surface area will be increased proportionately. This could then easily result in a nonlinear, but not necessarily cubical, increase in the Kozeny factor similar to that found in the above determinations.

Conversely, if the fiber aspect ratio is increased by increasing the width of the fiber, at a constant thickness the size of the flow channels in the plane of the fiber mats will be decreased significantly. This in turn will also cause pronounced increases in flow resistance, or more specifically, Kozeny factor. Whether or not these increases would be linear is not easily ascertainable at this point. However, it is contended that since the aspect ratios of the fibers

used in this study were varied by changing the width and thickness simultaneously, some degree of nonlinearity should be present in the Kozeny factor-aspect ratio relationships.

Theoretical treatments of flow past isolated elliptical cross-section cylinders (35, 36), with the flow perpendicular to the major axis of the cylinder, do result in nonlinear relationships describing the increase in flow resistance with increasing cylinder axis ratio. Unfortunately, unlike the trends found in this study, these relationships describe functions which initially increase very rapidly and then gradually approach asymptotic values of flow resistance. However, divergences from theoretical treatments, such as these, are not surprising when consideration is given to the complexity of fiber networks and the multitude of flow interactions occurring in such systems.

In the light of these findings, an attempt was made to extend Happel's (7) free surface model to include flow through porous media composed of elliptical cross-section fibers. The mathematical details of such a procedure have been included in Appendix III. In this treatment the creeping flow equations, as well as the equation of continuity, were transformed to an elliptic, cylindrical coordinate system. The boundary conditions, of zero shear stress at the outer fluid envelope and zero velocity at the fiber surface, were then defined. Examination of any one component of the creeping flow equations then revealed the extremely involved nature of such a treatment. In order to complete such a solution, elliptic harmonic functions would have to be found which would accurately describe the pressure behavior at various points within the fluid envelopes. These functions would then be substituted for the various pressure gradients in the creeping flow equations. Attempts would subsequently be made to solve these extremely complex equations, and if a successful solution were found, it would be related to the drag force on isolated elliptical-cross-section cylinders. The

force per unit length of cylinder would then be related to the pressure gradient and subsequently to Darcy's permeability coefficient.

Unfortunately, such a rigorous solution would require an unjustifiable amount of time. Hopefully, the initial equations, presented in Appendix III, can be used as starting points for future efforts in this area.

In order to obtain a uniform mathematical relationship, describing the dependence of Kozeny factor on both porosity and aspect ratio, curves of Fig. 11 were redrawn as shown in Fig. 20. In this case, the points for the 1.0 aspect ratio fibers were taken from previous investigations (10) which were completed while using nylon 66 or glass fibers. This was considered necessary in order to avoid the probable inclusion of misleading effects which resulted because of the greater deformability of the fibers used in this study. Admittedly, fiber deformability may have caused some undetected problems when investigating the higher aspect ratio fibers. However, examination of the compressibility results, which were presented in Fig. 18, revealed that the loading pressures required to reach a given porosity with the higher aspect ratio fibers were considerably lower than those required for the circular fiber mats. As a result, it is not expected that fiber deformability was a significant factor at porosities above 0.6 for the higher aspect ratio fibers.

The data obtained at 0.5 porosity has not been included in this figure because of possible fiber deformability effects, and because it was necessary to extrapolate the $\underline{s}$-ϵ relationships from 0.6 to 0.5 porosity in order to obtain the surface area values needed to calculate that data.

By using these smoothed relationships, it is possible to express the dependence of Kozeny factor on porosity and aspect ratio as

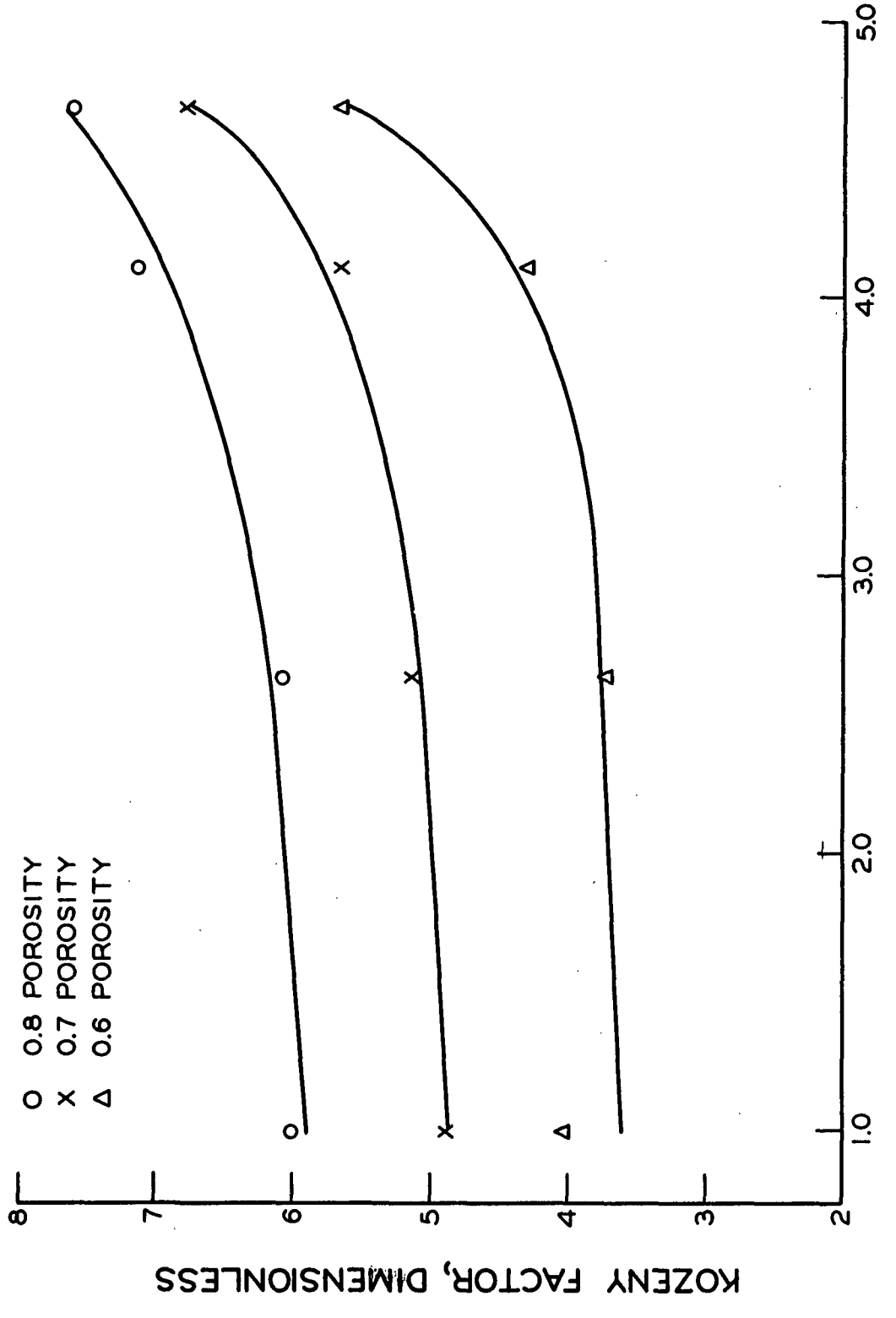

Figure 20. Smoothed Relationships of Kozeny Factor versus Aspect Ratio

$$k = -12.29 + 42.9\,\epsilon - 24.5\epsilon^2 + (1.90 - 10.9\epsilon + 9.6\epsilon^2)(AR) - (0.18 - 1.61\epsilon + 1.45\epsilon^2)(AR)^2 \quad (31)$$

over the porosity range from 0.6 to 0.8, and for aspect ratios up as high as 4.69:1.

This equation should be of general applicability, over the range indicated, and should not depend too severely on the experimental limitations of this investigation. If in the future, fundamentally sound reasons can be advanced, which prove that the fiber mat compressibility correction, as presented in an earlier section of this thesis, is a valid correction, this equation will still be generally applicable provided the values of Kozeny factors are increased by approximately 6%.

APPLICABILITY OF THESE RESULTS TO OTHER FIBROUS SYSTEMS

On occasion, there have been doubts expressed about the validity of using the values of Kozeny factors found for circular fibers when calculating the hydrodynamic properties of wood pulp fiber mats. In light of the results of this study, such procedures should not be in serious error as long as the fiber aspect ratios remain less than approximately 3:1. At higher ratios, there is a very pronounced effect on the value of Kozeny factor, and any use of the values obtained from circular fiber data should be avoided. Fortunately, examination of photomicrographs of wood fiber cross sections, which had been freeze dried to prevent the collapse of the fiber lumen (37), revealed that most wood fibers have aspect ratios less than 3.5:1, until after drying. However, upon drying, the fiber lumen collapse and some of the fiber aspect ratios increase to values as high as 10:1, although most of the fibers still have aspect ratios less than 4:1. Consequently, studies involving the use of dried wood fibers should have provisions for accounting for the effects of these higher aspect ratios. If an appropriate estimate of the distribution of fiber cross-sectional aspect ratios can be surmised

for the fibers comprising the porous medium, the proper Kozeny factor to be used in Equation (5) can be estimated by using weighted averages of the Kozeny factors, which were calculated for each aspect ratio, from Equation (31). For example, if the fiber mat being studied contains 20% of 5:1 aspect ratio fibers and 80% circular fibers, the Kozeny factor can be calculated from Equation (31) for 1.0 and 5.0 aspect ratios and the two averaged together, through a weighted averaging procedure where the value obtained for circular fibers is weighted 4 times that of the 5:1 aspect ratio fibers.

Such an estimate of Kozeny factor could then be used to calculate $\underline{S}_{\underline{v}}$ and $\underline{v}$, the fiber specific volume, from plots of the so-called rectified data (10). This would give the investigator a reasonable estimate of the uncontacted surface area present in such fiber mats. This value could then be used, in conjunction with other surface area estimates, to arrive at the bonded or contact area present in fiber mats at those conditions. Attempts could subsequently be made to relate this bonded area to the mechanical and structural properties of that fiber system. However, it should be pointed out that, as the compacting pressure on a fiber mat is increased, either through static loading or through the frictional drag resistance of the permeating fluid, the fibers will deswell at the contact points and this will cause an effective reduction in fiber specific volume, as well as fiber specific surface area. Such a simultaneous change in $\underline{v}$ and $\underline{S}_{\underline{v}}$ could possibly cause some confusion in the final interpretation of the rectified data.

CONCLUSIONS

The results of this investigation revealed that the Kozeny factor is related to the fiber cross-sectional aspect ratio in a nonlinear manner. Quadratic expressions have been found to represent the relationships. These relationships became more and more dependent upon fiber aspect ratio as the porosity was decreased. In the range of aspect ratios up to 3:1 there is very little effect of fiber cross-sectional shape on fluid flow resistance. However, beyond aspect ratios of 3:1, the Kozeny factor was found to increase significantly. Whether or not this factor continues to increase at higher aspect ratios has not been determined.

The validity of the light-scattering technique for estimating surface areas within thick fiber mats has been checked and found to be quite good. A linear relationship between the specific scattering coefficient and the microscopically determined surface area of nylon 6 fiber was established at unit porosity.

Reasonably good agreement was found between the surface areas estimated through use of the light-scattering procedure and those calculated by means of a modified form of the statistically derived equations of Onogi and Sasaguri. Both procedures indicate that contact areas above 20% of the total area are not very likely, even for the higher aspect ratio fibers, at porosities as low as 0.5.

SUGGESTIONS FOR FUTURE WORK

It has been frequently suggested that the Kozeny factor for pulp fiber mats be determined experimentally. However, due to the complex nature of such systems, perhaps systematic studies of the effects of the various papermaking processes on the cross-sectional shape of wood fibers would be more adventageous. If precise estimates of the cross-sectional shapes of these fibers were available, the Kozeny factor could be calculated from studies similar to the present one.

As an extension of the work just completed, it may be advantageous to increase the range of fiber aspect ratios studied to 15:1 or higher. This would test the hypothesis that the Kozeny factor continues to rise sharply at aspect ratios greater than 5:1. It might also be of value to repeat the work of this study while using noncircular cross-section glass fibers. This would possibly eliminate errors associated with the various estimates of surface area within the fiber mats.

In reference to surface area determinations, the range of applicability of the light-scattering technique could be extended considerably by designing a system capable of supporting higher compressive loads. The applicability of the technique could also be increased by designing a sample holder which would permit optical measurements, over a wide range of porosities, on fully saturated fiber mats.

In terms of theoretical approaches to flow through porous media, it would be of considerable value to complete the solution of Happel's free surface model for elliptical cross-section fibers. As was mentioned earlier, the initial equations needed for such a project have been included in Appendix III.

A more thorough investigation of the compressibility behavior of fiber mats composed of fibers of various cross sections should certainly be of considerable interest.

ACKNOWLEDGMENTS

It is virtually impossible to acknowledge all the people who assisted materially in the successful completion of this study. To these people the author extends his sincere appreciation.

In particular, the author would like to acknowledge the help and encouragement of the late Dr. W. L. Ingmanson, chairman of his thesis advisory committee, and to Mr. H. Meyer and the late Dr. G. R. Sears, the members of his advisory committee.

The assistance of the following people is also gratefully acknowledged:

Messrs. B. D. Andrews and O. C. Kuehl for their assistance in the design, construction, and operation of the permeability apparatus.

Dr. J. A. Van den Akker and Mr. L. Dearth for their assistance in planning and executing the various light-scattering experiments.

Mr. J. Hankey for preparing the photomicrographs of the synthetic fiber cross sections.

Mr. M. Filz for his aid in the construction of several pieces of equipment used in this study.

The American Enka Corporation, of Enka, North Carolina, for supplying the required fiber samples, gratis.

Special acknowledgment should be given to my wife, Mary Lou, for her encouragement and especially for her typing of the original manuscript of this dissertation.

NOMENCLATURE

a'' = minor axis ellipse

A = cross-sectional area of a test specimen perpendicular to the direction of macroscopic flow, $cm.^2$

A_c = average projected area of contact between fibers in a bed, $cm.^2$

A_{rc} = total contact area within a fiber bed, $cm.^2$

A_F = cross-sectional area of a fiber, $cm.^2$

AR = aspect ratio, dimensionless

b = distance between parallel plates, cm.

b'' = major axis of ellipse

c = fiber mat concentration, g./cc.

c'' = focal point of ellipse

cb = abbreviation for chlorobenzene

d = fiber diameter, cm.

exp = base of Naperian logarithms

F = fraction of the projected area that is in actual contact, dimensionless

F_d = drag force

K = permeability coefficient, $cm.^2$

K_o = proportionality factor in Darcy's equation

k = Kozeny factor, dimensionless

L = thickness of a test specimen, cm.

L_1 = length of parallel plates, cm.

ℓ = free segment length between contact points in a fibrous bed, cm.

ℓ_o = characteristic segment length, cm.

N_c = total number of contact points in a fibrous bed, dimensionless

N_o = slope of the compressibility relationship, obtained when using dry fiber mats

N_w = slope of the compressibility relationship, obtained when using fully saturated fiber mats

$N_x N_y N_z$ = probability distribution for the number of fiber segments in the X, Y, and Z directions, respectively, dimensionless

M = mathematical factor used in compressibility equations

ΔP = overall pressure drop across a test specimen, dynes/cm.^{2}

P_L = compressive load, cm. H_2O

Q = mass flow rate per unit width, g./cm.^{2}

R_o = absolute reflectance of a fibrous sheet backed by a black body

R_o' = corrected value of R_o

S_v = surface area of a bed per unit volume of the particles which compose the bed, cm.^{2}/cc.

s = specific scattering coefficient, cm.^{2}/g.

sW = scattering power

T = absolute optical transmittance of a fibrous bed

T' = corrected value of T

t = thickness of individual fibers, cm.

U = superficial linear approach velocity in permeability system, cm./sec.

v = hydrodynamic specific volume of the fibers in a bed, cc./g.

v_x, v_y = x and y components of fluid velocity, respectively, cm./sec.

W = basis weight, g./cm.^{2}

W_1 = weight of fiber in a bed, g.

w = projected width of a fiber, cm.

x = x coordinate

y = y coordinate

z = z coordinate

α, β = intercept and slope of light-scattering versus porosity relationships, respectively

γ_{R_o} = ratio of true reflectance to reflectance value obtained when standard was in sample holder

γ_T = ratio of true transmittance to transmittance value obtained when standard was in sample holder

$\delta(\ )$ = Dirac delta function

ϵ = porosity or fractional void volume of a porous medium, dimensionless

μ = fluid viscosity, g./(cm. sec.)

$\gamma(\underline{\ell})$ = frequency probability used to represent the distribution of $\underline{\ell}$, dimensionless

γ = contour of ellipse

$\rho_{\underline{b}}$ = apparent density of fibrous bed, g./cc.

$\rho_{\underline{F}}$ = fiber density, g./cc.

η = angular elliptical coordinate

$\psi(\underline{A_F})$ = frequency probability used to represent the distribution of $\underline{A_F}$, dimensionless

LITERATURE CITED

1. Lamb, H. Hydrodynamics. 6th ed. London, Cambridge University Press, 1932. 738 p.

2. Mokadain, R. G., Trans. Am. Soc. Mech. Eng. 83E:208(1961).

3. Whitaker, S., Chem. Eng. Sci. 21:291-300(March, 1966).

4. Muskat, M. The flow of homogeneous fluids through porous media. New York, McGraw-Hill, 1937. 763 p.

5. Kozeny, J., Akad. Wiss. Wien., Math. – naturw. Kl. 36(abt IIa):271-306(1927).

6. Carman, P. C. Flow of gases through porous media. New York, Academic Press, 1956. 182 p.

7. Happel, J., A.I.Ch.E. Journal 5, no. 2:174-7(1959).

8. Davis, C. N., Proc. Inst. Mech. Engrs. (London) Bl:185(1952).

9. Carroll, C. W. Unpublished work. Appleton, Wisconsin, The Institute of Paper Chemistry, 1965.

10. Ingmanson, W. L., and Andrews, B. D., Tappi 46, no. 3:150-5(1963).

11. Bliesner, W. C. Tappi 47, no. 7:392-400(1964).

12. Onogi, S., and Sasaguri, K., Tappi 44, no. 12:874-80(1961).

13. Arnold, E. W., Tappi 46, no. 4:250-6(1963).

14. Kubelka, P., and Munk, F., Z. tech. Physik 12, no. 11a:593-601(1931).

15. Van den Akker, J. A., Tappi 32, no. 11:498(1949).

16. Davis, M. N., Paper Trade J. 111, no. 14:40-4(1940).

17. Parsons, S. R., Tech. Assoc. Papers 25:360(1942).

18. Ratliff, F. Y., Tappi 32, no. 8:357(1949).

19. Leech, H. J., Tappi 37, no. 8:343(1954).

20. Haselton, W. R., Tappi 38, no. 12:716-23(1955).

21. Ingmanson, W. L., and Thode, E. F., Tappi 42, no. 1:83(1959).

22. Swanson, J. W., and Steber, A. J., Tappi 42, no. 12:986(1959).

23. Hardacker, K. W., Tappi 45, no. 3:237(1962).

24. Ingmanson, W. L., Tappi 35, no. 10:439(1952).

25. Hardacker, K., and Van den Akker, J. A. Unpublished work. Appleton, Wisconsin, The Institute of Paper Chemistry, 1965.

26. Chipalkatti, H. R., Giles, C. H., and Vallance, D. G. M., J. Chem. Soc. 1954: 4375-90.

27. Gibson, K. S. Spectrophotometry. National Bureau of Standards Circ. No. 484, Sept., 1949.

28. Dearth, L. Unpublished work. Appleton, Wisconsin, The Institute of Paper Chemistry, 1965.

29. Van den Akker, J. A. Theory of the optical properties of pulp. TAPPI MONOGRAPH Series No. 27:17-39(1963).

30. Myer, W. T., Jr. The rheology of synthetic fiber suspensions. Doctor's Dissertation. Appleton, Wisconsin, The Institute of Paper Chemistry, 1962. 189 p.

31. Wilder, H. D., Tappi 43, no. 8:715-20(1960).

32. Chang, N. L. Unpublished work, Appleton, Wisconsin, The Institute of Paper Chemistry, 1965.

33. Van den Akker, J. A. In Bolam's The formation and structure of paper. Vol. I. p. 205-41, London, England, Tech. Sect. British Paper & Board Makers' Assoc., 1962.

34. Pao, R. H. F. Fluid mechanics. New York, Wiley and Sons, 1961.

35. Bairstow, L., Cave, B. M., and Lang, E. D., Royal Soc. of London Phil. Trans., 123:383-432(1923).

36. Lamb, H. Hydrodynamics. 6th. ed. New York, Dover, 1945.

37. Farrar, N. O. Unpublished work. Appleton, Wisconsin, The Institute of Paper Chemistry, 1964.

C

APPENDIX I

COMPUTER CALCULATIONS

```
C          THIS PROGRAM IS DESIGNED TO CALCULATE THE KOZENY FACTOR FOR
C     THE FOUR POINT ONE TO ONE FIBER.  IN ORDER TO ADAPT IT TO
C     OTHER FIBERS, THE STATEMENTS DEFINING SV2 AND SPV MUST BE CHANGED

C     T IS THE TEMPERATURE OF THE PERMEATING FLUID
C     EL IS THE FIBER MAT THICKNESS
C     WGT IS THE WEIGHT OF THE FIBER MAT
C     SLOPE IS THE SLOPE OF THE FLOW RATE VERSUS PRESSURE DROP DATA
C     VISC IS THE FLUID VISCOSITY
C     CONC IS THE FIBER MAT CONCENTRATION
C     POR IS THE FIBER MAT POROSITY
C     SPV IS THE SPECIFIC VOLUME OF THE FIBER
C     PERC IS THE PERMEABILITY COEFFICIENT
C     SV2K IS THE SQUARE OF THE SPECIFIC SURFACE TIMES KOZENY FACTOR
C     FK IS THE KOZENY FACTOR
C     SV IS THE SPECIFIC SURFACE
C     SV2=100000.*(13.2+7.14*POR+3.86*POR**2) FOR RX 1167 (LIGHT SCATT.)
C     SV2=100000.*(21.+7.8*POR+2.9*POR**2) FOR RX 1164 (LIGHT SCATT.)
C     SPV=0.9007 FOR ALL OTHER FIBER SAMPLES


      DIMENSION T(20), EL(20), SLOPE(20)
5     READ, N, WGT
      DO 1 I=1,N
      1 READ, T(I)
      DO 2 I=1,N
      2 READ, EL(I)
      DO 3 I=1,N
      3 READ, SLOPE(I)
      DO 4 I=1,N
      SPV=0.873
      VISC=1./(2.1482*((T(I)-8.435)+SQRTF(8078.4+(T(I)-8.435)**2))-120.)
      CSLOP=102.4*SLOPE(I)
      CONC=.008673*WGT/EL(I)
      POR=1.-SPV*CONC
      PERC=2.54*(VISC*EL(I))/CSLOP
      SV2K=POR**3/(((1.-POR)**2)*PERC)
      SV2=100000.*(12.4+8.1*POR+5.32*POR**2)
      FK=SV2K/SV2
      SV=SV2**0.5
      PRINT,POR,PERC,SV,FK
4     CONTINUE
      PAUSE
      GO TO 5
      END
```

APPENDIX II

DYE ADSORPTION

As was mentioned in the text of this report, an attempt was made to use a dye adsorption technique of measuring surface area within fiber mats. Preliminary work in the area was concerned with adsorbing a layer of dye onto the fiber surfaces, while using aqueous systems. Dye concentrations ranging from 2×10^{-5} molar to 7.5×10^{-4} molar were used. The consistency of the fiber suspensions varied from 0.5% up to 3% and the dye bath temperature was maintained between 20 and 30°C.

The dyes investigated in this study, along with their Color Index numbers, are as follows:

"Pontacyl" Fast Black N2B	C.I. 27075
Du Pont Milling Yellow 5G	C.I. 18950
Du Pont Milling Red 3B	C.I. 24810
Du Pont "Napthanil" AS Fast Red Salt RCN	C.I. 37505
"Pontachrome" Brown Hn	C.I. 13250
"Pontachrome" Black TA	C.I. 14645
"Ponolith" Fast Black P Liquid	
Chromacyl Black W	C.I. 15711
Capracyl Red B	C.I. Acid Red 182
Capracyl Brown RD	C.I. Acid Brown 29
"Monastral" Fast Green GFNP Paste	

When it was found that the dyes penetrated into the swollen fibers, an attempt was made to use nonswelling solvents from which the fibers could be dyed. The solvents used, as well as the dyes tried in each, are as follows:

Acetone	Du Pont Milling Red 3B-C.I. 24810
Butyl stearate	Celanthrene Fast Pink 3B Picric acid
Cyclohexane	p-Nitrophenol Du Pont Oil Red – C.I. 26105 Celanthrene Fast Pink 3B
Dioctyl phthalate	Celanthrene Fast Blue 2G C.I. 62500 Celanthrene Fast Pink 3B C.I. 62015
Magic Bros. Inc. Oil 470	Acetamide Yellow CG C.I. 11855 Acetamide diazo Black 3b C.I. 11255 Picric acid

Methanol	Du Pont Milling Red 3b C.I. 24810
Mineral Salt Oil	Calco Oil Red N-1700
	Celanthrene Fast Pink 3B
Mobil Certrex 39	Celanthrene Fast Pink 3B
Phenyl ether	Sudan IV C.I. 26105

Unfortunately, none of the above combinations provided reasonable values of the surface area values needed. Consequently, further investigations in this area were stopped. However, it should be made clear that, in principle, this technique should be suitable for determining surface areas and despite the failures of this investigation, the procedure should not be discarded as inapplicable to other systems.

APPENDIX III

EXTENSION OF HAPPEL'S "FREE SURFACE MODEL"

As an extension to Happel's (7) free surface model approach to flow through porous media composed of circular cross-section fibers, a free surface model has been described for elliptical cross-section fibers. Figure 21 is a representation for such a system. In this representation, $\underline{a}''_o$ and $\underline{b}''_o$ are the minor and major axes, respectively, of the fiber cross section, and $\underline{c}''$ is the focal point of the ellipse. A confocal elliptical fluid envelope is visualized around the fiber such that the fiber bed porosity can be defined as

$$\epsilon = 1 - a''_o b''_o / a''_1 b''_1 \tag{32}$$

where $\underline{a}''_1$ and $\underline{b}''_1$ are the minor and major axes, respectively, of the fluid envelope. However, since

$$a'' = c'' \cosh\lambda \tag{33}$$

and

$$b'' = c'' \sinh\lambda \tag{34}$$

where λ is defined as the contour of the ellipse, the porosity can be represented as

$$\epsilon = 1 - (\sinh 2\lambda_o)/(\sinh 2\lambda_1) \tag{35}$$

where λ_o and λ_1 refer to the fiber and fluid envelope surfaces, respectively.

Expressed in rectangular coordinates, the creeping motion equations for the case of two-dimensional flow are given by

$$\partial P/\partial x = \mu(\partial^2 v_x/\partial x^2 + \partial^2 v_x/\partial y^2) \tag{36}$$

$$\partial P/\partial y = \mu(\partial^2 v_y/\partial x^2 + \partial^2 v_y/\partial y^2) \tag{37}$$

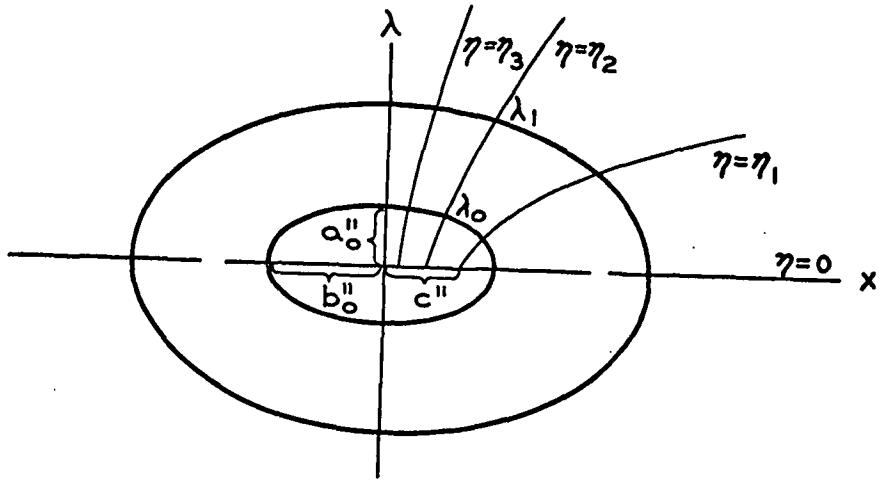

Figure 21. Elliptical Cross-Section "Free Surface Model"

whereas the continuity equation is

$$\partial v_x/x + \partial v_y/\partial y = 0 \qquad (38).$$

However, since definitions of the boundary conditions of the elliptical components of the system are virtually impossible, the above equations were converted to an elliptic cylindrical coordinate system. The transformations were effected, in the usual manner, through the use of the tranformation equations

$$x = c'' \cosh \lambda \cos \eta \qquad (39)$$

$$y = c'' \sinh \lambda \sin \eta \qquad (40)$$

where η is the angular component of this coordinate system. The various transformed equations of motion are:

$$\partial P/\partial\lambda = c'\mu \{[(\sin 2\eta \sinh 2\lambda - 1/4 \sin^2 2\eta + 1/2 \sinh^2 2\lambda) D^{-3/2} - 1/2 (\sinh^2 2\lambda) D^{-1/2}] v_\lambda + [(1/2 \sinh^2 2\lambda - \sin 2\eta \sinh 2\lambda - 1/4 \sin^2 2\eta) D^{-3/2} + D^{-1/2} \sinh^2 2\lambda] v_\eta - (\sin 2\eta + 1/2 \sinh 2\lambda) D^{-1/2} \partial v_\lambda/\partial\lambda + (\sin 2\eta - 1/2 \sinh^2 2\lambda) D^{-1/2} \partial v_\eta/\partial\eta + 1/2 \sin 2\eta D^{-1/2} (\partial v_\lambda/\partial\eta + \partial v_\eta/\partial\eta) + (\partial^2 v_\lambda/\partial\lambda^2 + \partial^2 v_\eta/\partial\eta^2) D^{+1/2}\} \quad (41)$$

$$\partial P/\partial\eta = c'\mu \{[(\sinh 2\lambda \sin 2\eta + 1/2 \sin^2 2\eta - 1/4 \sinh^2 2\lambda) D^{-3/2} - (1/2 \sin^2 2\eta) D^{-1/2}] v\lambda + [(\sinh 2\lambda \sin 2\eta + 1/2 \sin^2 2\eta - 1/4 \sinh^2 2\lambda) D^{-3/2} - (1/2 \sin^2 2\eta) D^{-1/2}] v_\eta + (\sinh 2\lambda - 1/2 \sin 2\eta) D^{-1/2} \partial v_\lambda/\partial\eta - (\sinh 2\lambda + 1/2 \sin 2\eta) D^{-1/2} \partial v_\eta/\partial\eta + 1/2 D^{-1/2} \sinh 2\lambda (\partial v_\lambda/\partial\lambda + \partial v_\eta/\partial\lambda) + (\partial^2 v\lambda/\partial\eta^2 + \partial^2 v_\eta/\partial\eta^2) D^{+1/2}\}. \quad (42)$$

whereas the equation of continuity is

$$c'\rho (1/2 \sinh 2\lambda)(D^{-1/2} v_\lambda) + 1/2 \sin 2\lambda (D^{-1/2} v_\eta) + (\partial v_\lambda/\partial\lambda + \partial v_\eta/\partial\eta) D^{-1/2} = 0 \quad (43)$$

where

$$D = \sinh^2\lambda + \sin^2\eta \quad (44).$$

The boundary conditions, of zero shear stress at the surface of the fluid envelope, i.e. at

$$\lambda_1 = 1/2 \sinh^{-1} [(\sinh 2\lambda_o)/(1 - \epsilon)] \quad (45)$$

and zero velocity at the fiber surface, i.e., at

$$\lambda_o - \sinh^{-1} (b'_o/c') \quad (46)$$

are then employed in the solution of the above equations.

Unfortunately, due to time limitations, further work on the solution of these relationships has been abandoned. Hopefully, these equations will serve as convenient starting points for future work in this area.

APPENDIX IV

EXPERIMENTAL DATA

In view of the extremely large volume of data collected during the permeability determinations, it has been decided to report the slopes of the various flow rate – pressure drop relationships instead of the individual flow rate and pressure drop measurements. In all cases, the statistical correlation coefficients, relating the pressure drops to the flow rates, were greater than 0.999, when the data were treated in a linear regression analysis. Table VI is a summary of the permeability data obtained from fiber mats composed of fibers of each aspect ratio.

Table VII is a summary of the results obtained from the light-scattering determinations.

Table VIII includes the data obtained from the fiber mat compressibility studies.

TABLE VI

PERMEABILITY DATA

Fiber Rx-1169

Mat Thickness, inches	Mat Weight, g.	Temperature, °C.	Pressure Drop/ Flow Rate, (cm. cb. sec./cm.)[a]
0.3638	7.088	23.1	49.01
0.3249	"	23.1	60.30
0.3006	"	23.1	66.65
0.2760	"	23.6	74.68
0.2308	"	23.6	89.88
0.2054	"	24.2	104.81
0.1879	"	24.2	116.71
0.1725	"	24.2	129.81
0.3466	6.878	22.6	56.03
0.3254	"	22.0	63.17
0.3066	"	22.0	69.19
0.2832	"	22.1	76.49
0.2633	"	22.1	83.66
0.2436	"	22.0	90.40
0.2297	"	22.0	97.75
0.2112	"	22.0	109.76
0.1895	"	22.0	127.27
0.1704	"	22.0	149.53
0.3522	7.254	21.3	53.54
0.3221	"	21.6	60.04
0.2975	"	21.7	66.22
0.2746	"	21.7	73.59
0.2503	"	21.7	82.47
0.2293	"	21.9	91.64
0.2073	"	22.0	102.13
0.1864	"	22.0	117.14
0.1666	"	22.0	134.33
0.1451	"	22.1	158.56
0.1284	"	22.0	182.13
0.1137	"	22.0	205.75
0.3603	7.430	21.6	57.84
0.3268	"	21.7	65.85
0.3062	"	21.7	71.70
0.2502	"	21.8	93.55
0.2247	"	21.9	107.30
0.1979	"	21.9	126.47
0.1742	"	21.9	145.78
0.1496	"	22.0	176.18
0.1275	"	22.1	211.00
0.1166	"	22.1	231.59

[a] See end of table for footnote.

TABLE VI (Continued)

PERMEABILITY DATA

Fiber Rx-1167

Mat Thickness, inches	Mat Weight, g.	Temperature, °C.	Pressure Drop/ Flow Rate, (cm. cb. sec./cm.)[a]
0.2946	7.447	23.8	79.3
0.2694	"	24.0	89.4
0.2428	"	23.9	100.2
0.2259	"	23.9	107.2
0.1977	"	24.0	126.0
0.1764	"	23.9	143.9
0.1562	"	24.0	164.3
0.1353	"	24.0	190.6
0.1188	"	23.9	215.3
0.1002	"	23.9	237.8
0.2666	7.459	23.1	115.4
0.2436	"	23.3	129.6
0.2224	"	23.3	144.3
0.2003	"	23.3	163.9
0.1790	"	23.3	187.6
0.1613	"	23.4	213.3
0.1413	"	23.4	252.2
0.1248	"	23.4	287.7
0.1070	"	23.4	338.9
0.0906	"	23.4	389.4
0.2628	7.377	23.7	114.5
0.2384	"	24.1	129.3
0.2167	"	24.2	147.0
0.1982	"	24.3	167.5
0.1761	"	24.3	200.2
0.1587	"	24.3	236.1
0.1404	"	24.3	287.2
0.1227	"	24.2	348.5
0.1052	"	24.3	437.8
0.0891	"	24.2	516.9

[a]See end of table for footnote.

TABLE VI (Continued)

PERMEABILITY DATA

Fiber Rx-1165

Mat Thickness, inches	Mat Weight, g.	Temperature, °C.	Pressure Drop/ Flow Rate, (cm. cb. sec./cm.)[a]
0.2771	7.146	22.7	106.96
0.2328	"	22.7	141.20
0.2095	"	22.8	169.97
0.1832	"	22.9	209.73
0.1634	"	22.9	252.33
0.1432	"	23.0	308.80
0.1245	"	23.0	382.84
0.1088	"	23.1	459.27
0.0863	"	23.2	599.44
0.2853	7.166	24.0	89.87
0.2414	"	24.1	109.50
0.2172	"	24.0	124.00
0.1927	"	24.1	145.70
0.1735	"	24.1	168.00
0.1562	"	24.1	194.20
0.1378	"	24.1	227.60
0.1216	"	24.1	257.60
0.1062	"	24.1	293.00
0.0868	"	24.1	338.10
0.2824	7.140	22.8	99.60
0.2486	"	23.0	116.80
0.2241	"	23.0	131.20
0.2028	"	23.0	145.30
0.1809	"	23.0	163.80
0.1645	"	23.1	183.10
0.1466	"	23.2	204.80
0.1286	"	23.2	235.20
0.1106	"	23.3	271.50
0.0853	"	23.3	319.10

[a]See end of table for footnote.

TABLE VI (Continued)

PERMEABILITY DATA

Fiber Rx-1164

Mat Thickness, inches	Mat Weight, g.	Temperature, °C.	Pressure Drop/ Flow Rate, (cm. cb. sec./cm.)[a]
0.2528	7.368	23.6	154.8
0.2363	"	24.0	165.8
0.2121	"	24.0	196.0
0.1895	"	24.0	231.5
0.1695	"	24.1	276.7
0.1508	"	24.1	334.4
0.1323	"	24.1	417.5
0.1168	"	24.2	515.3
0.0988	"	24.3	640.2
0.0808	"	24.3	768.6
0.2517	7.380	24.0	186.0
0.2287	"	24.1	206.7
0.2032	"	24.2	246.1
0.1816	"	24.2	300.2
0.1623	"	24.3	370.6
0.1413	"	24.3	489.4
0.1249	"	24.3	621.0
0.1085	"	24.3	810.7
0.0894	"	24.2	1148.4
0.2596	7.538	23.7	151.3
0.2426	"	23.9	166.9
0.2148	"	24.0	210.8
0.1934	"	24.1	259.5
0.1672	"	24.1	340.1
0.1455	"	24.1	449.5
0.1285	"	24.1	563.8
0.1126	"	24.0	695.0
0.0965	"	23.9	857.0
0.0829	"	23.9	999.0

[a]See end of table for footnote.

TABLE VI (Continued)

PERMEABILITY DATA

Fiber Rx-1164

Mat Thickness, inches	Mat Weight, g.	Temperature, °C.	Pressure Drop/ Flow Rate, (cm. cb. sec./cm.)[a]
0.2612	7.330	23.7	188.9
0.2290	"	24.0	212.5
0.2031	"	24.0	262.6
0.1774	"	24.1	342.9
0.1584	"	24.1	430.9
0.1393	"	24.2	560.9
0.1221	"	24.1	727.1
0.1076	"	24.1	941.8
0.0945	"	24.1	1168.6
0.0828	"	24.1	1404.3
0.2673	7.358	23.9	180.7
0.2389	"	24.0	204.0
0.2107	"	24.2	253.4
0.1864	"	24.2	323.0
0.1729	"	24.3	378.4
0.1512	"	24.3	505.2
0.1329	"	24.3	671.4
0.1165	"	24.3	905.4
0.0996	"	24.3	1268.5

[a] cb. Represents Chlorobenzene.

TABLE VII

OPTICAL DATA

Fiber Rx-1169

Mat Thickness, inches	Mat Weight, g.	T	R_o
0.267	1.283	10.4	57.7
0.218	"	10.3	57.5
0.205	"	10.2	57.3
0.169	"	10.2	57.2
0.145	"	10.2	57.1
0.114	"	10.0	56.9
0.091	"	9.7	56.8
0.237	1.138	11.2	57.0
0.192	"	11.0	56.6
0.166	"	10.8	56.2
0.123	"	10.6	55.8
0.103	"	10.4	55.5
0.077	"	10.4	55.3

Fiber Rx-1167

0.204	1.259	8.1	59.2
0.162	"	8.1	59.0
0.128	"	7.9	58.1
0.093	"	7.7	57.2
0.074	"	7.7	56.6
0.060	"	7.7	56.2
0.214	1.305	8.0	61.3
0.170	"	7.9	61.1
0.137	"	7.7	60.5
0.102	"	7.4	59.5
0.079	"	7.2	58.6
0.062	"	7.0	57.8

TABLE VII (Continued)

OPTICAL DATA

Fiber Rx-1165

Mat Thickness, inches	Mat Weight, g.	$\underline{T}$	$\underline{R}_o$
0.191	1.140	8.4	59.9
0.152	"	8.0	59.3
0.106	"	7.7	58.0
0.078	"	7.5	57.3
0.052	"	7.5	56.1
0.034	"	7.7	55.9
0.185	1.398	6.8	59.3
0.149	"	6.6	58.6
0.127	"	6.6	58.2
0.105	"	6.6	57.9
0.086	"	6.6	57.6
0.060	"	6.6	56.6

Fiber Rx-1164

0.208	1.129	8.6	62.5
0.166	"	8.4	62.1
0.122	"	8.2	61.1
0.091	"	7.8	60.0
0.063	"	7.8	58.8
0.045	"	7.9	58.0
0.191	1.136	8.0	61.6
0.154	"	7.8	60.8
0.126	"	7.7	60.4
0.087	"	7.4	59.1
0.070	"	7.3	58.4
0.047	"	7.4	57.4

TABLE VIII

FIBER MAT COMPRESSIBILITY DATA

Fiber Rx-1169

Load, cm.H_2O	Mat Thickness, inches	Mat Weight, g.	Solids Concn., g./cc.
8.02	0.4773	7.056	0.128
13.1	0.4632	"	0.132
22.9	0.4408	"	0.138
37.7	0.4169	"	0.146
62.3	0.3905	"	0.156
96.4	0.3667	"	0.166
145.8	0.3422	"	0.178

Fiber Rx-1167

88.0	0.3432	7.404	0.186
13.1	0.3289	"	0.194
22.9	0.3129	"	0.204
37.7	0.2981	"	0.214
62.3	0.2818	"	0.227
96.4	0.2670	"	0.239
145.8	0.2514	"	0.254

Fiber Rx-1165

8.0	0.3420	7.297	0.184
13.1	0.3300	"	0.191
22.9	0.3132	"	0.201
37.7	0.2968	"	0.212
62.3	0.2788	"	0.226
96.4	0.2613	"	0.241
145.8	0.2432	"	0.259

Fiber Rx-1164

8.0	0.2802	7.104	0.217
13.1	0.2678	"	0.229
22.9	0.2528	"	0.242
37.7	0.2393	"	0.256
63.3	0.2248	"	0.272
96.4	0.2118	"	0.289
145.8	0.1998	"	0.307

TABLE VIII (Continued)

FIBER MAT COMPRESSIBILITY DATA

Load, cm.H_2O	Mat Thickness, inches	Mat Weight, g.	Solids Concn., g./cc.
Fiber Rx-1165 (Freeze Dried)			
9.7	0.3097	6.265	0.190
14.8	0.2878	"	0.205
24.7	0.2659	"	0.222
39.4	0.2461	"	0.240
64.0	0.2263	"	0.261
98.1	0.2092	"	0.282
147.5	0.1935	"	0.305

The Institute of Paper Chemistry

Appleton, Wisconsin

Doctor's Dissertation

The Hydrolysis of Cellobiose in the Presence of Ferric Ion

Karl V. Kraske

June, 1963

THE HYDROLYSIS OF CELLOBIOSE IN THE PRESENCE OF FERRIC ION

A thesis submitted by

Karl V. Kraske

B.S. 1957, University of Maine
M.S. 1959, Lawrence College

in partial fulfillment of the requirements
of The Institute of Paper Chemistry
for the degree of Doctor of Philosophy
from Lawrence College,
Appleton, Wisconsin

June, 1963

TABLE OF CONTENTS

SUMMARY

A study of the various reactions of ferric ion with cellobiose was undertaken in order to gain a better understanding of the degradation of cellulose in the presence of the ferric ion.

A preliminary study of the ferric ion-cellobiose-water system showed that both hydrolysis products and oxidation products were formed from the cellobiose at 100°C. Because ferrous ion was formed in these experiments and was reoxidized upon exposure of the sample to the air, oxygen was excluded from the reaction mixture until the sample had been stabilized.

The presence of a complex of cellobiose with the ferric ion in solution was indicated spectrophotometrically. The same method was used to confirm the existence of a complex of glucose with the ferric ion. The complex of the ferric ion and the carbohydrate was concluded to be a necessary intermediate for both the hydrolysis due to the ferric ion and the oxidation of the carbohydrate.

Work with a cyclic glycol, linear glycols, and a series of sugars was done to determine the probable sites on the carbohydrates for reduction of the ferric ion. The polyhydric alcohols showed no evidence of reaction with the ferric ion under the conditions used in this work. The reactivity of the sugars increased as the proportion of the sugar in the aldehyde form increased. It is believed that the reaction occurs through a complex of the ferric ion and the enediol form of the sugar.

The effect of the ferric ion upon the hydrolysis of the glycosidic bond of cellobiose was studied by comparing the rate of formation of glucose in reactions containing ferric ion with the rate of formation of glucose in reactions without ferric ion. It was found that the ferric ion influenced the hydrolysis of the glycosidic bond in two ways.

The first way was the direct acidic effect of the metal ion. It was concluded that ferric ion acts in a manner similar to that of the proton in the acid-catalyzed hydrolysis of glycosidic bonds. It is proposed that the ferric ion affects the glycosidic bond by chelating with the 6-carbon hydroxyl group on the aglycon and the oxygen of the glycosidic bond. Another possibility for reaction at the glycosidic bond is chelation of the ferric ion with the 6-carbon hydroxyl and the ring oxygen of the glycosyl moiety of cellobiose.

The second way that the ferric ion influences the hydrolysis of cellobiose is by the production of protons during the reduction of the ferric ion by the carbohydrate. The resulting decrease in pH increases the hydrolysis rate.

It was concluded that the direct action of the ferric ion upon the hydrolysis of cellobiose is equivalent to the action of an equal concentration of protons. This conclusion was reached because the rate constant of hydrolysis of cellobiose did not vary during the reaction containing ferric ion. Ferrous ion had no effect upon the hydrolysis of cellobiose. It was concluded that Czepiel's report (5) of ferrous ion accelerating the degradation of cellulose could be explained by air oxidation of the ferrous ion to the ferric ion which, subsequently, would degrade the cellulose.

It was hypothesized that for a metal ion to directly catalyze the hydrolysis of cellobiose, the ion must have an affinity for electrons greater than that required for simple co-ordinate bonding with the cellobiose. The ions that fulfill this requirement exhibit the greater electron affinity (acidity) as oxidizing power. The zinc ion was selected to demonstrate whether or not the ability of an ion to co-ordinate with cellobiose is sufficient to catalyze the hydrolysis of cellobiose

since the zinc ion complexes with carbohydrates, but is not an oxidizing agent. The zinc ion had no effect on the hydrolysis of cellobiose.

It was concluded, therefore, that the acidic properties of the ferric ion are such as to cause hydrolysis of the glycosidic bond. The electrophilic properties of this ion that are responsible for this action are best described by the Usanovich concept of acidity. The Lewis theory of acidity is not sufficient, as it does not distinguish between the properties of the ferric ion and the zinc ion. It was further concluded that the oxidizing and hydrolysis-catalyzing properties of the ferric ion, as shown by reaction with cellobiose, are sufficient to account for the degrading action of iron salts upon cellulose.

INTRODUCTION

Many research workers have noticed that certain metal ions have an effect upon the stability of cellulose (1-7). Some investigators were concerned with the effect of the metal ion on tensile strength (1-3), others with the effect on color stability (4-5).

Czepiel (5) connected the two effects, showing that metal salts had a parallel effect on the lowering of the degree of polymerization of cellulose and on the formation of colored materials. Aluminum, cupric, ferrous, and ferric sulfates were shown to be increasingly good accelerators of the degradation of cellulose. Other metal salts (cadmium, lanthanum, magnesium, and manganese) had the opposite effect, that of increasing the stability of the cellulose. Czepiel examined the effects of some of the salts upon cellulose in a low oxygen (<0.1%) atmosphere. The effects of the metal salts upon the degree of polymerization were still present, although somewhat diminished.

On this basis, he hypothesized that the hydrated metal ion hydrolyzed in the presence of the cellulose, producing protons which directly catalyzed the hydrolysis of the cellulose. However, he called attention to the fact that his data did not support this mechanism completely. The aluminum ion is highly acid, and would hydrolyze to a large extent in the pulp slurries used. Yet, the effect of the aluminum was much less than the effect of the less acidic ferrous and cupric ions.

The idea that metal salts can contribute to the hydrolysis of cellulose has been advanced by others (6, 7). Young (6) found that bamboo could be hydrolyzed to glucose in molten $FeCl_3 \cdot 12H_2O$. Torii (7) stated that iron and manganese increased hydrolysis during the oxidation of cellulose by nitric acid.

The contribution of the metal ions to the degradation of cellulose seemed to be through the hydrolysis of the glycosidic bond, but could not be accounted for by protons from hydrolysis of the metal ion. The transition-metal ions are noted for being acidic in nature. It seemed possible that these metal ions could interact with the cellulose directly to influence the electron shift about the glycosidic bond that results in hydrolysis of that bond.

The ion must exhibit two features in order to accomplish this hydrolytic action. The ion must co-ordinate with or near the oxygen atom of the glycosidic bond. The acidity of the ion must be such that the resultant electron shift about the glycosidic bond will be sufficient to cause fission of that bond.

In order to provide a basis for such a hypothesis, the following topics will be discussed:

the acid hydrolysis of glycosidic bonds,
the concepts of acids and bases,
the complexing of carbohydrates with transition-metal ions, and
the oxidation of polyhydric substances by transition-metal ions.

THE ACID HYDROLYSIS OF GLYCOSIDIC BONDS

REACTION MECHANISMS

The acid hydrolysis of glycosidic bonds is thought to be a unimolecular decomposition of the protonated glycoside, since the first-order rate constant is proportional to the Hammett acidity function of the hydrolysis solution (8, 9). Two mechanisms for hydrolysis have been discussed by Shafizadeh (10) and presented in Fig. 1. The two mechanisms differed in that one formed a cyclic carbonium-ion intermediate, and the other an acyclic carbonium-ion intermediate. Experiments

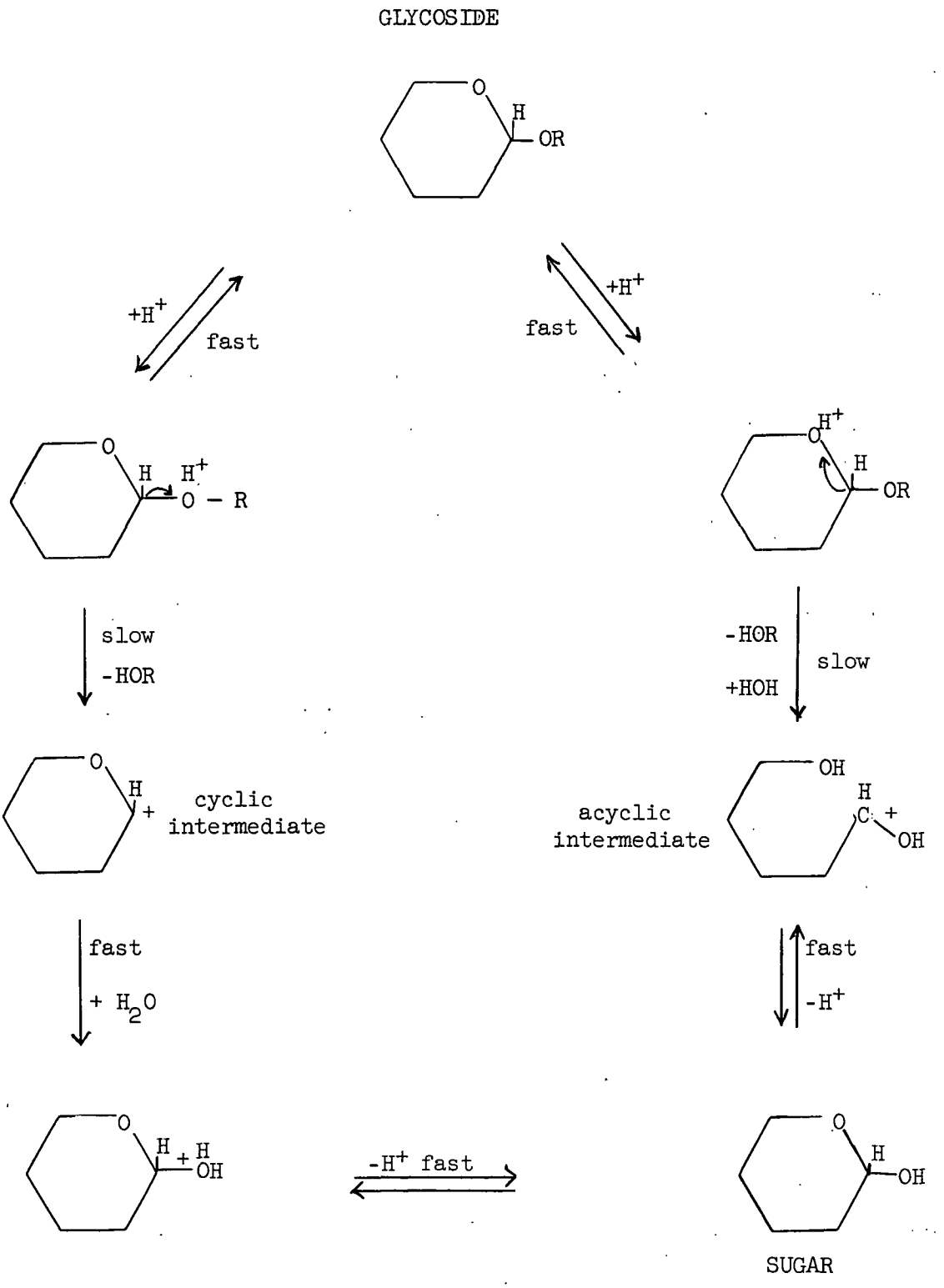

Figure 1. Proposed Pathways for the Acid Hydrolysis of Glycosides (10)

with water enriched with H_2O^{18} (9) led to the belief that the reaction occurs with fission of the glycosyl-oxygen bond as follows:

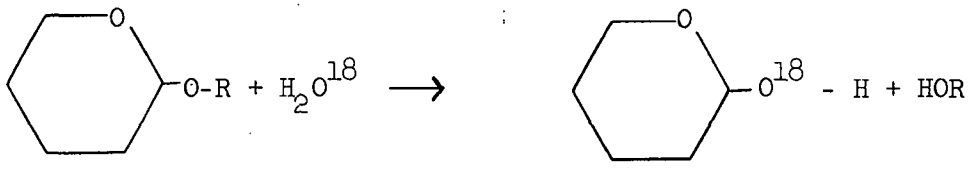

Further experiments (11) determining initial enrichment of H_2O^{18} revealed that the reaction probably proceeded through the cyclic carbonium ion instead of the alternate acyclic mechanism as had been previously postulated. This does not exclude the possibility that the acyclic mechanism might be involved in certain conditions (12).

Effect of Substitution on the Glycoside

One method of stabilizing the glycosidic bond is to mask the reactive center. Methyl-2-amino-2-deoxy glucopyranoside is thought to be stable because the positively charged amino group decreases the concentration of lyonium ions about the glycosidic bond (13). Other substituents affect hydrolysis by modifying the strain or conformational stability of the molecule (13). Also, some substituents are thought to have a polar effect upon the glycosidic bond, either retarding or accelerating hydrolysis by attracting or repelling electrons from the glycosyl portion of the molecule (14).

THE CONCEPT OF ACIDS AND BASES

A general review of the acid-base concept has been given by Moeller (15). A summary of the pertinent points will be given here.

The Bronsted concept of acid-base phenomena is probably the most widely understood theory, although too limited to adequately explain these phenomena. Here, the acidic property is considered to be the proton, and the acid-base relationship is:

$$\text{conjugate acid } (BH)^+ \rightleftharpoons \text{base } (B) + H^+$$

or

$$\text{acid } (AH) \rightleftharpoons \text{conjugate base } (A^-) + H^+.$$

From these relationships, it can be seen that a material can be an acid (or a base) without actually exhibiting properties of an acid. A substance cannot exhibit the properties of an acid unless a base is present to accept the proton, and a base must be in the presence of an acid to display basicity. Thus, acid-base reactions are actually competitions for protons.

$$\text{acid}_1 + \text{base}_2 \rightleftharpoons \text{acid}_2 + \text{base}_1$$

The Lewis theory of acidity is more general in that it eliminates the necessity of the proton as the acidic particle. The Lewis definition of an acid is: An acid is a group (atom, ion, molecule) that has available unfilled orbitals. This group will tend to share electrons with other groups with available electron pairs. Consequently, a base is a group with electron pairs available for donation. It can be seen that this concept embraces the Bronsted theory completely.

Lewis

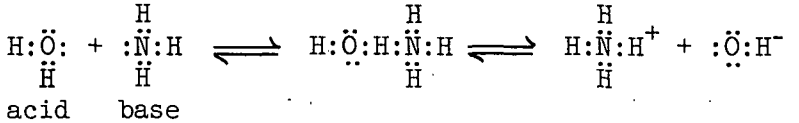

acid base

Bronsted

$$H_2O \rightleftharpoons H^+ + OH^-$$

acid conjugate base

$$NH_3 + H^+ \rightleftharpoons NH_4^+$$

base conjugate acid

$$H_2O + NH_3 \rightleftharpoons NH_4^+ + OH^-$$

$$\text{acid}_1 + \text{base}_2 \quad \text{acid}_2 + \text{base}_1$$

The increased generality of the Lewis theory enables the acid-base concept to be extended to systems containing no protons.

$$ZnCl_2 + 2Cl^- \rightleftharpoons \begin{bmatrix} & Cl & \\ Cl & Zn & Cl \\ & Cl & \end{bmatrix}^{-2}$$

It can be seen that the Lewis concept extends the idea of the acid-base reaction to cover the field of co-ordination chemistry. Here, the central metal ion is a Lewis acid and the ligand is the Lewis base.

Occasionally in the literature, an author states that a substance does not act as a Lewis acid but as a Bronsted acid. This does not imply that the Lewis acid theory is not valid, but that the exhibition of the acidic nature of the substance takes place through the donation of a proton. For instance, Gould (16) stated that transition-metal ions are often thought of as Lewis acids, but, in the case of aqueous solutions of ferric ion, the metal ion is a Bronsted acid.

$$Fe(H_2O)_6^{+3} \rightleftharpoons Fe(OH)(H_2O)_5^{+2} + H^+$$

Actually, the ferric ion is acting as a Lewis acid, attracting the electrons of the oxygen of the co-ordinated water molecules, effectively weakening the O-H bond. If another Lewis base were to replace the co-ordinated water, the electrons of the new base would be similarly affected.

Usanovich, in a comprehensive acid-base theory, defined an acid as any material which neutralizes bases, gives up cations, or combines with anions or electrons. Bases are materials which form salts with acids, give up anions or electrons, or combine with cations. The value of this further generalization is that it recognizes oxidation-reduction reactions as being another case under the acid-base theory. Under the Lewis theory, oxidation-reduction reactions differ from co-ordination

reactions in that the latter share electrons, and thus are included in the Lewis theory, while the former involve complete transfer of the participating electrons. The Usanovich theory makes no such distinction, but states that the nature of acidity and oxidizing power are the same.

Thus, the theory covering acid-base reactions has been greatly expanded so that it now recognizes as acids all proton donors (Bronsted acids), electrophilic agents (Lewis acid), and oxidizing agents (Usanovich acids). A solution of transition-metal ions in the oxidized state, therefore, has an acidity greater than that measurable by the hydrogen-ion content of the solution.

THE COMPLEXING OF TRANSITION-METAL IONS WITH CARBOHYDRATES

The carbohydrates are classified as amphiprotic materials, i.e., the hydroxyl groups can react as bases with materials which are stronger acids than the hydroxyl groups, or as acids with groups that are more basic. Some of the transition-metal ions (notably the ferric ion) are quite acidic; thus, it is quite possible that electron sharing can occur between the hydroxyl groups and the metal ions. There are, however, other electron-donating locations on the glycosidic molecule. Using the glucopyranoside structure both as a general structure and as the specific glycoside of interest to this thesis, both the glycosidic oxygen and the ring oxygen have unshared, sterically accessible electron pairs. In the case of cellobiose (4-O-(β-D-glucopyranosyl)-D-glucose), both the ring and the glycosidic oxygens are accessible from the same angle, presenting a strong electronegative center on the molecule.

There are many examples in the literature of complexes of transition elements with polyhydric alcohols, aldoses, and related compounds. In alkaline solution, ferric ion complexes with mannitol, glycerol, sucrose, or glucose to a degree

sufficient to prevent the hydrous ferric oxide from precipitating (17-19). Pecsok and Sandera (20) stated that ferric ion complexes with gluconic acid over a wide pH range. The first evidence of a complex occurred at a pH of about three. It was assumed by Pecsok and Sandera that the δ-hydroxy proton is the most easily replaced of all the protons including the carboxyl protons.

Delaney (21) attempted to determine the stoichiometry of a ferric ion-glucose complex in the system: ferric chloride, hydrochloric acid, water, and glucose. The numerous chloro-complexes of the ferric ion interfered with most of the spectrophotometric attempts to determine a complex. However, the limited spectrophotometric data, together with the fact that ferric ion accelerated the mutarotation of α-glucose, was used to infer the presence of a ferric ion-glucose complex. Delaney attributed the complex solely to the beta form of glucose.

The oxidation of glycols by several metal ions has been explained through the complexing of the ion and the glycol. Drummond and Waters (22) stated that the manganic ion (a very strong oxidizing agent) did not attack olefins or monohydric alcohols, but readily attacked and oxidized glycols in a manner similar to the action of ceric salts. It was stated that this was indicative of a cyclic intermediate.

Arndt, Loewe, and Ayca (23) showed that several stable enediols (ascorbic acid, reductone, coumarindiol) formed colored materials upon the addition of ferric chloride. Furthermore, the color disappeared as the ferric ion was reduced to the ferrous state. The methyl ether of coumarindiol, as presented in Fig. 2, could not form the complex, did not color, and did not reduce the ferric ion.

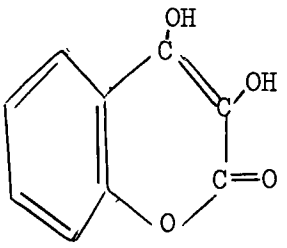

Coumarindiol

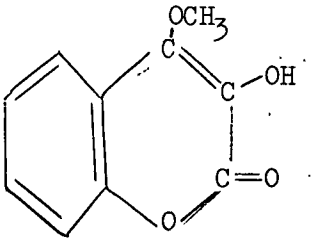

Methyl-O-coumarindiol

Figure 2. Comparative Structures of Compounds Used to Demonstrate Enediol Chelation of Ferric Ion

OXIDATION OF SOME ORGANIC MATERIALS BY TRANSITION-METAL IONS

There are many cases where transition-metal ions are thought to oxidize organic molecules through the formation of a co-ordinate bond. If this were true, the more acid the metal ion (acidity increases with increasing positive charge and decreasing ionic radius), the more likely such a reaction would be. Of course, the organic molecule also affects the results. Just as one could not speak of the strength of an acid without referring to the base, one cannot refer to the oxidizing potential of a system without knowing the reducing agent. Some of these investigations involved solutions of the metal ions and of 1,2 di-oxy compounds: ferric ion with various stable enediols (23), cupric ion with acetoin (24), ceric ion with 2,3 butanediol (25), and manganic ion with glycols (22). In all of the above, a complex of the metal to the oxygen of the organic molecule was postulated as a major step leading to electron transfer.

These reactions proceed with rapid salt formation (co-ordination) followed by relatively slow electron transfer and breakdown into more stable forms. Consequently, many of this type of oxidation are irreversible and have monomolecular decomposition of an activated complex as the rate-controlling step.

Arndt, Loewe, and Ayca (23) proposed the following pathways for the reaction of ferric ion with enediols:

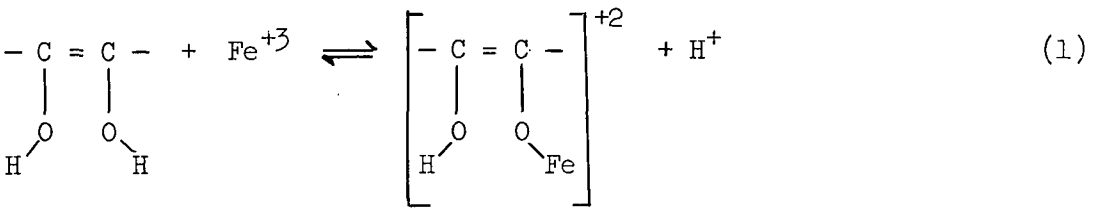

(1)

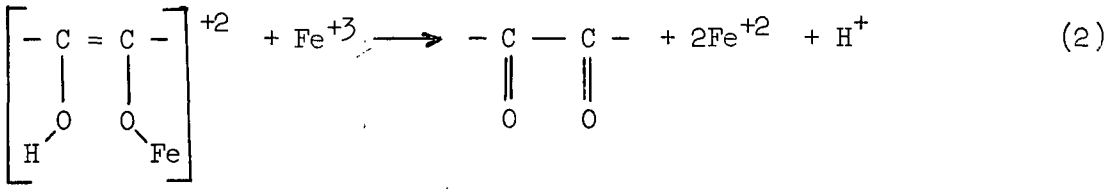

(2)

A colored material was formed by the addition of the ferric ion to the enediol. Monohydric alcohols are only slightly stronger bases than water (13, 26). Therefore, aqueous solutions of the alcohol and metal are only weakly associated. The chelating ability of the dihydroxy compound enables it to form a more stable salt than the monohydric alcohols. Arndt and co-workers regarded Step (1) as a simple replacement, probably reversible, of a proton during complexing. This author regarded their data as indicating that Step (1) might better be written as two steps:

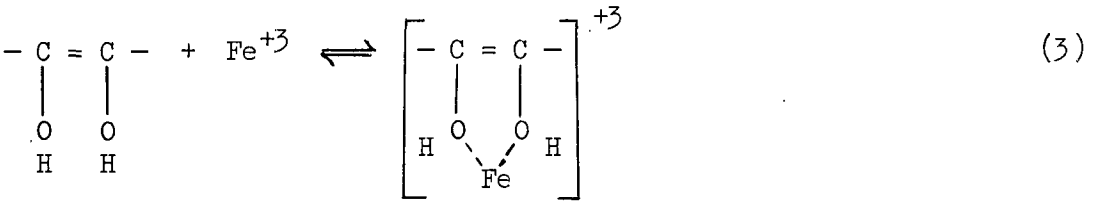

(3)

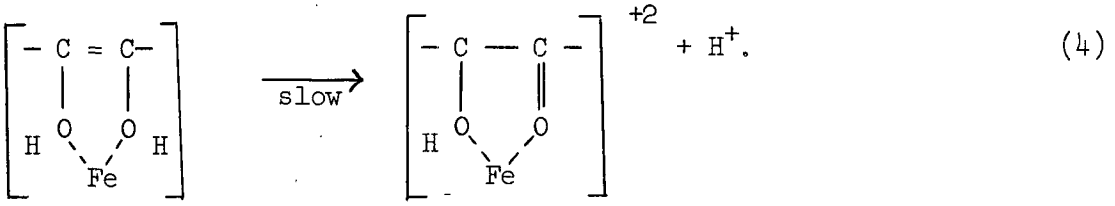

(4)

This conclusion was reached because an increase in the hydrogen ion concentration accelerated the reaction.

Stannett (27) stated that the hydrogen ion released in the oxidation of poly-hydroxy compounds by ceric ion came not from the hydroxyl group, but from the hydrogen directly bonded to the carbon backbone.

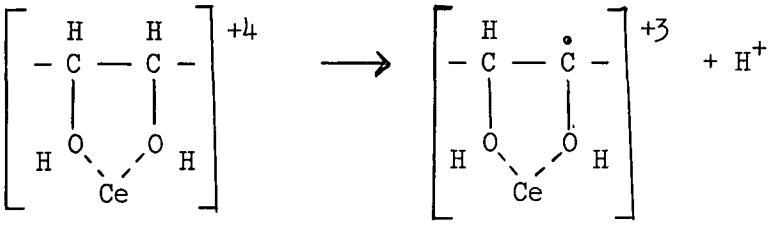

PRESENTATION OF THE PROBLEM

The fact that metal ions, either directly or indirectly, have a profound influence upon the hydrolysis of glycosidic bonds is evident from the preceding discussion. Czepiel's (5) hypothesis that the hydrolysis of the glycosidic bond was accelerated by the protons from the hydrolysis of the hydrated ion has been acknowledged as being a contributing factor, but not the sole source of acceleration.

Hydrolysis of glycosides is believed to be catalyzed by an acidic particle, the proton. Although aqueous solutions of transition-metal ions are sometimes thought to exhibit their acidity by the production of protons during the hydrolysis of the hydrated ion, some of these ions have an effective acidity beyond the proton-donating concept. The Usanovich concept of acids states that total acidity is a combination of proton-donating ability, co-ordinating power, and oxidizing power. Thus, transition-metal ions of high ionic charge, capable of oxidizing other materials, would have an acidity far greater than that measured by the pH of its solution in water. If this were true, then the order of influence of metal ions on the degradation of cellulose found by Czepiel would seem logical ($Fe^{+3} > Fe^{+2} > Cu^{+2} > Al^{+3}$) with the exception of the ferrous ion.

There seems to be a reasonable explanation for the promotion of the ferrous ion in this series. Ferrous sulfate is quite stable in acidic solution, enough so that it has been used as a primary standard in the past. However, $Fe(OH)_2$ is a reducing agent with an oxidizing potential considerably more negative than the Fe^{+2} ion

$$(Fe^{+2} \longrightarrow Fe^{+3} + e^- \; ; \; E_o = -0.74 \text{ v.})$$

$$(Fe(OH)_2 + OH^- \longrightarrow Fe(OH)_3 + e^- \; ; \; E_o = 0.65 \text{ v.}) \quad (28).$$

Kaden and Fallab (29) have shown that when the ferrous ion was complexed with an oxygen of an organic molecule, the oxidation of the ferrous ion was greatly accelerated. Silverman and Dodson (30) reported that electron transfer between the oxidation states of iron occurred much more rapidly through an oxygen bridge.

Czepiel (5) prepared the ferrous-salt-containing cellulose by slurrying the cotton linters in a ferrous ion solution, then air drying the pads formed from the slurry. This author believes that much of the ferrous ion was oxidized to the ferric state during the drying period.

It would appear that certain transition-metal ions could act directly as an acidic particle to catalyze the hydrolysis of the glycosidic bond. The metal ion could act by co-ordinating at or near the glycosidic bond, thus affecting the electron density at the glycosidic bond. A bridge-activated complex, as proposed by Taube and Myers (31), would be another possibility for affecting the electron distribution.

ANALYSIS OF THE PROBLEM AND EXPERIMENTAL APPROACH

The hypothesis that transition-metal ions can induce hydrolysis of glycosidic bonds by affecting the electron density of the oxygen atom in the glycosidic bond has been shown to be probable by evidence from the literature. Further evidence was necessary to prove the direct action of the metal ion. The following course of experiments was undertaken to establish this evidence:

Cellobiose was chosen as the glycoside for these experiments. This problem is of particular interest in the field of cellulose chemistry, so it was desired to maintain a close relationship to the type of bond found in cellulose. Cellobiose, as the simplest of the glucosans, fulfills this ideal, and the products of hydrolysis are amenable to analysis.

The ferric ion was chosen as the acidic particle, since it was the most acidic of the metal ions investigated by Czepiel (5), and had the greatest effect upon the degradation of cellulose.

It was thought that the metal ion would affect the hydrolysis of cellobiose through a complex. Spectrophotometric evidence was obtained to show that complexing occurs between the ferric ion and glucose or cellobiose.

A preliminary qualitative set of reactions of cellobiose solutions with and without ferric ion present was carried out to determine if the ferric ion had any effect upon the hydrolysis of cellobiose. It was found that the reactions carried out in the presence of the metal salt produced a significantly larger quantity of glucose, as was expected. However, one of the reactions produced a quantity of other materials, presumably oxidation products from reaction with the metal ion.

Because of this evidence of oxidation, work was done to determine the site on the organic molecule that was responsible for the reduction of the metal ion. Linear glycols, a cyclic glycol, and a series of sugars were investigated to discover probable pathways for the oxidation-reduction reaction.

There are several possibilities for catalysis of hydrolysis of glycosidic bonds in a ferric-ion-containing system. Protons present in solution initially, both from acid added to adjust pH and from hydrolysis of the metal salt, would catalyze the reaction. Another source of catalysis would be protons produced during the oxidation of a carbohydrate by the ferric ion. A final source of catalysis would be the direct action of the metal ion upon the atoms of the glycosidic bond. The latter two sources of catalysis are the major points of interest to this thesis. These points were investigated by comparison of the rates of hydrolysis of cellobiose in a ferric sulfate solution with the rate of hydrolysis of cellobiose in a solution without the ferric ion of the same initial pH and ionic strength. Also investigated in the same manner were the effects of sodium sulfate (used to adjust the ionic strength) and the effects of the ferrous ion upon the hydrolysis of cellobiose. The combination of these results are interpreted to explain the significance of the direct contribution of the metal ion on the hydrolysis of glycosides.

RESULTS AND DISCUSSION

COMPLEXING IN FERRIC ION-CELLOBIOSE AND FERRIC ION-GLUCOSE SYSTEMS

EXPERIMENTAL METHODS

Two general methods have been used to analyze data for the presence of coordinate compounds in a system. The more commonly used method has been termed the method of continuous variation (32) in which the ratio of the metal to the ligand was varied, while the total molarity of the system was kept constant. The variation of the measured function from the sum of the ideal behavior of the two components was plotted vs. the composition of the solution. The composition of the complex was then indicated by a maximum (or a minimum) in the plot.

The second method has been termed the method of limiting logarithms (33). If a complex existed in equilibrium with its dissociated forms, then the following relationship should hold:

$$aA^{+} + bB \rightleftharpoons A_aB_b^{+}$$

where

A = the metal ion

a = coefficient for the metal ion

B = the ligand molecule, and

b = coefficient for the ligand.

Then the equilibrium constant

$$K = (A_aB_b^{+})/(A^{+})^{a}(B)^{b}$$

where

( ) = concentration in consistent units.

Then, $\log K = \log(A_a B_b^+) - \log(A^+)^a - \log(B)^b$

or $\log(A_a B_b^+) = \log(A^+)^a + \log(B)^b + \log K.$

When a complex shows an absorption maximum independent of the spectra of other species, Beer's Law may be assumed to hold at that frequency, i.e., absorbance ($\underline{a}$) $\propto$ ($\underline{A}_{\underline{a}}\underline{B}_{\underline{b}}^+$). Therefore, $\log \underline{a} \propto \log (\underline{A}^+)^{\underline{a}} + \log \underline{K} + \log (\underline{B})^{\underline{b}}$. When the equilibrium constant of the co-ordination reaction is small, the equilibrium concentrations of the metal ion and the ligand may be assumed equal to the initial concentrations. If the concentration of one of the constituents of the complex was held constant while the other was varied, then

$$\log a \propto a \log (A^+) + C_1$$

and

$$\log a \propto b \log (B^+) + C_2.$$

Therefore, if the logarithm of the optical density were plotted against the logarithm of the concentration of either the ligand or the metal, while the other was held constant, the plot should yield a constant slope equal to the coefficient of the varied component.

This method was termed the method of limiting logarithms since, at high concentrations, interaction of the species interferes with the relationship.

Delaney (21) attempted to work with the method of continuous variation for a ferric chloride-glucose system, but the many ferric-anion complexes confused the interpretation of the data so the method of limiting logarithms was used.

The method of limiting logarithms was used in this thesis to show that a complex between ferric ion and glucose, and ferric ion and cellobiose exists. A 0.1M ferric sulfate solution was both the solvent and the reference solution for

the spectrophotometric study. Ten milliliters of the reference solution was added to a weighed quantity of the carbohydrate. The absorbance of the solution containing the carbohydrate, referred to the ferric sulfate solution, was determined near the maximum absorption wavelength of the complex (410 to 420 mμ). Spectra of the complex are shown in Fig. 3.

RESULTS

Work with a constant concentration of ferric ion (either as the sulfate or chloride) and a varying amount of glucose or cellobiose yielded data which may be found in Fig. 4 and 5. The absorbance was measured close to the wavelength where maximum absorption occurred in the solution. A plot of log a vs. log(carbohydrate) had a slope of 1, indicating that a complex had formed involving one molecule of the carbohydrate.

Attempts to use this method for the determination of the number of ferric ions involved in the complex failed. The high absorbance of the ferric ion solutions compared to that of the complex prevented work near the maximum absorption wavelength of the complex.

QUALITATIVE STUDY OF THE EFFECT OF FERRIC ION UPON CELLOBIOSE

A preliminary study of the system ferric ion, cellobiose, and water was made to determine the type of reaction and the conditions favoring the reactions desired. Cellobiose solutions were heated for 77 hours at 100°C. The ferric ion content and the pH were the variables. The solutions were compared chromatographically after heating. The conditions and data are given in Table I.

The samples were exposed to the atmosphere several times when the solutions were chromatographed after the reaction period. During the several days the

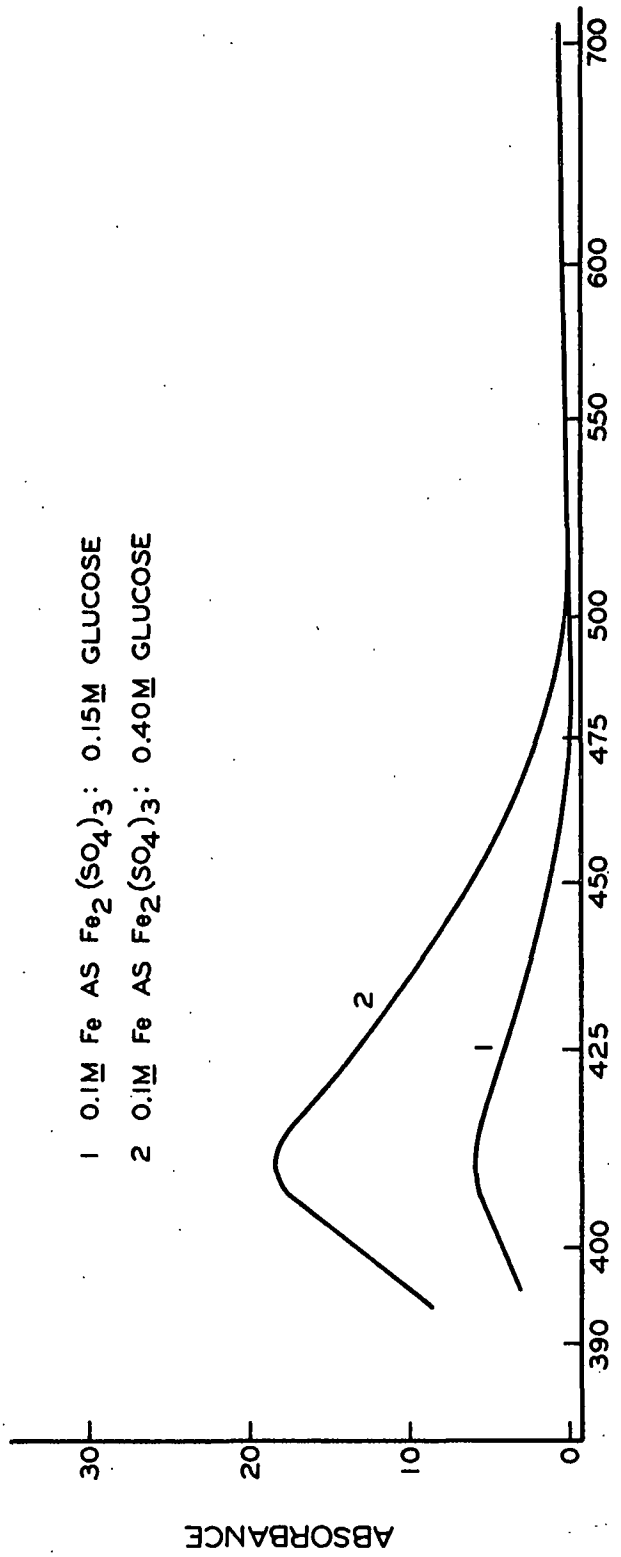

Figure 3. Spectra of the Ferric Ion-Glucose Complex

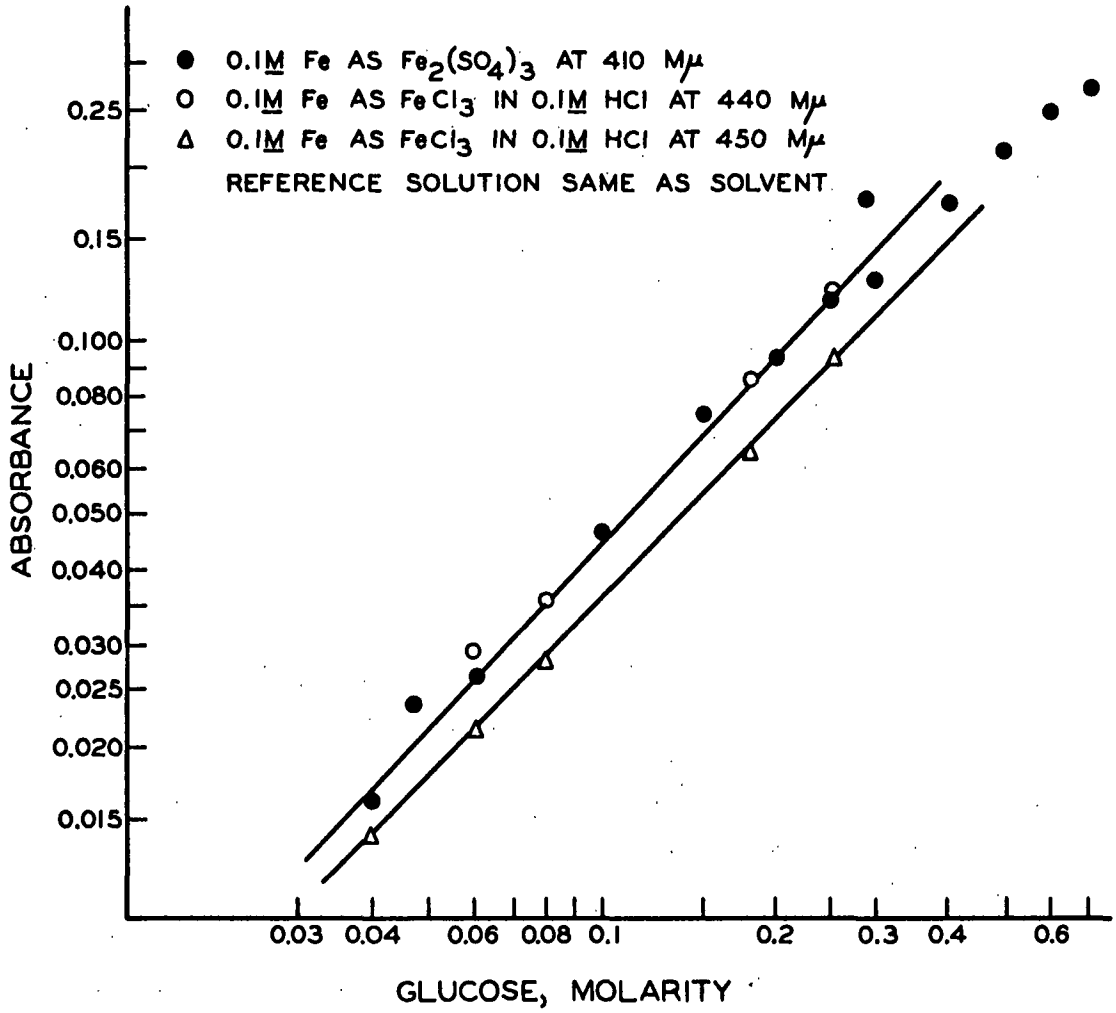

Figure 4. Ferric Complex of Glucose

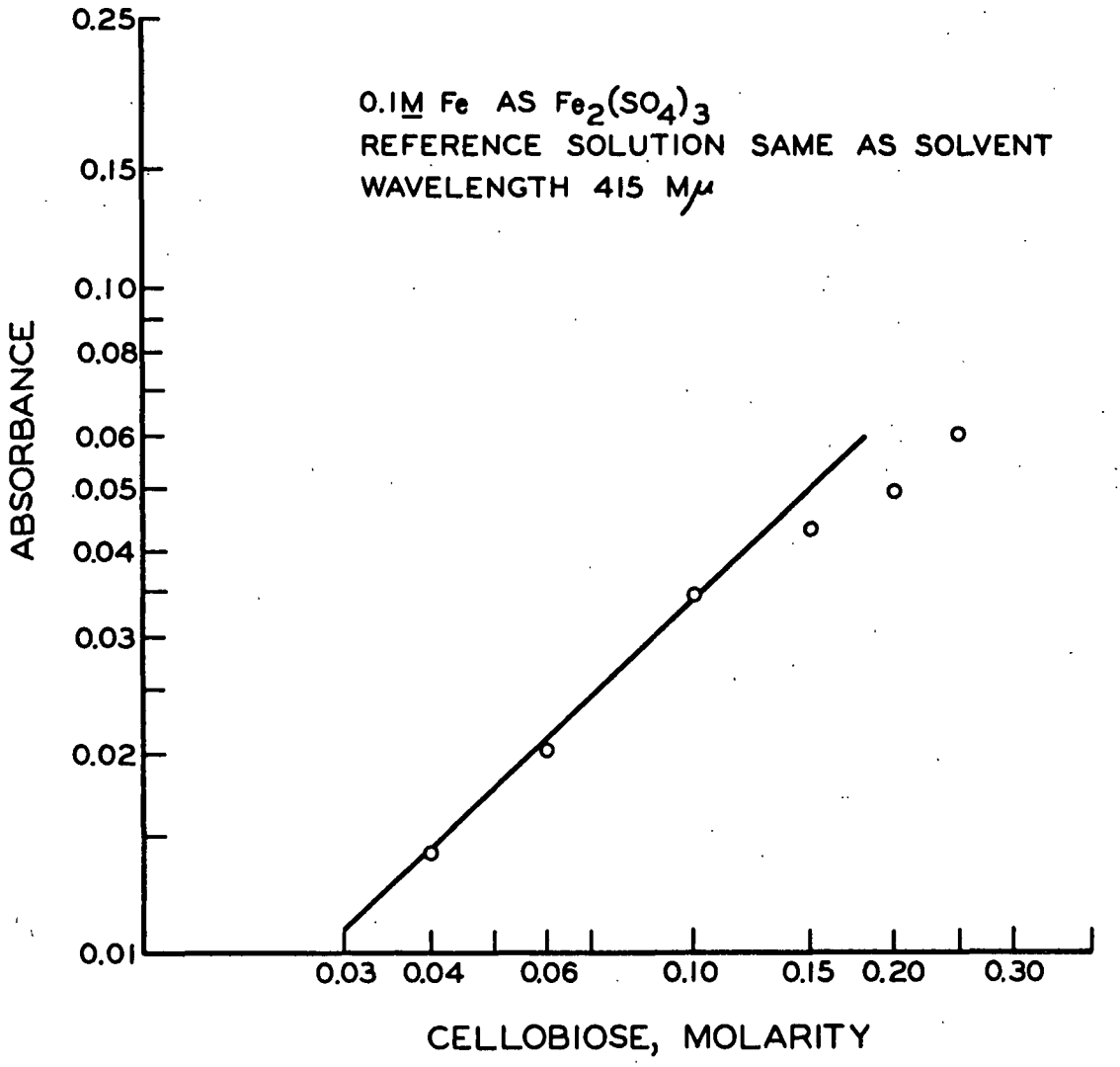

Figure 5. Ferric Complex of Cellobiose

TABLE I

CHROMATOGRAPHIC COMPARISON OF CELLOBIOSE-FERRIC SULFATE SOLUTIONS

Reaction Conditions: 77 Hours at 100°C.

	Control	Solution 1	Solution 2
Cellobiose, g.	0.192	0.192	0.192
Ferric ion, μg.	0	2040	2040
pH, initial	5	3	6
pH, final	3.9	1.9	4.5
Volume, ml.	10	10	10
R_g of spots[a,b]	0.4	0.4	0.4
	1.0	1.0	0.6
			1.0
			3.2[e]
			5.2[e]
R_g of spots[a,c]	0.4	0.4	0.04
	1.0	1.0	0.4
		0.1[d]	0.6
			1.0
			1.3
			2.0

[a]Developed in 8:2:1 (ethyl acetate:pyridine:water).

[b]Sprayed with p-anisidine·HCl to detect reducing compounds.

[c]$AgNO_3$ in the developer, NH_3 vapor to detect most organic oxygen compounds.

[d]This spot appeared after the sample had been exposed to the air for several days.

[e]These spots appeared on the initial chromatogram only.

samples were exposed to the air, Solution 1 showed a new spot with an R_g value of about 0.1, and Solution 2 became very dark, both presumably due to atmospheric oxidation, as subsequent samples did not show this effect when efforts were made to exclude as much air as possible.

An estimate of the relative degradation of the samples would be: Control < Solution 1 < Solution 2. In terms of the production of glucose, Solutions 1 and 2 were about equal, both considerably greater than the control solution. The solution containing ferric ion at a higher pH definitely showed more oxidation than did the solution at the lower pH. At the higher pH, the ferric ion is paired with more hydroxide ions. These ion pairs have been shown to facilitate electron transfer reactions (31). (See the discussion concerning the electron transfer through oxygen bridging on page 16.)

REDUCTION OF FERRIC ION IN SOLUTION WITH CARBOHYDRATE

EXPERIMENTAL

The remaining experiments were carried out at the same ionic strength except where specified. The ionic strength was adjusted to a value of 1.5 moles per liter with sodium sulfate. This ionic strength was chosen because it made possible the choice of a wide variety of concentrations and ions without making a large change in the ionic atmosphere.

In order to investigate the catalytic action of ferric ion on the hydrolysis of cellobiose, the pH was maintained relatively low to eliminate as much as possible the previously shown oxidizing action of the ferric ion at a higher pH. The analytical procedures were complicated by the need to reduce oxidation of the carbohydrate by lowering the pH of the reaction mixture. The lower pH would cause

a higher rate of acid-catalyzed hydrolysis of the cellobiose. Too low a pH would reduce the program to a search for small differences between large numbers. At a pH of 1.80 at room temperature, there was virtually no more color change in the solution upon adding small amounts of concentrated sulfuric acid, indicating that the equilibrium in the reaction

$$Fe(H_2O)_n^{+++} \rightleftharpoons FeOH(H_2O)_{n-1}^{++} + H^+$$

is such that most of the metal present is in the form of the ferric ion. Using the value of $K_h = 6 \times 10^{-3}$ (16), a 0.01M ferric sulfate solution would be 25% in the $FeOH^{++}$ state. According to Arden (34), the rate of precipitation is dependent upon the concentration of the $FeOH^{++}$ ion. The percentage of the original ferric ion present as $FeOH^{++}$ was quite low because the ferric ion solution with no sodium sulfate rapidly precipitated after a few minutes at 90°C., while the solution with added salt remained stable for days at 90°C. It was concluded that the presence of sodium sulfate suppressed the hydrolysis of the hydrated ferric ion.

It was decided to do as much work as possible under a low oxygen content atmosphere because the qualitative work had shown such a marked sensitivity to oxygen, even at room temperature. To accomplish this purpose, the reaction was carried out in a 100-ml. flask with three capillary openings. A schematic diagram of this flask appears in Fig. 6. One capillary was stoppered, being opened only for sampling, one served as an inlet port for prepurified nitrogen, and the third, bearing a condenser, served as an outlet for the gas.

A current of nitrogen was passed through the flask at room temperature for an hour after the introduction of the reaction mixture into the flask. Then the flask was completely immersed in the controlled temperature oil bath. The oil bath was controlled uniformly to $\pm$ 0.12°C. At this point, the outlet nitrogen stream was shut off to maintain a small positive pressure of nitrogen in the reaction vessel.

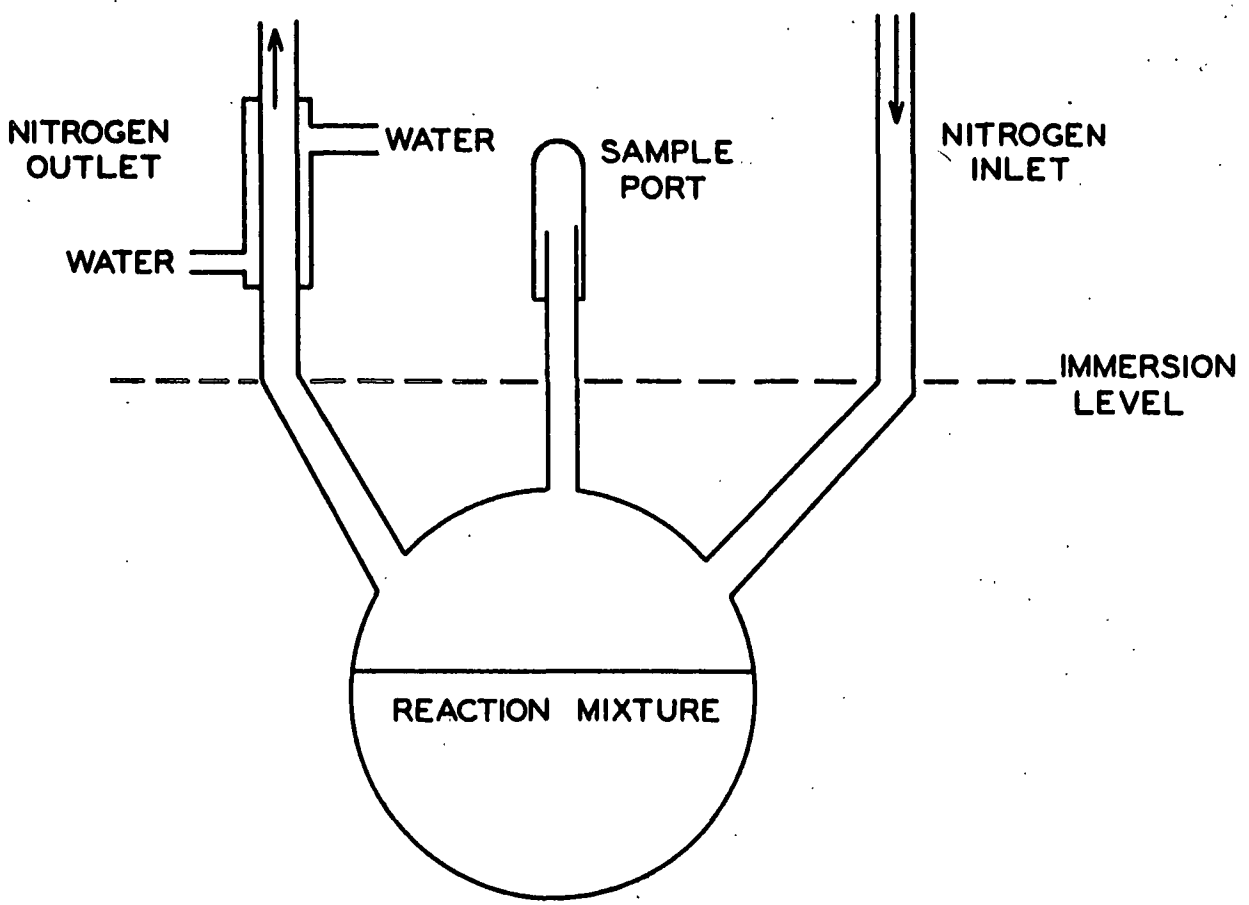

Figure 6. Schematic Diagram of the Reaction Vessel

The procedure for taking the sample was as follows: The rubber cap was removed from the sampling orifice. A syringe with a long needle was inserted in the orifice, keeping the needle point above the surface of the liquid. The syringe was filled with gas, removed from the flask, and emptied. This was repeated several times. The syringe was then inserted in the liquid and about one half to one milliliter of liquid drawn up. The syringe was removed from the flask, inverted, and the gas bubble driven out. The syringe was inserted into the flask again, and a quantity of liquid greater than the desired sample size drawn up. The Cheney-type adapter was then utilized to get a reproducible sample volume. The samples were then treated for the specific analysis desired. Ferrous ion was determined as an 1.10-phenanthroline complex by a procedure given in Appendix III. Glucose was separated from the rest of the

reaction mixture by paper chromatography. The glucose was eluted from the paper, then determined by a spectrophotometric method using alkaline ferricyanide as described in Appendix IV.

Early in the investigation of the system ferric ion-cellobiose, it was noticed that a time-dependent production of ferrous ion occurred. At this time, it was also noticed that the pH dropped a significant amount over the course of the reaction.

It is known that several metal ions attack glycols in acidic solutions with the production of a proton. Ceric ion (25) and manganic ion (22) are believed to react in this manner. Kaden and Fallab (29) mentioned that ferric ion reacts with dihydroxy compounds in the following manner:

$$Fe^{+3} + H_2Z \rightarrow Fe^{+2} + H^+ + HZ\cdot$$

Arndt, Loewe, and Ayca (23) presented evidence that ferric ion reacts with enediols with the formation of a proton for each ferric ion reduced. Drummond and Waters (22) have demonstrated that manganic ion does not oxidize olefinic compounds and monohydric alcohols. Since the ferric-ferrous couple is a much less powerful oxidizer than the manganic-manganous couple, it is assumed that the ferric ion attacks the enediols through the adjacent hydroxyl groups, forming a five-membered ring.

In order to see if the ferric ion system was analogous to the above systems, a series of qualitative spot tests were run for several polyhydroxy compounds. An 8% solution of the polyhydroxy compound in ferric sulfate stock solution (0.01 molar in ferric ion, total ionic strength 1.5 moles per liter, pH at room temperature 1.80) was used. The spot test used to judge the extent of the reduction of

ferric ion to ferrous ion was as follows: One drop of 0.1% o-phenanthroline solution was placed on a piece of filter paper and allowed to dry. Then one drop of the reaction mixture was placed on top of the dry spot. The resultant color was judged against the color developed by the reaction of glucose with ferric ion at the same reaction time. The relative rates of reaction were: ethylene glycol $\simeq$ inositol $<<$ sorbitol $<<$ glucose $<$ ribose. Based on the enediol requirement, sorbitol seemed to be out of place in this series. Two of the glycols, ethylene glycol and inositol, did not react with ferric ion, but sorbitol gave evidence of reaction.

The sorbitol used was chromatographed in 8:2:1 (ethyl acetate:pyridine:water) for two days. Upon spraying with p-anisidine hydrochloride, a reagent used for detecting reducing groups, a definite spot was obtained. This spot was within the general sorbitol spot obtained by spraying with permanganate-periodate.

It was concluded that the glycol groupings did not contribute to the reduction of the ferric ion. The potential carbonyl of the organic molecule was necessary for the reduction of ferric ion to proceed at an appreciable rate.

Cantor and Peniston (35) gave a listing of the amounts of the aldehyde form present in aqueous solution for various sugars, based on polarographic data. Later, others (36, 37) have stated that the quantities listed were too high, but that the relative order of the compounds was probably unaffected. The order given, with increasing ease of formation of the reducing form, was: glucose $<$ mannose $<$ galactose $<$ xylose $<$ arabinose $<$ ribose.

RESULTS

A study of the rate of formation of ferrous ion in various carbohydrate solutions was employed to determine the effect of the potential reducing group. The

determinations were run in the flask, described previously, designed to prevent oxygen from interfering with the reaction. The data from these experiments are given in Fig. 7. The relative rates of reaction were: solvent (0.01M ferric ion, 0.48M sodium sulfate, initial pH of 1.80 at room temperature) < cellobiose < glucose < galactose < ribose.

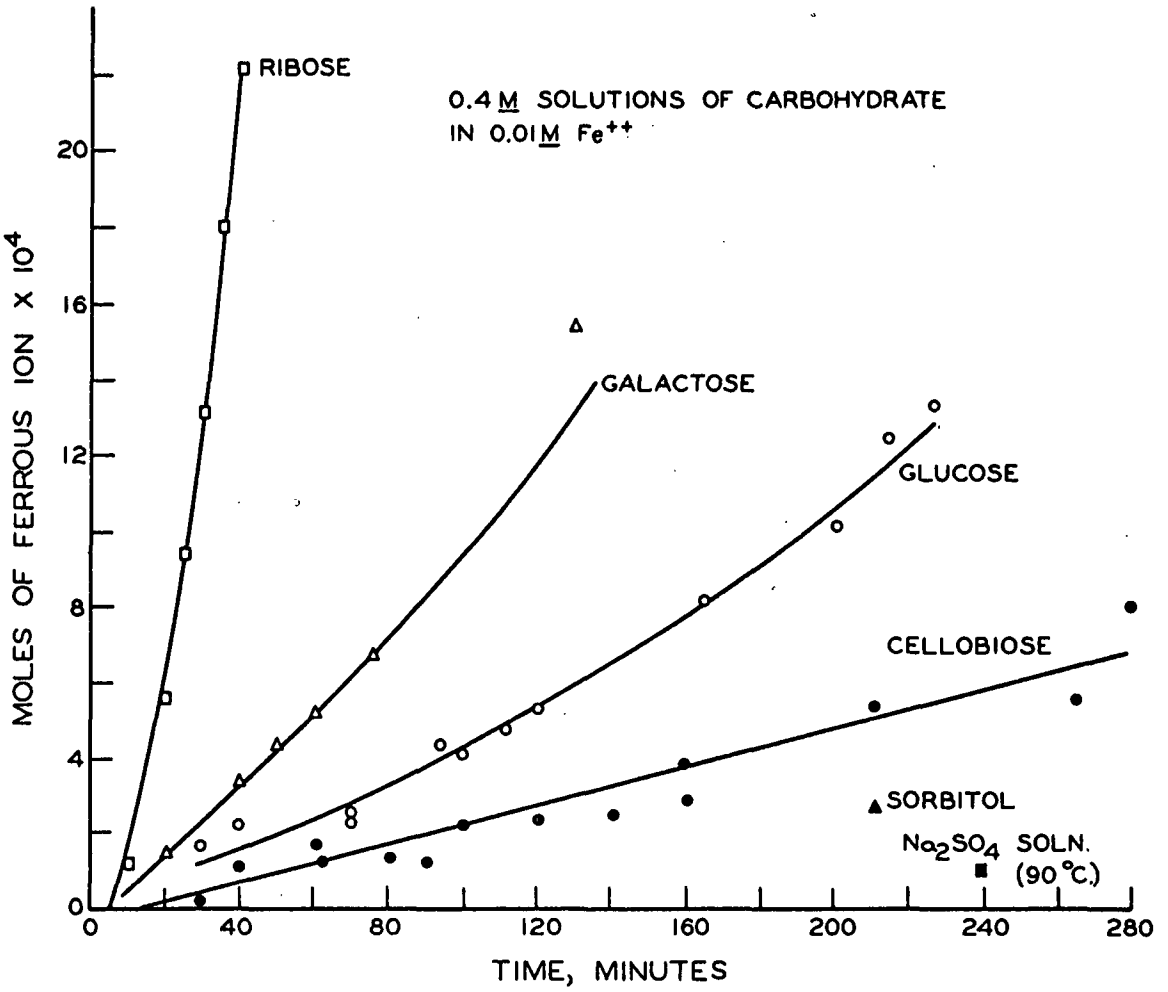

Figure 7. Reduction of Ferric Ion by Polyhydric Substances

The reaction between carbohydrates and ferric ion could not be described by a simple kinetic equation. The shape of the ferrous-ion-*vs.*-time curve, as given in Fig. 8, resembled that of the product curve of a set of consecutive reactions [e.g., see Glasstone (38)]. Residual oxygen in the solution would delay the appearance of the ferrous ion. However, the maximum amounts of oxygen that could possibly be present could not cause a delay as large as that shown in Fig. 8.

The rate of production of ferrous ion depends upon the quantity of glucose present. An experiment was carried out to determine the rate of consumption of glucose and the rate of formation of ferrous ion in a solution 0.01*M* in ferric ion and 0.02*M* in glucose. The data from this reaction are presented in Fig. 9. There was no change in the glucose concentration as measured by the procedure given in Appendix IV during the period when most of the ferric ion had been reduced. It is probable that the glucose actually was oxidized during the reaction with ferric ion, but the oxidation products were reduced by the hydrous ferrous oxide formed when the sample was treated to remove iron prior to chromatography. Therefore, the amount of cellobiose reacted may be calculated from the glucose determined by this method without correction for loss by oxidation.

If the complex of ferric ion with the carbohydrates occurred with the rapid ionization of the hydroxyl proton, the observed decrease in pH would be very rapid. An experiment was arranged so that the change in pH with time was recorded for a reaction of cellobiose with ferric ion. The results, as shown in Table II, indicate that the rate of change in the pH of the reaction mixture is about the same as the rate of reduction of the ferric ion. This result supports the theory that the decrease in pH of the solution results from the oxidation of the carbohydrate by the ferric ion. Another factor that affects the pH of the solution is the difference in the degree of hydrolysis of the ferric and ferrous ions. This

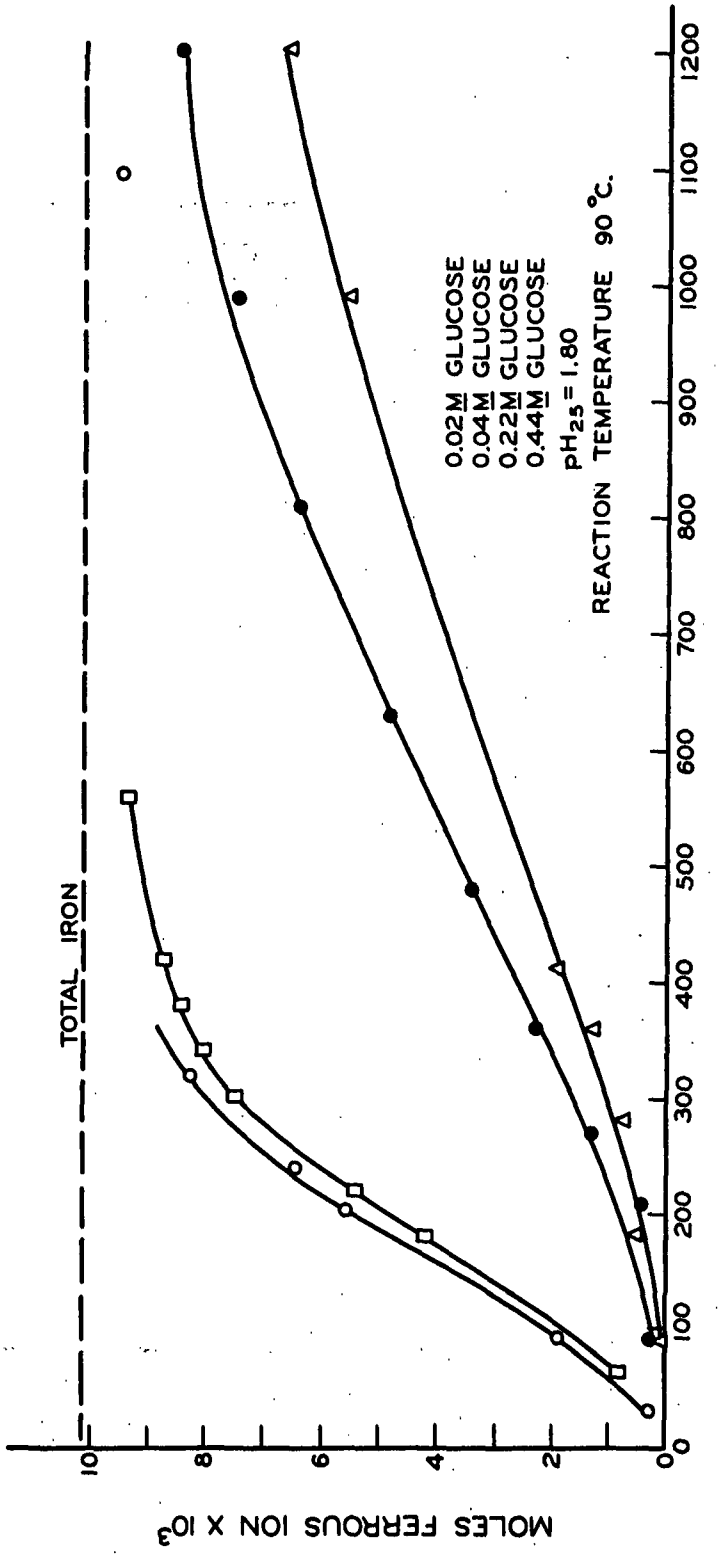

Figure 8. The Effect of Glucose Concentration Upon Ferric Ion Reduction

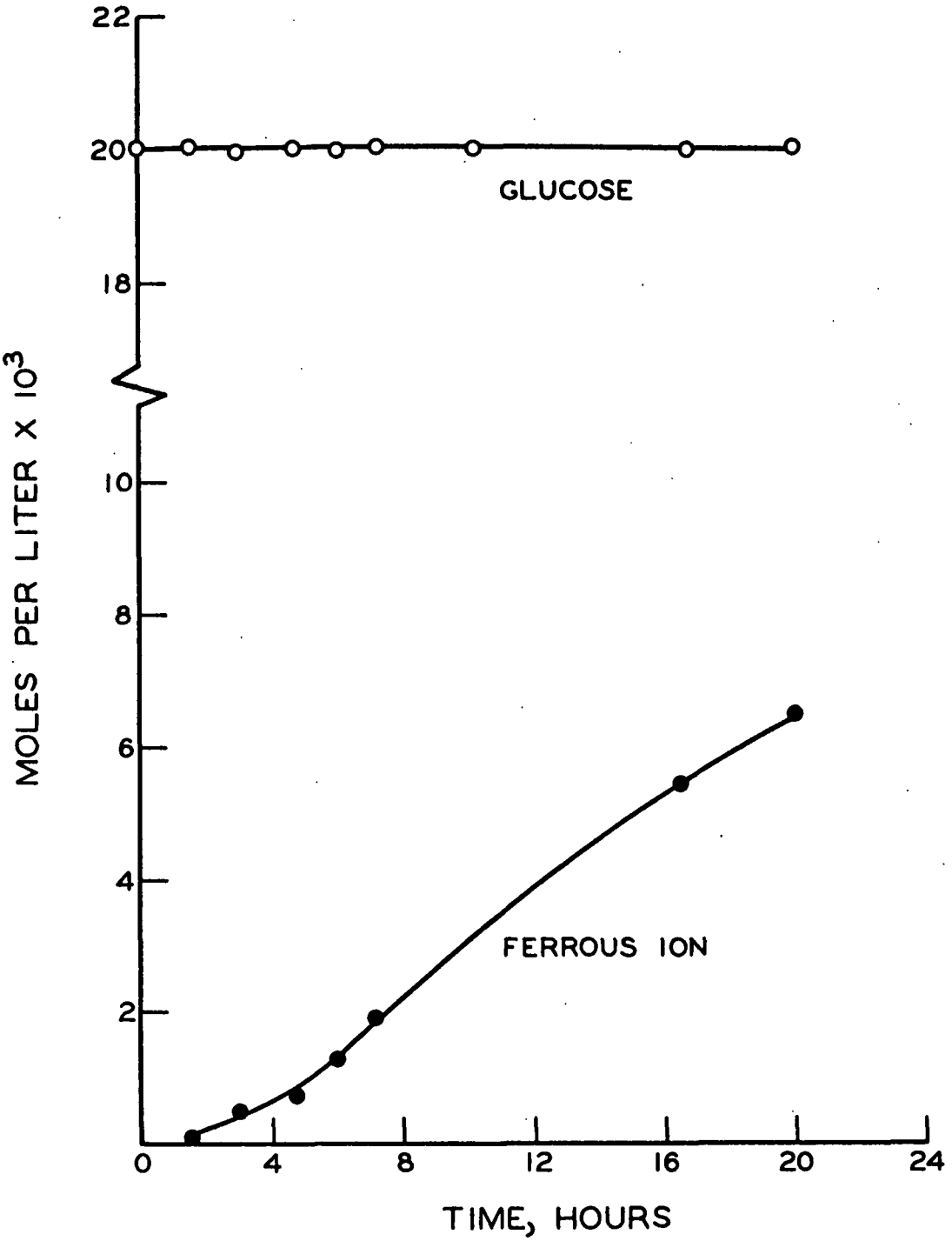

Figure 9. The Reaction of Glucose With 0.01M Ferric Ion at 90 ± 0.01°C., pH = 2.59, Ionic Strength = 1.5M

effect would be small because the ferric ion was hydrolyzed only to a minor extent under reaction conditions (p. 27). Since ferrous ion is less acid than the ferric ion, this effect would be opposite to the effect of the increase of proton concentration by oxidation.

TABLE II

THE DECREASE IN pH DURING THE REACTION OF CELLOBIOSE WITH FERRIC ION AT 90 ± 0.01°C.

Time, hr.	pH at 90°C.[a]	Fraction of Ferric Ion Reduced
0	2.59	0.000
0.50	2.60	0.020
5.00	2.55	0.303
11.00	2.57	0.730
23.00	2.52	> 0.910

[a]These values are for a particular trial, not averages, and therefore reflect the accuracy of the pH measurement as well as the experimental trend.

The following observations were made in these experiments:

1. Ferric ion was reduced to ferrous ion by aqueous solutions of carbohydrates.
2. Polyhydroxy alcohols did not reduce ferric ions.
3. The rate of reduction of the ferric ion increased with an increased amount of the aldehyde form of the carbohydrate available in solution.
4. The pH of the reaction mixture showed a definite decrease during the reduction of ferric ion to ferrous ion.

It was concluded that the glycol groups of the carbohydrates did not have a significant part in the reduction of the ferric ion. Therefore, only the reducing end of the carbohydrate molecule entered the reaction. It is probable

that the ferric ion does not react with the aldol form of the sugar as such, but reacts with the tautomeric enediol form (22, 23). There is some controversy whether the enediol form of the sugar can exist in acid solution. Speck (39) discussed this point and concluded that the enediol does exist in acid solutions, based on the isomerization of glucose in acids, and the known acid catalysis of enolization.

It was also concluded by analogy with data from the literature that the drop in pH occurred from the production of protons by oxidation of the carbohydrate by the ferric ions. (See the section on Oxidation of Some Organic Materials by Transition-Metal Ions, page 12.)

THE HYDROLYSIS OF CELLOBIOSE IN THE PRESENCE OF FERRIC ION

EXPERIMENTAL

The conditions, equipment, and methods used in carrying out these cellobiose hydrolysis experiments were the same as those discussed on page 26 for the experiments determining the reduction of ferric ion in the presence of carbohydrates. The extent of hydrolysis was determined by analysis of samples taken in the manner described on page 28.

The sample (1.03 ml.) to be used for analysis of glucose was neutralized to quench the reaction and remove most of the iron from the solution as the hydrous oxide before chromatographic separation of the carbohydrates. An appropriate amount of saturated sodium bicarbonate was placed in a 25-ml. Erlenmeyer flask from a semi-micro buret. The amount used was determined from the amount of the saturated sodium bicarbonate solution necessary to adjust 10 ml. of the reaction mixture to a pH of 5 to 6.

A small amount of analytical-grade Celite was placed in the same flask. The flask was flushed with nitrogen and covered with a serum bottle cap. The sample was added by syringe. The resultant iron hydroxide-Celite slurry was filtered through glass wool in a disposable pipet. The iron-free filtrate was then spotted on chromatographic paper for separation of the carbohydrates. The glucose fraction was analyzed quantitatively by an alkaline ferricyanide method given in Appendix IV.

There were several possible sources of catalysts for hydrolysis in the solutions:

1. Protons present from added sulfuric acid,
2. Protons from the hydrolysis of the metal ions,
3. Protons resulting from the oxidation of the organic substrate by the metal ion, and
4. The metal ion itself directly catalyzing the hydrolysis.

The initial pH of the hydrolysis solutions was held constant (1.80 at room temperature) in order to control the concentration of protons initially present in solution. Thus, if the results of the reaction of an iron-containing solution were to be compared to the results of a control containing no iron, Factors 1 and 2 above would be held constant, leaving the differences in the two reactions to be accounted for by Factors 3 and/or 4.

If the only sources of catalysts for hydrolysis of the glycosidic bond that are present in the iron-containing system and are not present in the control are the protons produced in the oxidation of the carbohydrates and/or the direct acidic effect of the metal ion, the results would follow a predictable course. The hydrolysis of glycosides is a first-order reaction (9). The first-order rate equation for this reaction may be written as:

$$d(G)/dt = -k(G) \qquad (1)$$

where

($\underline{G}$) = concentration of glycoside, and

$\underline{k}$ = first-order reaction rate constant.

Acidic-Metal-Ion Catalytic Effect

In the case where the acidic metal ion acting as a Usanovich acid is the only additional factor, the rate expression is:

$$d(C)/dt = -k_H(C) - k_U(C) = -(k_H + k_U)(C) \qquad (2)$$

where

($\underline{C}$) = concentration of cellobiose

$\underline{k_H}$ = first-order rate constant, a function of the hydrogen ion concentration

$\underline{k_U}$ = first-order rate constant, a function of the Usanovich acid concentration

$\underline{t}$ = time in seconds.

This equation would integrate to:

$$\ln (C)/(C_o) = -(k_H + k_U)t \qquad (3)$$

where ($\underline{C_o}$) equals the initial concentration of cellobiose.

Thus, a plot of the negative logarithm of ($\underline{C}$)/($\underline{C_o}$) vs. time would yield a linear function with a slope greater than the slope of the control-reaction plot by the additional factor $\underline{k_U}$.

Protons-from-Oxidation Catalytic Effect

The reaction rate constant would vary if the hydrolysis were accelerated only by the protons produced in the oxidation of the carbohydrate by the ferric

ion with no catalytic effect by the metal ion *per se*. Since hydrolysis is monomolecular only at the rate-determining step (Fig. 1) and depends upon the concentration of hydrogen ions (9), Equation (1) may be rewritten:

$$d(C)/dt = -k'(H)(C) \qquad (4)$$

where

k' = first-order rate constant, independent of the hydrogen ion concentration, and

(H) = concentration of hydrogen ions.

In this case, the concentration of hydrogen ions is not constant, but increases with time until the ferric ion is all reduced to the ferrous state and then remains constant. Therefore, Equation (4) can be expressed for this system as:

$$d(C)/dt = -k'[(H_i) + (H_t)](C) \qquad (5)$$

where

(H_i) = initial concentration of hydrogen ion, and

(H_t) = concentration of hydrogen ion that is a function of ferric ion concentration and time.

This equation may be integrated to the form:

$$\ln (C)/(C_o) = -k'[(H_i)t - \int_o^t (H_t)dt] \qquad (6)$$

where (H_t) varies from zero to (Fe_o), the initial ferric ion concentration.

In this case, a plot of the logarithm of $(C)/(C_o)$ vs. time does not yield a straight line. The initial slope is equal to that of the control hydrolysis of the same initial pH. The final slope is equal to that of a control hydrolysis with the pH adjusted to equal the final pH of the iron-containing hydrolysis.

RESULTS

Three sets of hydrolyses of cellobiose were carried out. All were in a solution of the same ionic strength (1.5M). The first two were of the same initial pH (2.59 at 90°C.); the first was 0.01M in ferric ion, while the second (defined as a control) contained no ferric ion. The third hydrolysis, also a control, had a pH of 2.50 at 90°C., the final pH of the iron-containing hydrolysis. The data from these reactions are presented in Fig. 10, 11, and 12. The functions plotted in these figures had small, negative intercepts. The failure of the function to pass exactly through the origin may be attributed to the small amount of reaction occurring during the time required for the reaction vessel and contents to heat up. The rate constants are presented in Table II.

TABLE II

THE EFFECT OF FERRIC ION UPON THE REACTION RATE CONSTANT OF THE HYDROLYSIS OF CELLOBIOSE AT 90°C.

(Ionic strength adjusted to 1.5M with sodium sulfate)

Fe^{+3} Content, M	pH at 90°C.		First-Order Rate Constant, k $sec.^{-1} \times 10^6$
	Initial	Final	
0.00	2.59	2.59	1.02 ± 0.04
0.01	2.59	2.51	1.33 ± 0.02
0.00	2.50	--	1.32 ± 0.03

The iron-containing hydrolysis gave a plot of the logarithm of $(C)/(C_o)$ vs. time which was linear to the origin with a slope greater than that of the control hydrolysis at the same initial pH. However, the pH decreased, indicating that the conditions existing in the reaction were not valid for the case described by Equation (2) for the acidic-metal-ion catalytic effect. The decrease in pH resulted from the reduction of the iron from the ferric to the ferrous state, with the

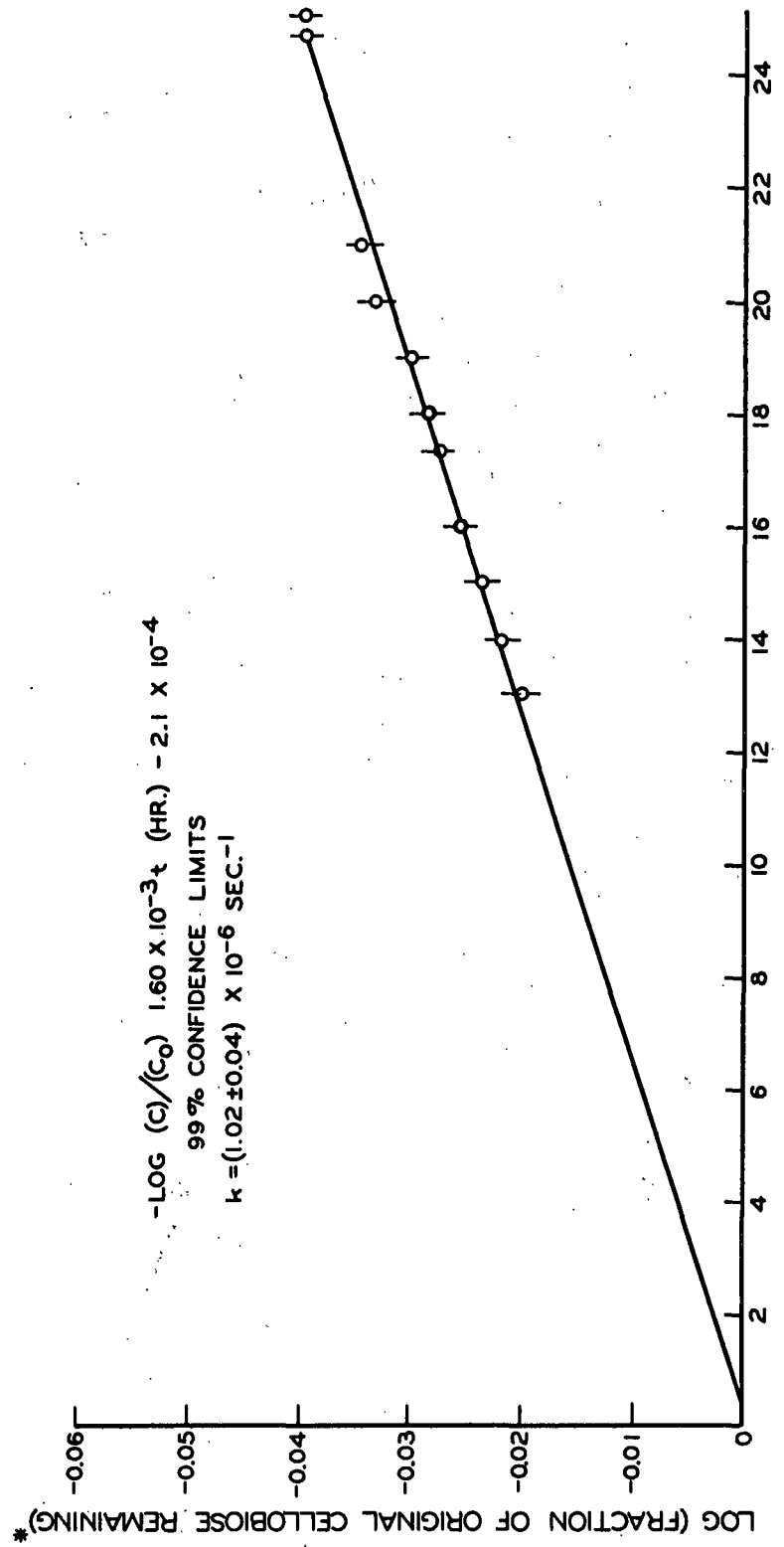

Figure 10. Hydrolysis of Cellobiose at: 90°C., No Ferric Ion, pH = 2.59, Ionic Strength = 1.5M

*Calculated from glucose production data as described in Appendix V.

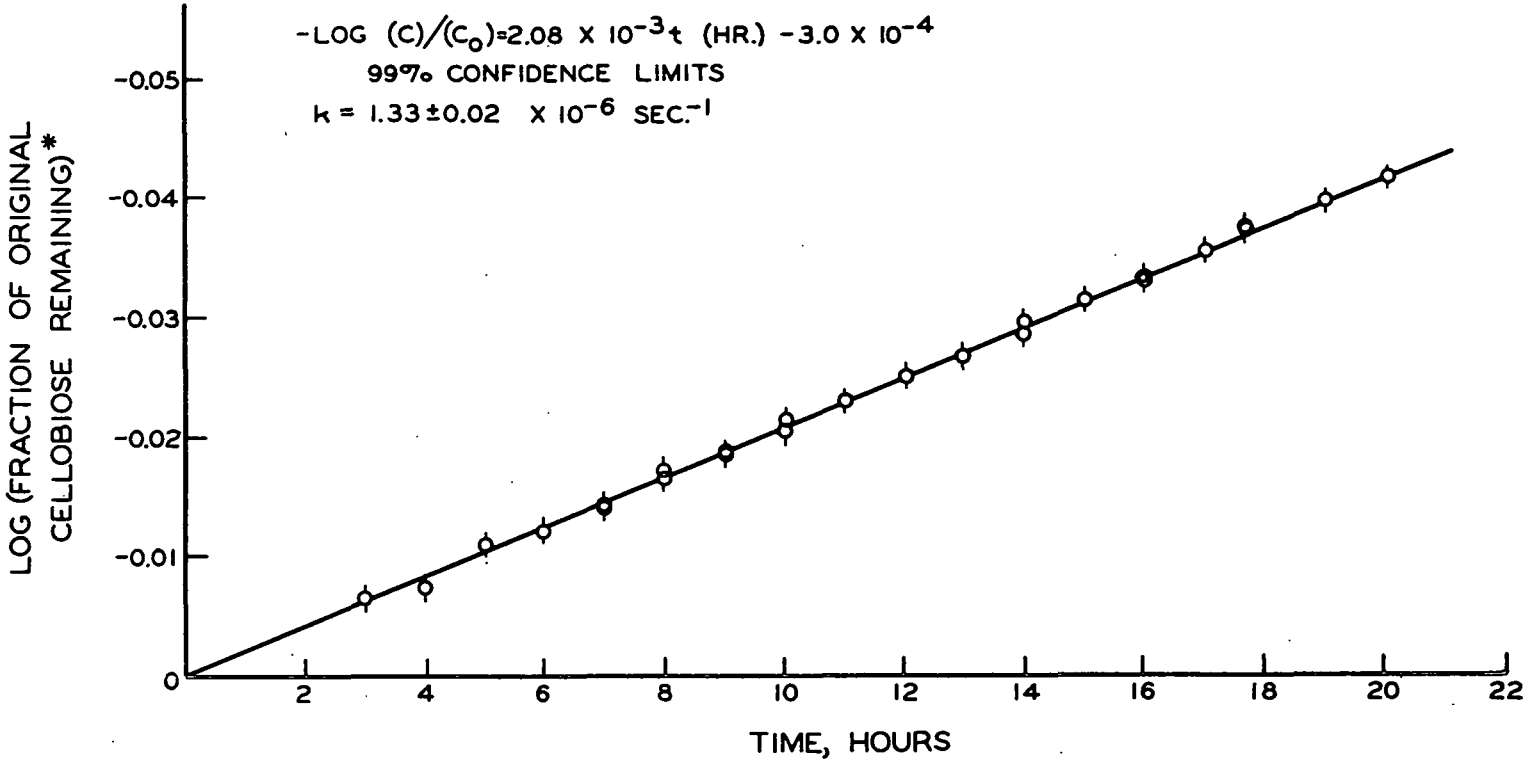

Figure 11. Hydrolysis of Cellobiose at: 90°C., Ferric Ion (0.01M), pH = 2.59, Ionic Strength = 1.5M

*Calculated from glucose production data as described in Appendix V.

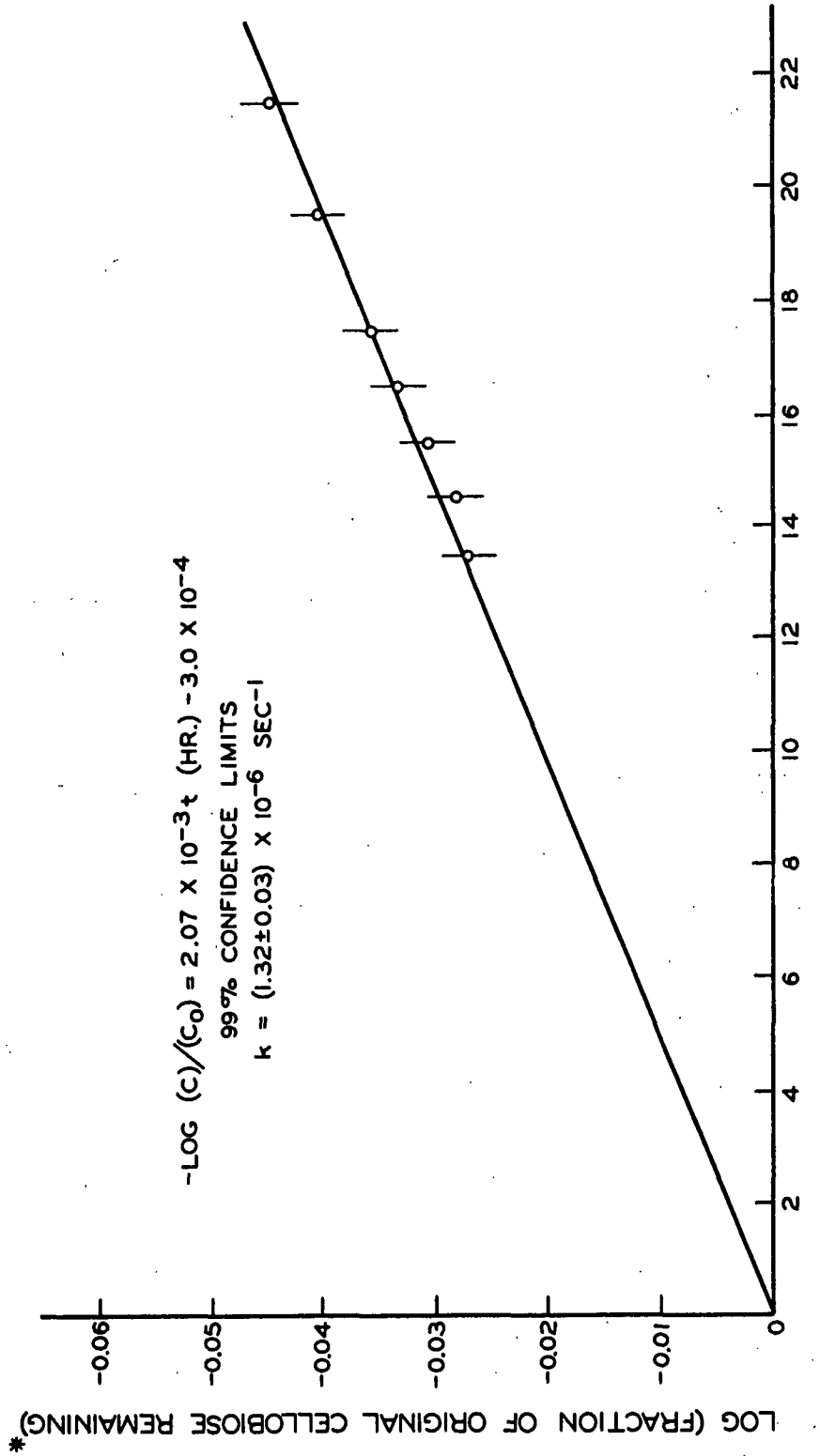

Figure 12. Hydrolysis of Cellobiose at: 90°C., No Ferric Ion, pH = 2.50, Ionic Strength = 1.5M

*Calculated from glucose production data as described in Appendix V.

resulting mole-for-mole production of protons. Since the initial and final hydrolysis rate constants are identical, the conditions for the case described in the section Protons-from-Oxidation Catalytic Effect (p. 38) are not maintained in this reaction. It is apparent that both of the previously described catalysts, metal ions and protons from oxidation, play a part in this reaction.

It is further noted that the reaction rate constant of the ferric-ion-containing hydrolysis of cellobiose is identical with the rate constant for the control hydrolysis that had an initial pH equal to the final pH of the ferric-ion-containing reaction. From this, it is concluded that the ferric ion has exactly the same effect upon the hydrolysis of cellobiose as the hydrogen ion. These data imply that the ferrous ion has no catalytic effect upon the hydrolysis of cellobiose.

A second possible explanation for the linearity of the first-order-rate plot for the hydrolysis containing ferric ion is that the hydrolysis of cellobiose is a general acid-catalyzed reaction. If this were the case, the hydrated ferric ion would catalyze the reaction by proton donation. However, the hydrolysis of glycosides is thought to be specific acid-catalyzed (9, 40), based on the linear relationship of the logarithm of the reaction rate constant to the Hammett acidity function.

There is a third possibility for the relationship of the ferric ion and the catalysis of hydrolysis of the glycosidic bond. In this case the ferric ion would oxidize the cellobiose, creating a product with an unstable glycosidic bond which would hydrolyze very rapidly. The increase in the hydrolysis of cellobiose in the system containing ferric ion should have a one to one relationship with the reduction of the ferric ion. The oxidized portion of the hydrolyzed cellobiose would be reduced in the separation procedure, so that the method used for analysis of

glucose would be a valid measure of the rate of cellobiose loss. Comparative data on the ferrous ion production and the increase in the cellobiose reacted in the ferric-ion-containing reaction over the control reaction are presented in Table III.

TABLE III

RELATIONSHIP OF FERROUS ION FORMATION AND INCREASE OF CELLOBIOSE HYDROLYSIS

Time, hr.	Ferrous Ion, g.-ion/l.	Cellobiose, M (increase over control)
5.00	0.00309	0.0012
6.00	0.00392	0.0016
9.83	0.00685	0.0024
12.00	0.00805	0.0030
17.12	0.00929	0.0041

The Effect of Ferrous Ion Upon the Hydrolysis of Cellobiose

It was necessary to obtain data on the effect of ferrous ion upon the hydrolysis of cellobiose since the hydrolysis of cellobiose in the presence of ferric ion has been shown to be concurrent with the reduction of ferric ion to ferrous ion. The conditions used in these experiments were intended to be representative of the entire reaction period when ferrous ion was being produced. The initial pH of the reaction mixtures containing ferric ion was 2.59; the final pH was 2.51. The pH of 2.54 was selected for the hydrolysis system containing ferrous ion. The ionic strength was adjusted to the value used previously, 1.5M. A hydrolysis of cellobiose at the same pH was used for a control. The data are presented in Fig. 13 and 14. The resultant reaction rate constants, given in Table IV, show that the ferrous ion had no significant effect upon the hydrolysis of cellobiose.

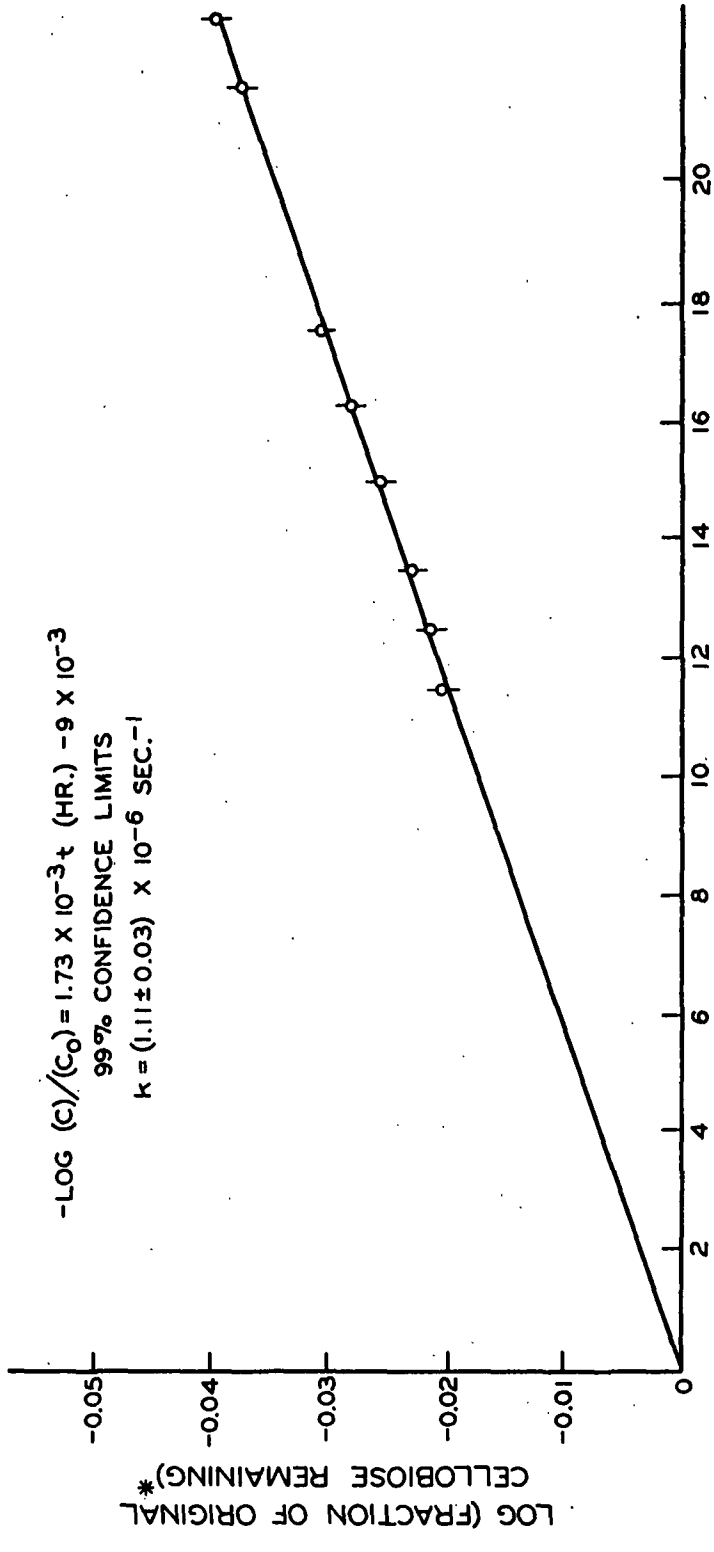

Figure 13. Hydrolysis of Cellobiose at: 90°C., No Ferrous Ion, pH = 2.55, Ionic Strength = 1.5M

*Calculated from glucose production data as described in Appendix V.

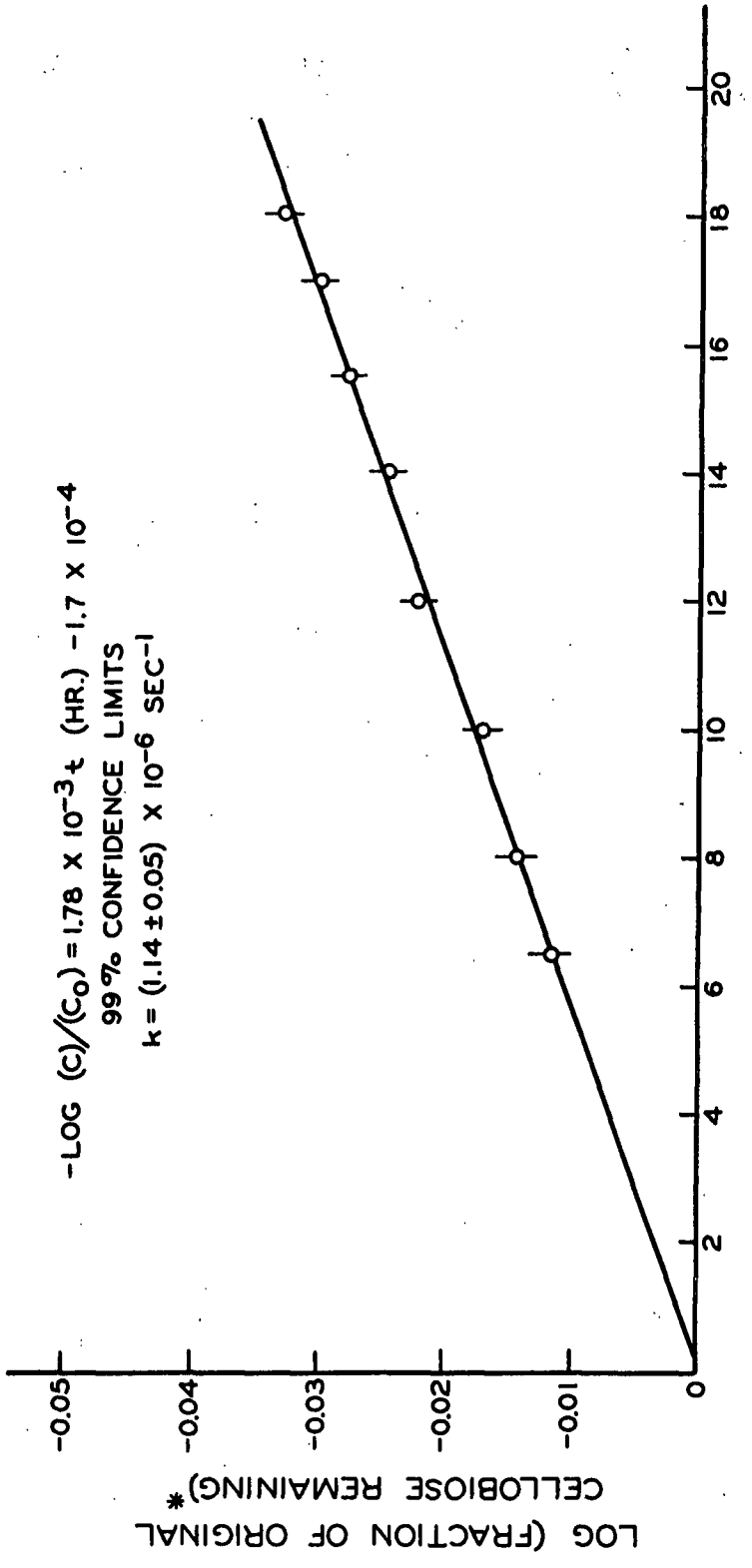

Figure 14. Hydrolysis of Cellobiose at: 90°C.,
Ferrous Ion (0.01M), pH = 2.54, Ionic Strength = 1.5M

*Calculated from glucose production data as described in Appendix V.

Although the rate constants are statistically identical, the slightly higher value is in line with the corresponding slightly lower pH.

TABLE IV

THE EFFECT OF FERROUS ION UPON THE REACTION RATE CONSTANT FOR THE HYDROLYSIS OF CELLOBIOSE AT 90°C.

(Ionic strength adjusted to 1.5M with sodium sulfate)

Fe^{+2} Content, M	pH at 90°C.	First-Order Rate Constant, k $sec.^{-1} \times 10^6$
0.00	2.55	1.11 ± 0.05
0.01	2.54	1.14 ± 0.03

The Effect of the Sodium Sulfate Upon the Acceleration of Hydrolysis of Cellobiose by Ferric Ion

Two trials were made to examine the reaction systems in the absence of the sodium sulfate used to adjust the ionic strength. The data are shown in Fig. 15 and 16. The rate constants listed in Table V show that the ferric ion maintained, and possibly enhanced, its catalytic effect in the absence of the sodium sulfate. The increased activity may have been due to the increased effective ferric ion concentration (less ion pair formation, due to lower sulfate ion concentration) or to the different relative amounts of the hydrolysis states of the ferric ion. Increased amounts of precipitate in the heated ferric ion solution indicated that more of the ferric ion was present as the $FeOH^{+2}$ ion pair (34).

TABLE V

THE EFFECT OF FERRIC ION UPON THE REACTION RATE CONSTANT OF THE HYDROLYSIS OF CELLOBIOSE AT 90°C. IN THE ABSENCE OF SODIUM SULFATE

Fe^{+3} Content, M	Ionic Strength, M	pH at 90°C.	First-Order Rate Constant, k $sec.^{-1} \times 10^6$
0.00	0.05	2.01	2.16 ± 0.10
0.01	0.08	1.98	3.67 ± 0.10

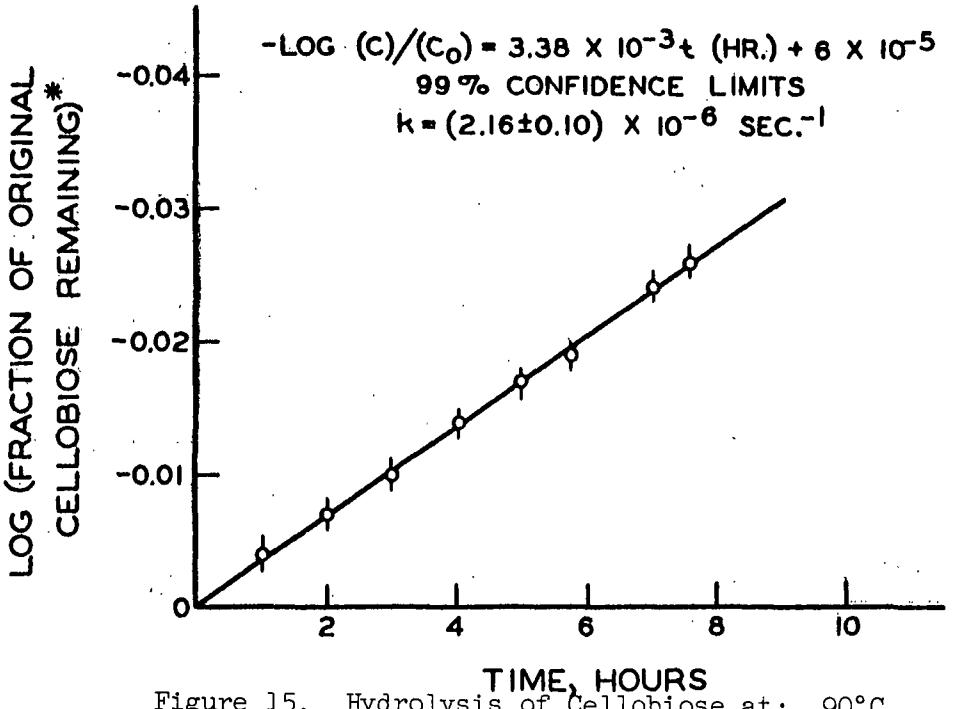

Figure 15. Hydrolysis of Cellobiose at: 90°C., No Ferric Ion, pH = 2.01, Ionic Strength = 0.05M

*Calculated from glucose production data as described in Appendix V.

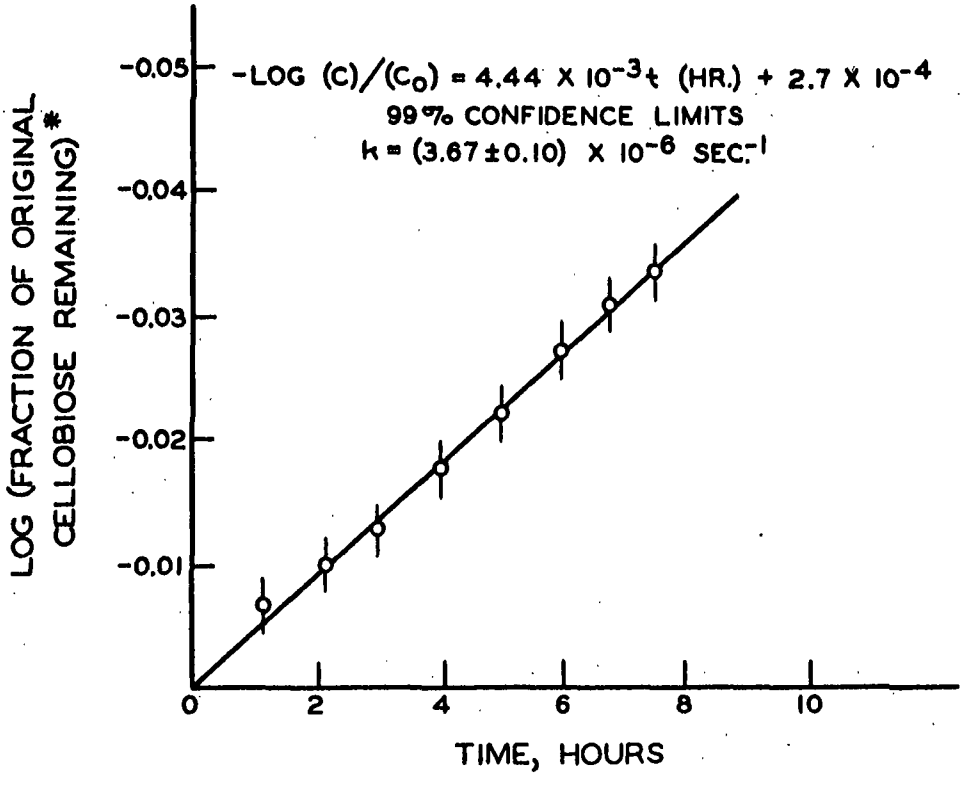

Figure 16. Hydrolysis of Cellobiose at: 90°C., Ferric Ion (0.01), pH = 1.98, Ionic Strength = 0.08M

*Calculated from glucose production data as described in Appendix V.

The following observations were made on the influence of the ferric ion upon the hydrolysis of cellobiose. A system containing:

1. an increasing quantity of protons, a known catalyst for the hydrolysis of glycoside,
2. a decreasing quantity of ferric ion, and
3. several inert materials (sodium sulfate, ferrous ion)

had a first-order reaction rate constant for the hydrolysis of cellobiose that did not vary with time. The rate constant for the hydrolysis of cellobiose in a system containing ferric ion was greater than the rate constant in a control system at the same initial pH containing no ferric ion. However, a control system with an initial pH equal to the final pH of the ferric-ion-containing reaction system had a rate constant for the hydrolysis of cellobiose that was identical to the rate constant in the ferric-ion-containing system.

The conclusions drawn from these facts are as follows:

1. The ferric ion is responsible for the increase in the rate of hydrolysis, both directly and indirectly.

2. The acidity of the ferric ion, as measured by its effect upon the hydrolysis of cellobiose, is equal to that of the proton. The initial rate constant of hydrolysis was equal to the rate constant later in the reaction when the ferric ion had been replaced by a ferrous ion and a proton.

3. The direct catalytic activity of the ferric ion is due to that part of the acidity of the ion that is not described by the Lewis theory of acids, but is covered by the Usanovich theory.

The Usanovich theory of acids extends the Lewis theory by recognizing that oxidizing power is a description of the affinity of a substance for electrons. It is this affinity for electrons beyond that which is necessary for the formation of

a simple co-ordinate bond between the metal ion and the carbohydrate that causes a sufficient shift in electron density at the glycosidic bond to permit hydrolysis to occur.

This last conclusion is based on the fact that the ferrous ion, the acidity of which is described completely by the Lewis theory, does not catalyze the hydrolysis of cellobiose. However, it is not known whether the ferrous ion complexes with cellobiose, although the ferrous ion is known to complex with other oxygen-group electron donors (29). The zinc ion is known to complex with glucose (41), and its acidity, like that of the ferrous ion, is adequately described by the Lewis acid concept, since the zinc ion is a very weak oxidizing agent.

THE EFFECT OF ZINC ION UPON THE HYDROLYSIS OF CELLOBIOSE

Kasbekar (42) hypothesized that a complex formed between $ZnCl^+$ and the glycosidic oxygen of cellulose. This complex was thought to be responsible for the loss in D.P. which occurs when cellulose is treated with vulcanizing-strength zinc chloride solution.

Jones (43) refuted the idea that zinc chloride accelerates hydrolysis of cellulose. He used an anthrone method to estimate the cellulose in solution in an aqueous zinc chloride solvent. Complete recovery could not be obtained until the cellulose solution was added into ethyl alcohol to separate the cellulose from the zinc chloride before the hydrolysis step. Dorcheus (44) found that zinc chloride did not interfere with the determination of monomeric glucose by the anthrone method, so the conclusion seems logical that zinc chloride retarded the hydrolysis of cellulose.

Snell (44) looked for a complex of zinc sulfate and glucose by the isopiestic method. The differences in vapor pressure from the predicted ideal were small but

significant, indicating the presence of at least one complex. This complex was interpreted as having the ratio of two zinc ions to each glucose molecule. It is assumed that zinc sulfate would also complex with cellobiose.

A hydrolysis of cellobiose was run in the presence of 0.01M zinc sulfate in order to show that complexing alone was not sufficient to accelerate the hydrolysis reaction. The data are presented in Fig. 17. The results, as given in Table VI, indicate that the zinc ion does not have an accelerating effect upon the hydrolysis of cellobiose. The difference in the means of the reaction rate constants may be attributed, at least partially, to the slight difference in pH of the reactions.

TABLE VI

THE EFFECT OF ZINC ION UPON THE REACTION RATE CONSTANT OF THE HYDROLYSIS OF CELLOBIOSE AT 90°C.

(Ionic strength adjusted to 1.5M with sodium sulfate)

Zn^{+2} Content, M	pH at 90°C.	First-Order Rate Constant, k, $sec.^{-1} \times 10^6$
0.00	2.59	1.02 ± 0.04
0.01	2.62	0.95 ± 0.07

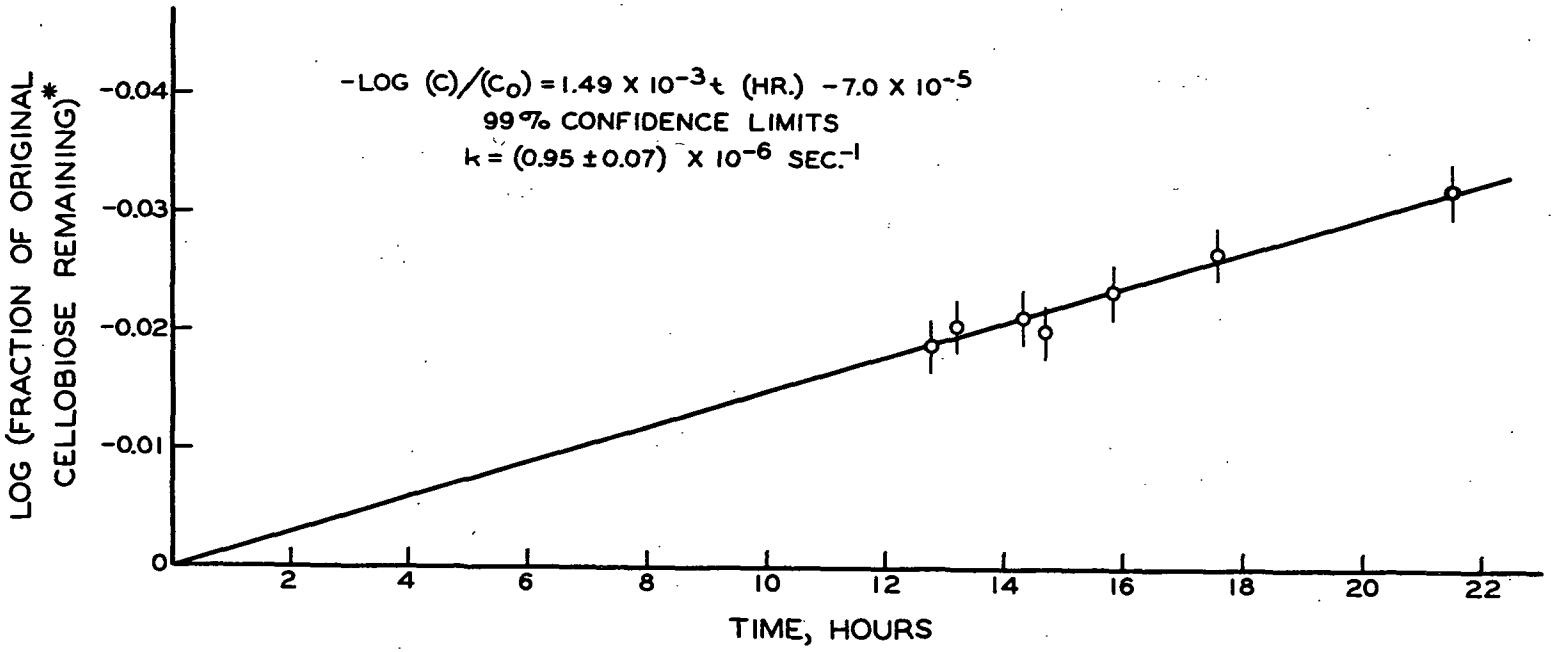

Figure 17. Hydrolysis of Cellobiose at: 90°C., Zinc Ion (0.01M), pH = 2.62, Ionic Strength = 1.5M

*Calculated from glucose production data as described in Appendix V.

INTERPRETATION OF RESULTS

Ferric ion affects the acid hydrolysis of cellobiose in two ways:

1. The hydrolysis is accelerated directly by the ferric ion acting as an Usanovich acid.

2. Cellobiose and the hydrolysis reaction product, glucose, are both oxidized by the ferric ion with the production of protons.

Both of these reactions are initiated by the complexing of the ferric ion to the carbohydrate, probably at different sites based on the present interpretations of these two reactions. The structure of cellobiose presents many electronegative sites to a strongly electropositive metal ion such as the ferric ion. The glycosidic bond, in particular, is surrounded by sterically accessible oxygen atoms as shown in Fig. 18 and 19.

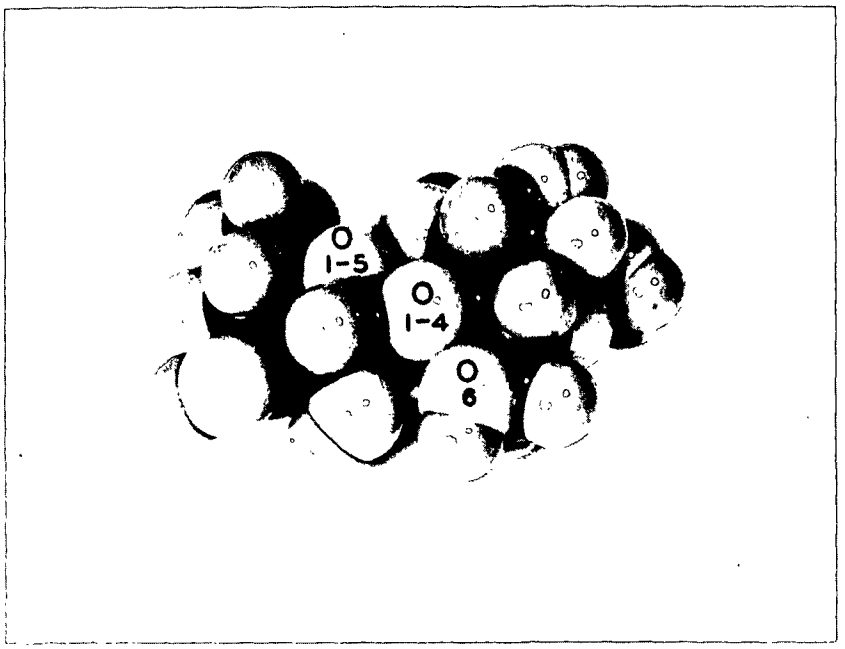

Figure 18. Hirschfelder Model of Cellobiose

(The numbered oxygen atoms refer to the positions in Fig. 19.)

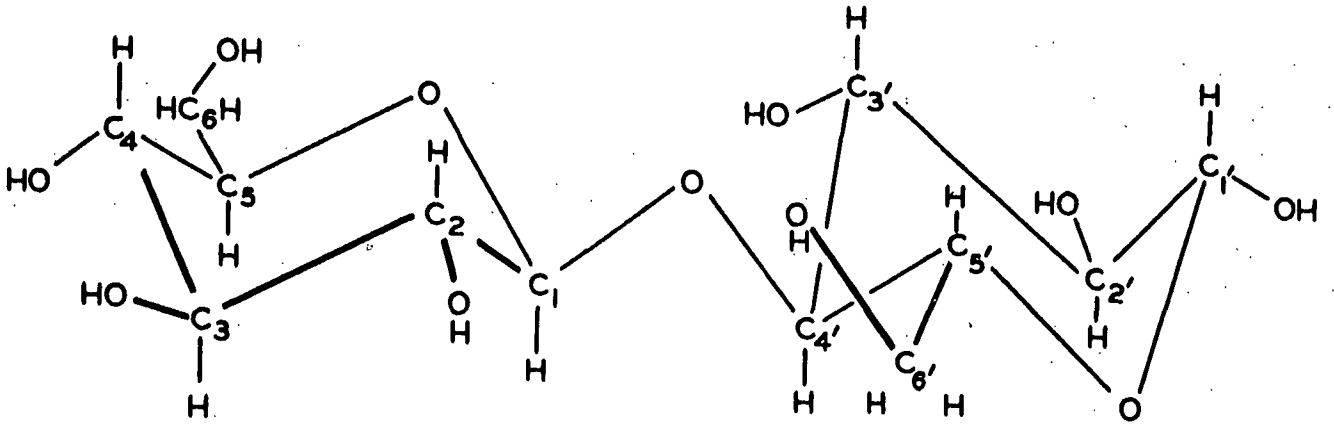

Figure 19. Configuration of Cellobiose

PATHWAYS FOR THE HYDROLYSIS OF CELLOBIOSE BY FERRIC ION

The primary hydroxyl group on the 6-carbon of the aglycon, glucose, can be positioned so that a six-membered ring can be formed by complexing the ferric ion with the oxygen of the primary alcohol and the oxygen of the glycosidic bond as in Fig. 20.

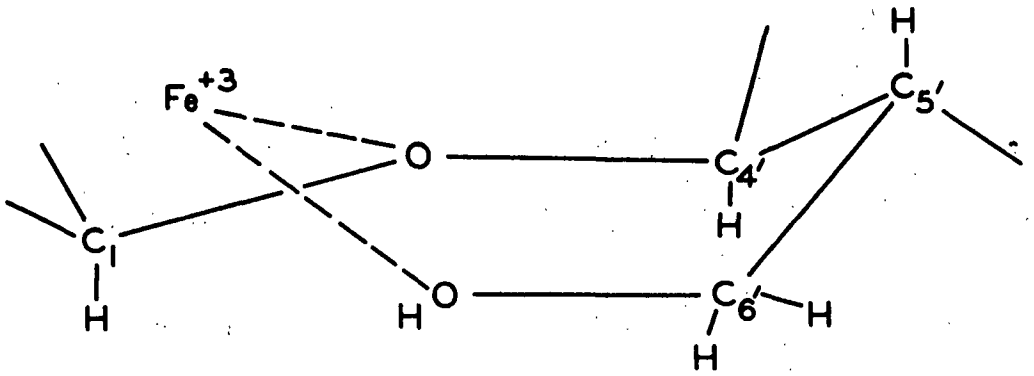

Figure 20. Schematic Diagram of a Possible Configuration of a Ferric Ion Complex of Cellobiose

This complex could act to affect the electron density at the glycosidic bond in a manner similar to that proposed for the cyclic carbonium-ion intermediate in Fig. 1. This same pathway using a ferric ion instead of a proton is shown schematically in Fig. 21.

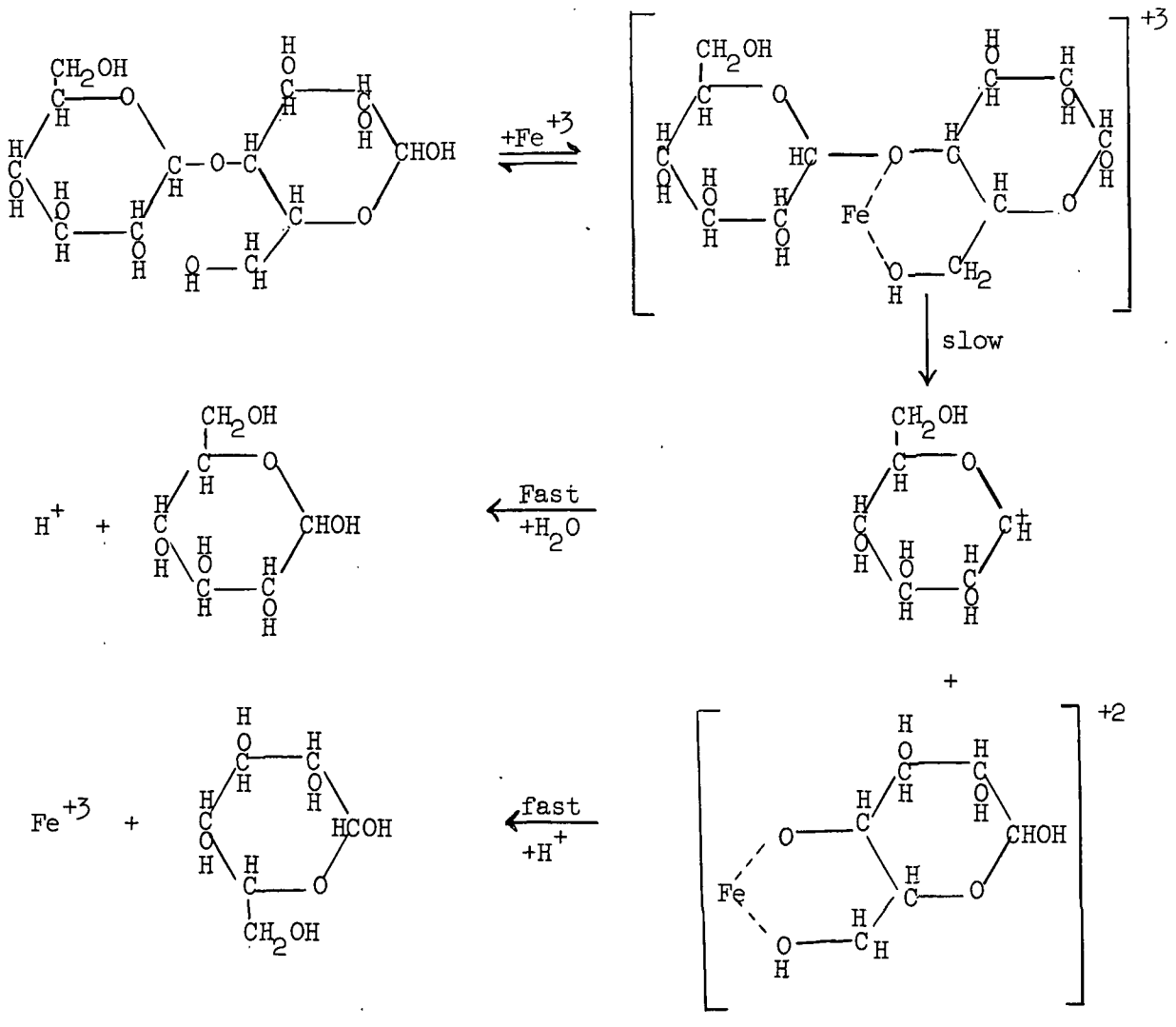

Figure 21. Proposed Pathway for the Ferric-Ion-Catalyzed Hydrolysis of Cellobiose

There is less possibility that the ferric ion could influence hydrolysis of the glycosidic bond through a complex formed with the glycosyl moiety of the cellulose. With the exception of a complex formed at the ring oxygen of the glycopyranoside group, the ferric ion would have to transmit its effect on the electrons through several bonds in order to reach the glycosidic bond.

However, the possibility exists that the ferric ion could form a bidentate complex with the primary hydroxyl on the 6-carbon and the ring oxygen of the glucopyranoside. The resultant complex could cause hydrolysis to occur through the

acyclic carbonium-ion intermediate as given in Fig. 1. This same pathway using the ferric ion instead of the proton is shown schematically in Fig. 22.

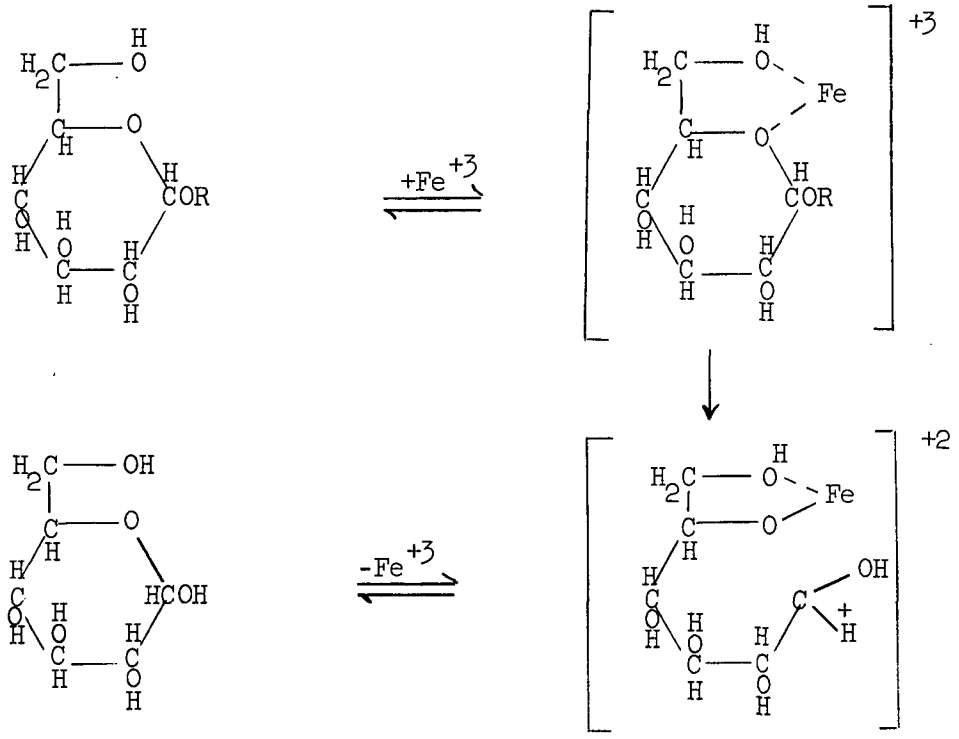

Figure 22. Proposed Pathway for the Ferric-Ion-Catalyzed Hydrolysis of Cellobiose

The relative degree of reaction that is due to each pathway could be studied by working with different glycosides. The pathway that results from the ferric complex with the aglycon could be demonstrated by using a suitable compound such as 4-O(β-D-xylopyranosyl)-D-glucose. The pathway resulting from the glucose complex could be evaluated by using a glucoside with a simple aglycon such as methyl glucoside.

A PATHWAY FOR THE OXIDATION OF CARBOHYDRATES BY FERRIC ION

It is hypothesized that the oxidation by the ferric ion of the carbohydrates studied in this work occurred through the enediol form of the sugar. The initial steps leading to the oxidation of glucose would be:

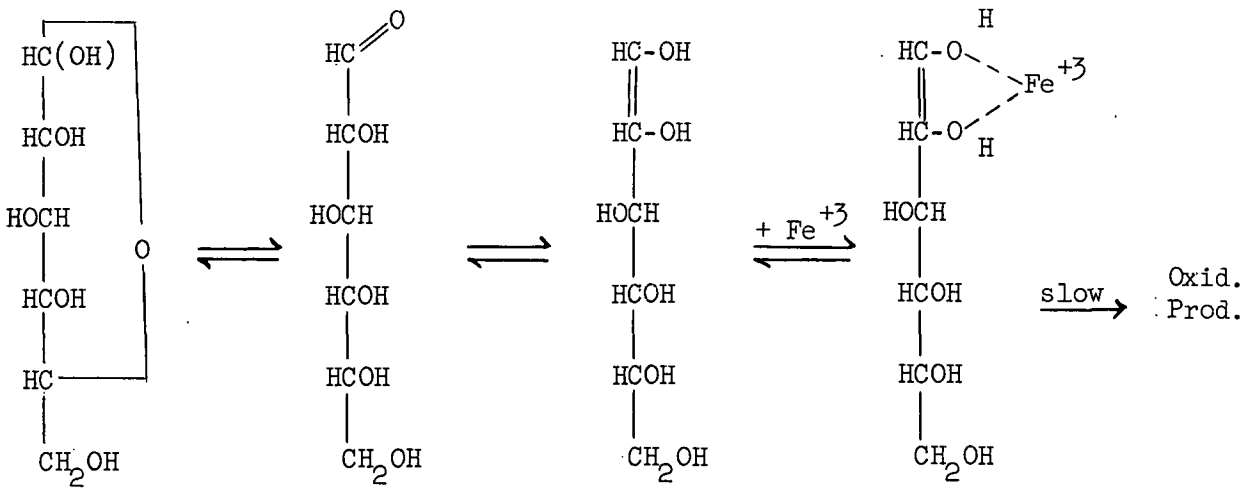

This study did not attempt to determine the nature of the reaction products.

INTERPRETATION OF REACTION IN THE FERRIC ION-CELLULOSE SYSTEM IN AIR

The hydrolysis of cellobiose in the presence of 0.01M ferric ion had a rate constant 30% higher than a hydrolysis of cellobiose under similar conditions without the ferric ion. Yet, Czepiel (5) showed that cellulose aged in the presence of ferric ion could show a degradation 300% greater than a similar sample without ferric ion. There are at least three possible explanations for this apparent discrepancy.

First, the comparative reactions (ferric-ion-containing and control) in the homogeneous system were comparatively easy to adjust to similar initial conditions. The cellulose-water-air system, however, defies a definition or a measurement of hydrogen ion concentration. Hence, the control could not compensate for the protons produced by hydrolysis of the metal ion.

Second, the hydrolysis of the glycosidic bond due to ferric ion might be a larger proportion of the total hydrolysis if it were compared to the hydrolysis of the glycosidic bond at a pH several units higher than used in this study.

Third, much more oxygen was present in Czepiel's work than in this study. Possibly, consecutive reactions could occur as follows:

$$R + Fe^{+3} \longrightarrow Fe^{+2} + \text{Oxid.} + H^{+}$$

$$2Fe^{+2} + \frac{1}{2}O_2 + 2H^{+} \longrightarrow 2Fe^{+3} + H_2O.$$

These reactions would account for a constant rate of hydrolysis and a constant rate of oxidation of cellulose. The total rate of degradation would be much greater than that occurring in an oxygen-free system.

It might be said that the oxidizing portion of the reactions being discussed here has no bearing on the reactions taking place in cellulose, since the ideal cellulose molecule has only one group that can form the enediol structure, and that group is at one end of the chain. However, it is recognized that natural cellulose has some carbonyl groups at the 2- and/or 3-carbon positions of the anhydro-glucopyranoside ring. These α-hydroxy-carbonyl groupings would be capable of forming reactive intermediates with the ferric ion.

ACKNOWLEDGMENTS

The author would like to express his appreciation to his committee, Dr. E. J. Jones, Mr. E. E. Dickey, and Dr. D. G. Williams for the advice and encouragement offered throughout this investigation.

The author also wishes to thank:

Dr. A. P. Dunlop of the Quaker Oats Company for consultation and a sample of 5-hydroxymethylfurfural.

Dr. M. L. Wolfrom, Dr. K. Ward, Jr., and Dr. J. W. Green for consultation.

LITERATURE CITED

1. Perti, S. L., Ranganathan, S. K., Subraman, T. S., and Sud, L. R., Nature 163, no. 4153:877-8(1949).

2. Bell, W. A., and Gibson, J. M., Nature 180:1065(1957).

3. Sihtola, H., Hentola, Y., Somer, V., Saarinen, A., Wigren, G., and Ulmanen, T., Paperi ja Puu 40:549-54(1958).

4. Langwell, W. H., Tech. Bull. Tech. Sect., Brit. Paper and Board Makers' Assoc. 29:21-8(1952); 29:52(1952); 30:170(1953); 36:199-207(1955).

5. Czepiel, T. P. The influence of selected metal traces on the color and color stability of purified cotton linters. Doctor's Dissertation. Appleton, Wis., The Institute of Paper Chemistry, 1959.

6. Young, K. P., Contrib. Inst. Chem., Nat'l. Acad. Peiping 1:171-80(1934); C.A. 29:2738.

7. Torii, J., J. Soc. Chem. Ind. Japan 46:26-31(1943); C.A. 43:19781.

8. McIntyre, D., and Long, F. A., J. Am. Chem. Soc. 76:3240-7(1954).

9. Bunton, C. A., Lewis, T. A., Llewellyn, D. R., and Vernon, C. A., J. Chem. Soc. 1955:4419-23.

10. Shafizadeh, F., Advan. Carbohydrate Chem. 13:9-61(1958).

11. Banks, B. E. C., Meinwold, Y., Rhind-Tutt, A. J., Sheft, I., and Vernon, C. A., J. Chem. Soc. 1961:3240.

12. Easty, D. B. The synthesis and acid hydrolysis of methyl alpha-D-gluco-pyranosiduronic acid. Doctor's Dissertation. Appleton, Wis., The Institute of Paper Chemistry, 1961.

13. Edward, J. T., Chem. & Ind. 1955:1102-4.

14. Whistler, R. L., and Richards, G. N., J. Am. Chem. Soc. 80:4888-91(1958).

15. Moeller, T. Inorganic chemistry, an advanced textbook. p. 306-32. New York, John Wiley & Sons, Inc., 1952.

16. Gould, E. S. Mechanism and structure in organic chemistry. New York, Henry Holt, 1960.

17. Mellor, J. W. Inorganic and theoretical chemistry. Vol. XIII. p. 834-6 New York, Longmans, Green and Co., 1937.

18. Batisse, E. M., Compt. Rend. 230:570-2(1950).

19. Traube, W., Kuhbier, F., and Harting, H., Ber. 66B:1545-56(1933).

20. Pecsok, R. L., and Sandera, J., J. Am. Chem. Soc. 77:1489-94(1955).

21. Delaney, J. C. Complexes of the system Fe (III), HCl, and glucose. Master's Dissertation. Lawrence, Kan., The University of Kansas, 1948.

22. Drummond, A. Y., and Waters, W. A., J. Chem. Soc. 1953:435-43.

23. Arndt, F., Loewe, L., and Ayca, E., Chem. Ber. 85:1150-60(1952).

24. Marshall, A. R., and Waters, W. A., J. Chem. Soc. 1960:2392-8.

25. Mino, G., Kaizerman, S., and Rasmussen, E., J. Am. Chem. Soc. 81:1494-6(1959).

26. Ingold, C. K. Structure and mechanism in organic chemistry. p. 726. Ithaca, Cornell University Press, 1953.

27. Stannett, V. T. Lecture given at The Institute of Paper Chemistry, 1961.

28. Hodgman, C. D., ed. Handbook of chemistry and physics. 34th ed. p. 1552-3. Cleveland, Chemical Rubber Publishing Co., 1952.

29. Kaden, T., and Fallab, S., Helv. Chem. Acta XLVI:714-20(1961).

30. Silverman, J., and Dodson, R. W., J. Phys. Chem. 56:846(1952).

31. Taube, H., and Myers, H., J. Am. Chem. Soc. 76:2103-11(1954).

32. Vosburgh, W. C., and Cooper, G. R., J. Am. Chem. Soc. 63:437-42(1941).

33. Bent, H. E., and French, C. I., J. Am. Chem. Soc. 63:568-92(1941).

34. Arden, T. V., J. Chem. Soc. 1951:350-63.

35. Cantor, S. M., and Peniston, Q. P., J. Am. Chem. Soc. 62:2113-21(1940).

36. Los, J. M., and Weisener, K., J. Am. Chem. Soc. 75:6346-7(1953).

37. Los, J. M., Simpson, L. B., and Weisener, K., J. Am. Chem. Soc. 78:1564-8 (1956).

38. Glasstone, S. Textbook of physical chemistry. 2d ed. Princeton, New Jersey, D. Van Nostrand Company, Inc., 1946.

39. Speck, J. C., Advan. Carbohydrate Chem. 13:79-80(1958).

40. Whalley, E., Trans. Faraday Soc. 55:798-808(1959).

41. Snell, J. B., and Williams, D. G. Unpublished work, 1961.

42. Kasbekar, G. S., Indian Pulp and Paper 3:465-7(1949).

43. Jones, E. J. Personal communication, 1961.

44. Dorcheus, S. H. Unpublished work, 1961.

45. Browning, B. L. Personal communication, 1960.

46. McBurney, L. F. In Cellulose and cellulose derivatives. Ott, E., and Spurlin, H. M., eds. p. 137. New York, Interscience Publishers, Inc., 1954.

47. Kolthoff, I. M., and Elving, P. J., eds. Treatise on analytical chemistry. Part I, Vol. 1. p. 374-7. New York, The Interscience Encyclopedia, Inc., 1959.

48. Snell, F. D., and Snell, C. T. Colorimetric methods of analysis. p. 235. Princeton, N. J., D. Van Nostrand Company, Inc., 1959.

49. Kesler, R. B., and Thompson, N. S. Personal communication, 1962.

APPENDIX I

THE EFFECT OF FERRIC ION UPON CELLULOSE

A series of trials was undertaken to show that the conditions for the degradation of cellulose by ferric ion were quite general. The amount of ferric iron retained, the state of the ferric ion, and the amount of moisture present were the variables to be tested.

EXPERIMENTAL

Preparation of Sample

Cotton linters (2.0 grams) were slurried in 1 liter of distilled water containing the desired quantity of ferric sulfate-sulfuric acid solution (the sulfuric acid was present to suppress hydrolysis, thus making the solution more stable). The pH of the slurry was adjusted to 3.0 for one group and 4.5 for another. The slurry was then filtered on a Buchner funnel, pressed, and air dried in a constant-humidity room at 51% R.H. One gram of the sheet was removed for iron determination and another portion for moisture determination. A 50-milligram aliquot of the remainder was weighed in the humidity room and transferred to a previously prepared sample tube, shown schematically in Fig. 23, designed so that there was a minimum of free space. These sample tubes were connected in series, then subjected alternately to a vacuum and flushing with nitrogen. Then several cubic feet of humidified nitrogen were passed through the tubes. The train of tubes ended with two weighing tubes containing a larger amount of cellulose for determining moisture content. Three moisture contents were used: 1.2, 6.2, and 80%. The last was obtained by injecting 0.2 ml. of water into the sample tube by hypodermic syringe. Finally, the tubes were sealed quickly in a very hot flame.

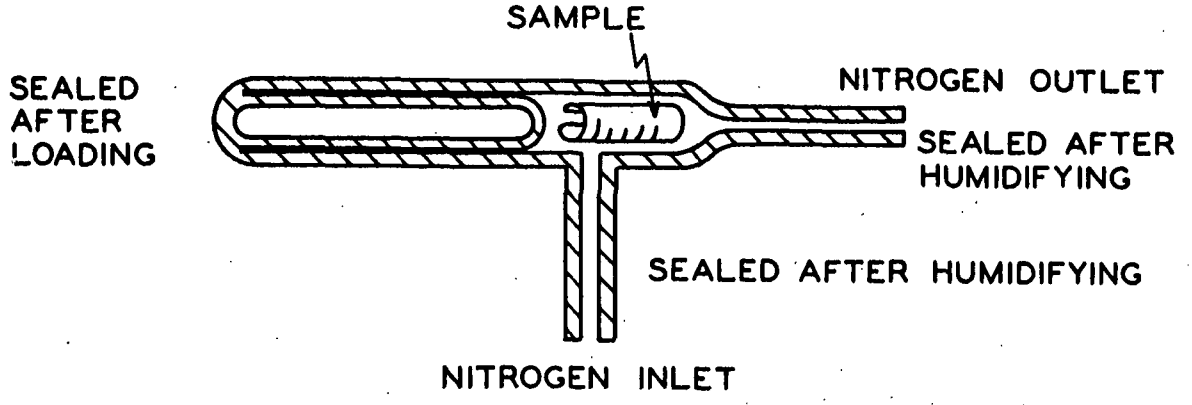

Figure 23. Schematic Diagram of a Sample Tube

The samples were heated by immersion in an oil bath at 110°C. for 48 hours. The samples were removed and quenched. Then the cold samples were opened, and the cellulose removed for the determination of viscosity in cupriethylenediamine.

Analytical Procedures

Determination of Iron

The procedures used for determining the ferric salt content of the cotton linters were used exactly as described by Czepiel (5). The method used involved removal of the organic material by oxidation with perchloric acid, leaving the metal salt in an acid solution. The ferric ion in solution was reduced to the ferrous state with hydroxylamine hydrochloride, and the total ferrous ion was determined as the complex of 1.10-phenanthroline.

Determination of the Intrinsic Viscosity of the Cellulose

The 50-mg. cellulose samples had been weighed exactly before they were sealed in the sample tubes and aged. These samples were placed in a serum bottle after aging and dispersed in 12.5 ml. of water. The bottle, closed with a serum bottle cap, was flushed with nitrogen. Then, 12.5 ml. of 1.0M cupriethylenediamine was

added from a needle-tipped buret. The sample was dispersed on a shaker for one hour. The viscosity of the resultant solution was determined by means of an Ostwald viscometer. The specific viscosity, η_{sp}, was calculated as $(\eta - \eta_o)/\eta_o = \eta_{sp}$, where η is the measured viscosity of the solution and η_o the viscosity of the solvent. Values of the reduced viscosity, $\eta_{sp}/\underline{c}$, were then calculated and used to determine the intrinsic viscosity $[\eta] = \lim_{\underline{c}\to 0} (\eta_{sp}/\underline{c})$ by a 1-point method from charts prepared for this purpose (45). The intrinsic fluidity, the reciprocal of the intrinsic viscosity, shows cellulose chain breakage more directly than intrinsic viscosity (46).

RESULTS

The data are presented in Fig. 24. The results of these experiments confirmed Czepiel's (5) observation that there is an apparent maximum in the effect of moisture content on the degradation of cellulose in the presence of ferric

The amount of degradation appeared to be a function of the iron content of the cellulose. The apparent effect of the difference in pH of the pulp slurries was to vary the retention of iron in the cellulose pad. At pH 4.5, most of the iron was present as a suspension of the hydrous oxide. At pH 3.0, little or none of the iron was present in an insoluble form.

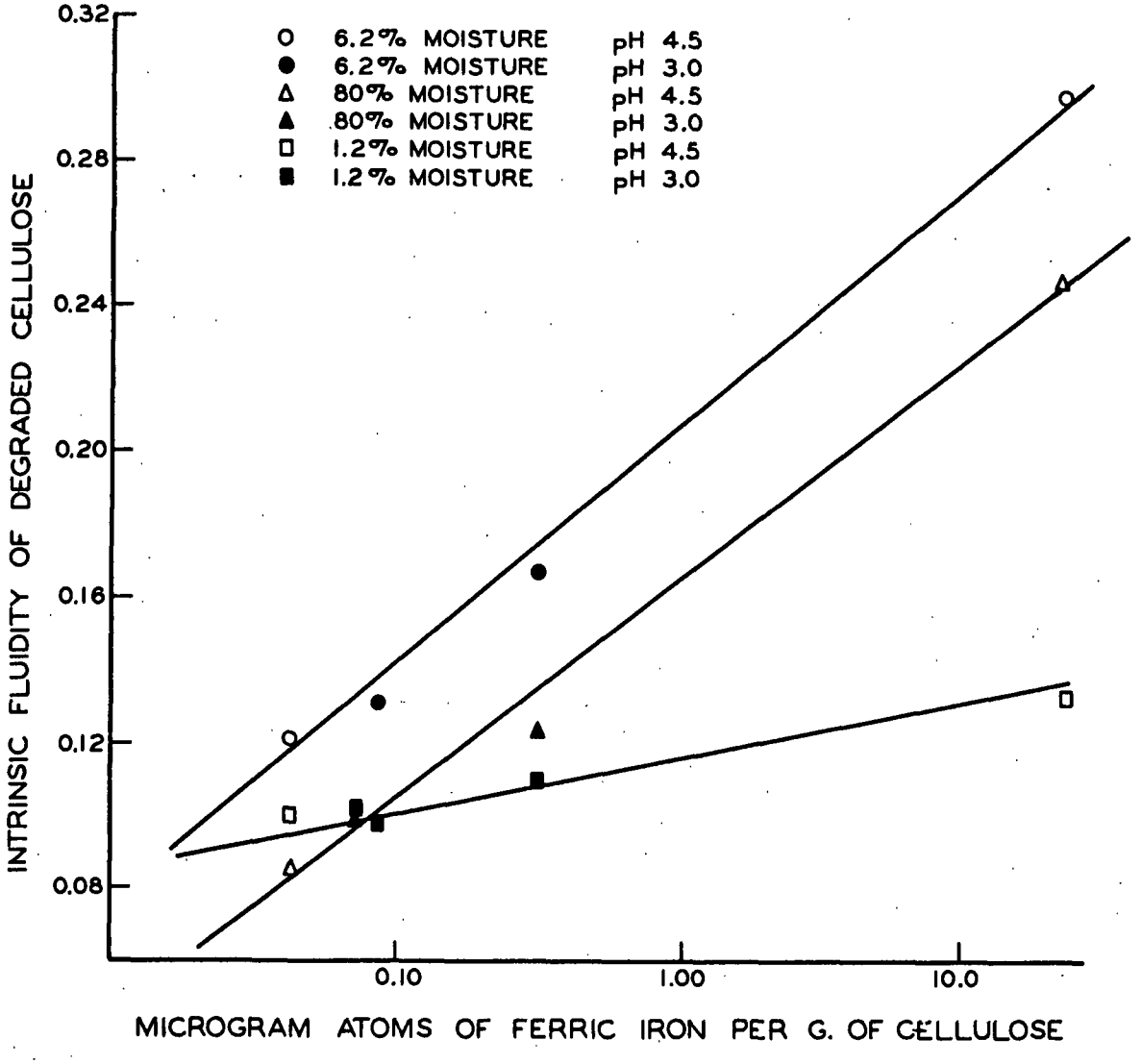

Figure 24. The Effect of Ferric Ion on Cellulose at 110°C.

APPENDIX II

THE EFFECT OF TEMPERATURE ON pH IN THE REACTION SYSTEM

The hydrogen ion content of the reaction system at reaction temperature is more fundamental for comparison than the hydrogen ion content at room temperature. A glass electrode suitable for use from 0 to 100°C. was used in conjunction with a Beckman Zeromatic pH meter to measure this quantity.

Two buffer solutions were used to bracket the experimental conditions. The temperature coefficients of both buffers were determined by the National Bureau of Standards (47). The two buffers were:

1. A solution of 0.05M potassium tetroxalate was made by dissolving 12.70 g. of $KH_3(C_2O_4)_2 \cdot 2H_2O$ in 1 liter of water. The pH was listed as 1.68 at 25°C. and 1.80 at 90°C.

2. A saturated solution of potassium hydrogen phthalate, supplied by Beckman, was the second buffer. The pH was listed as 4.01 at 25°C. and 4.20 at 90°C.

The method used to standardize the electrodes was as follows: A U-tube, formed of two vertical pieces of tubing slightly larger in diameter than the electrodes connected by a piece of much smaller tubing, was placed in the oil bath at 90°C. The buffer solution, potassium tetroxalate, was added, the electrodes immersed in solution, and the assembly allowed to come to temperature equilibrium. With the temperature compensator set at 90°C., the pH meter was adjusted to read pH 1.80. The solution was then removed by means of a syringe and replaced with another portion of the same buffer solution, which had been conditioned to 90°C. in a small closed flask. The meter was checked, and, if necessary, readjusted to pH 1.80. The solution to be checked (either sample or potassium hydrogen phthalate buffer) was placed in another preheated U-tube. The

electrodes were cleaned and transferred as quickly as possible to minimize the heat-up period. The pH was recorded when the value was constant; then the solution was replaced by fresh solution and rechecked.

It is apparent from the data presented in Table VII that temperature and the neutral salt content play a large part in the effect on the measured pH and upon the hydrolysis of the ferric ion. Therefore, it is necessary that the reaction experiments be compared on the basis of data established under reaction conditions.

TABLE VII

THE EFFECT OF TEMPERATURE ON THE pH OF REACTION MIXTURES

Sample	pH at 25°C.	pH at 90°C.	Lit. pH at 90°C.
KH phthalate buffer	4.01	4.23	4.20
0.01M Fe^{+3}	1.80	2.59	
Control	1.80	2.59	
Control	1.60	2.35	
0.01M Fe^{+3} + 8% glucose final pH	1.6	2.51	
Control	1.68	2.50	
0.01M Fe^{+2}	1.80	2.54	
Control	1.76	2.55	
0.01M Fe^{+3}, no Na_2SO_4	1.80	2.01[a]	
Control, no Na_2SO_4	1.80	1.98	

[a]This solution had a reddish-brown precipitate soon after reaching 90°C.

APPENDIX III

ANALYSIS FOR FERROUS ION IN A MIXTURE OF FERRIC AND FERROUS IONS (48)

Ten milliliters of 0.3% 1,10-phenanthroline was pipetted into a 50-ml. volumetric flask. To buffer the solution, 5 ml. of a 4% potassium hydrogen phthalate solution was added. An aliquot of the reaction mixture was removed from the reaction flask by syringe. After the sample was adjusted to 1.03 ml. by means of the Cheney-adaptor on the syringe, the needle tip of the syringe was placed under the surface of the phenanthroline solution in the volumetric flask, and the sample was delivered. The solution of the reddish ferrous-phenanthroline complex was then made to 50 ml. with distilled water. This solution was allowed to sit for 15 minutes at room temperature. A 5-ml. aliquot of this solution was diluted to 25 ml. in a volumetric flask. The optical density of this last solution was measured immediately at 512 mμ in a Beckman Model DU Spectrophotometer. The reference solution used for the spectrophotometric measurement was made in the preceding fashion from an aliquot of the reaction mixture at zero reaction time.

APPENDIX IV

ANALYSIS FOR GLUCOSE IN THE REACTION MIXTURE (49)

A sample of the reaction mixture was taken and treated to remove the iron present as described on page 36. The clear filtrate was spotted on Whatman no. 1 chromatographic paper. Two 50-microliter aliquots were spotted on a single 3-inch strip at the starting line. At either side of the quantitative spot, a guide spot of about 20 microliters of the sample was applied to the paper. After the spots were dried, the chromatogram was developed in 8:2:2:1 (butyl acetate:pyridine: ethanol:water) for approximately 50 hours. After developing, the sheets were dried, and the strips containing the guide spots at the edge of the sheets were cut off. These guide strips were sprayed with a reagent containing p-anisidine hydrochloride and chloroacetic acid to discover reducing compounds. The guide strips were then aligned with the sheet. A 4-inch portion of the center, containing the glucose spot, was cut out. The sheet containing the glucose was cut into 1/4-inch squares and placed in a test tube. The remainder of the sheet was sprayed with the p-anisidine reagent to determine if all of the glucose spot had been removed.

Twenty milliliters of an aqueous 0.2% benzoic acid solution was then added to the test tube containing the glucose-laden paper. The tubes were agitated and allowed to sit for an hour. At the end of this time, the tubes were emptied through a garlic press into a coarse sintered-glass funnel. The liquid was pressed from the paper into the funnel. The filtrate was collected in a suitable flask.

Standards containing known amounts of glucose were prepared from a synthetic reaction mixture composed of weighed quantities of glucose and cellobiose in the same solvent used to make the true reaction mixture. Two duplicate sets of chromatograms of different glucose content were prepared for every run. These standards were subjected to all of the procedures used for the unknowns except heating.

The filtrate was then analyzed for glucose on a Technicon AutoAnalyzer by a modification of the method developed by Technicon Controls, Inc., Chauncey, New York. This method determines spectrophotometrically the extent of reaction between the glucose and an alkaline ferricyanide solution.

The results from the analysis of the standards were plotted as the logarithm of the per cent transmission vs. glucose content. The concentration of glucose in each sample was obtained from this graph, using the results of analysis for each sample.

APPENDIX V

EXPERIMENTAL RESULTS

REDUCTION OF FERRIC ION TO FERROUS ION BY GLUCOSE

Ferric ion concentration: 0.0102 g. ion/liter
Ionic strength: 1.5M
Glucose concentration: 0.444M

Time, min.	Ferrous Ion, g. ion/l. x 10^2
Temperature: 80 ± 0.1°C.	
Run 145-2-18-62	
30	0.016
70	0.023
100	0.041
120	0.053
180	0.074
213	0.124
Run 145-2-19-62	
40	0.022
70	0.025
94	0.042
112	0.048
165	0.082
200	0.109
224	0.136
Temperature: 90 ± 0.1°C.	
Run 107-3-30-62	
30	0.027
95	0.187
204	0.553
240	0.641
320	0.825
1096	0.946

Temperature: 90 ± 0.1°C.

Run 114-4-26-62

Glucose concn.: 0.222M

Time, min.	Ferrous Ion, g. ion/l. x 10^2
60	0.083
180	0.420
220	0.540
300	0.750
340	0.805
380	0.845
420	0.875
558	0.935

Run 117-5-7-62

Glucose concn.: 0.020M

Time, min.	Ferrous Ion, g. ion/l. x 10^2
90	0.011
180	0.052
280	0.074
360	0.130
425	0.191
990	0.547
1200	0.650

Run 118-5-14-62

Glucose concn.: 0.040M

Time, min.	Ferrous Ion, g. ion/l. x 10^2
90	0.029
210	0.043
275	0.137
360	0.231
480	0.338
630	0.482
810	0.635
990	0.738
1200	0.835

REDUCTION OF FERRIC ION TO FERROUS ION BY CELLOBIOSE

Ferric ion concentration: 0.0102 g. ion/liter
Ionic strength: 1.5M
Cellobiose concentration: 0.234M

Time, min.	Ferrous Ion, g. ion/l. x 10^2
Temperature: 80 ± 0.1°C.	
Run 147-2-26-62	
30	0.0058
62	0.0134
90	0.0125
159	0.0382
210	0.0541
280	0.0810
Run 152-3-7-62	
40	0.0121
60	0.0179
80	0.0152
100	0.0233
120	0.0246
140	0.0264
160	0.0286
265	0.0560
Temperature: 90 ± 0.1°C.	
Run 156-3-14-62	
20	0.0161
35	0.0242
50	0.0318
65	0.0492
80	0.0873
95	0.0631
110	0.0744

Time, min.	Ferrous Ion, g. ion/l. x 10^2

Temperature: 90 ± 0.1°C.

Run 112-4-13-62

60	0.038
120	0.090
180	0.159
260	0.250
300	0.309
360	0.392
400	0.443
590	0.685
720	0.805
1025	0.929
1200	0.928
1250	0.905

REDUCTION OF FERRIC ION TO FERROUS ION BY RIBOSE

Initial ferric ion concentration: 0.0102 g. ion/liter
Ionic strength: 1.5M
Ribose concentration: 0.462M

Temperature: 80 ± 0.1°C.

Run 146-2-20-62

10	0.012
20	0.056
25	0.094
30	0.131
35	0.180
40	0.222

REDUCTION OF FERRIC ION TO FERROUS ION BY GALACTOSE

Ferric ion concentration: 0.0102 g. ion/liter
Ionic strength: 1.5M
Galactose concentration: 0.444M

Temperature: 80 ± 0.1°C.

Run 147-2-21-62

20	0.0148
40	0.0340
50	0.0438
60	0.0524
75	0.0676
130	0.1550

REDUCTION OF FERRIC ION TO FERROUS ION IN THE SOLVENT

Ferric ion concentration: 0.0102 g. ion/liter
Carbohydrate concentration: 0.000M
Ionic strength: 1.5M

Time, min.	Ferrous Ion, g. ion/l. x 10^2
Temperature: 90 ± 0.1°C.	
Run 116-5-3-62	
248	0.0058
1440	0.0238
2880	0.0510

HYDROLYSIS OF CELLOBIOSE AT 90 ± 0.1°C.

Cellobiose concentration: 0.234 mmoles/ml. = C_o
Ionic strength: 1.5M

Time, hr.	G, Glucose, mg./100 λ neutralized[a] reaction mixture	X, equiv. mmoles[b] per ml. reacted cellobiose	$\log \frac{C_o - X}{C_o}$
Run 105-3-28-62			
Ferric ion concentration: 0.0000 g. ion/liter Initial pH at 90°C. = 2.59			
13.00	0.344	0.0105	-0.0200
14.00	0.370	0.0113	-0.0216
15.00	0.400	0.0122	-0.0234
16.00	0.434	0.0132	-0.0254
16.00	0.438	0.0134	-0.0256
17.33	0.466	0.0142	-0.0273
18.00	0.484	0.0148	-0.0284
18.00	0.480	0.0146	-0.0282
19.00	0.504	0.0154	-0.0296
20.00	0.560	0.0171	-0.0330
21.00	0.578	0.0176	-0.0341
24.67	0.660	0.0202	-0.0393
25.00	0.660	0.0202	-0.0393

[a] V = 0.10 ml.

[b] Sample calculation for X

$$X = \frac{G \times 10 \times \frac{1.03 + V}{1.03}}{180 \times 2}$$

where V = the volume of neutralizing agent, ml., added to 1.03 ml. of sample.

Time, hr.	G, Glucose, mg./100 λ neutralized[a] reaction mixture	X, equiv. mmoles[c] per ml. reacted cellobiose	$\log \frac{C_o - X}{C_o}$
Run 132-7-28-62			
Ferric ion concentration: 0.0000 g. ion/liter Initial pH at 90°C. = 2.50			
13.50	0.470	0.0143	-0.0274
14.50	0.486	0.0148	-0.0284
15.50	0.528	0.0161	-0.0310
16.50	0.568	0.0173	-0.0334
17.42	0.608	0.0185	-0.0358
19.58	0.688	0.0210	-0.0408
20.65	0.754	0.0230	-0.0449
21.50	0.758	0.0231	-0.0452
Run 130-7-18-62			
Ferric ion concentration: 0.0000 g. ion/liter Initial pH at 90°C. = 2.55			
11.50	0.350	0.0107	-0.0203
12.50	0.364	0.0111	-0.0212
13.50	0.390	0.0129	-0.0227
15.00	0.438	0.0134	-0.0255
16.25	0.478	0.0146	-0.0280
17.50	0.522	0.0159	-0.0306
21.55	0.630	0.0192	-0.0372
22.75	0.666	0.0203	-0.0395
Run 109-4-5-62			
Ferric ion concentration: 0.0102 g. ion/liter Initial pH = 2.59			
7.00	0.236[b]	0.0076	-0.0143
8.00	0.280	0.0090	-0.0170
9.00	0.300	0.0096	-0.0182
12.00	0.406	0.0130	-0.0249
13.00	0.432	0.0138	-0.0265
15.00	0.506	0.0162	-0.0313
16.00	0.532	0.0171	-0.0330
17.00	0.570	0.0183	-0.0354
19.00	0.634	0.0203	-0.0395
20.00	0.664	0.0213	-0.0414

[a] V = 0.10 ml.

[b] V = 0.16 ml.

[c] See footnote p. 77.

Time, hr.	G, Glucose, mg./100 λ neutralized reaction mixture[a]	X, equiv. mmoles per ml. reacted cellobiose[b]	$\log \frac{C_o - X}{C_o}$
Run 111-4-11-62			
	Ferric ion concentration: 0.0102 g. ion/liter Initial pH at 90°C. = 2.59		
10.00	0.344	0.0110	-0.0210
11.00	0.374	0.0120	-0.0228
14.00	0.464	0.0149	-0.0285
14.00	0.476	0.0152	-0.0294
16.00	0.532	0.0171	-0.0329
17.67	0.600	0.0192	-0.0374
17.67	0.594	0.0190	-0.0371
16.00	0.532	0.0171	-0.0329
Run 119-5-21-62			
	Ferric ion concentration: 0.0102 g. ion/liter Initial pH at 90°C. = 2.59		
3.00	0.108	0.0035	-0.0055
4.00	0.120	0.0038	-0.0072
5.00	0.183	0.0059	-0.0110
6.00	0.200	0.0064	-0.0121
7.00	0.231	0.0074	-0.0140
8.00	0.270	0.0087	-0.0164
9.00	0.301	0.0096	-0.0183
10.00	0.330	0.0106	-0.0201
Run 120-6-9-62			
	Ferrous ion concentration: 0.01 g. ion/liter Initial pH at 90°C. = 2.54		
6.50	0.190	0.0060	-0.0115
8.00	0.234	0.0075	-0.0142
10.00	0.278	0.0089	-0.0169
12.50	0.360	0.0115	-0.0221
14.00	0.398	0.0128	-0.0243
15.50	0.448	0.0144	-0.0276
17.00	0.484	0.0150	-0.0299
18.00	0.526	0.0168	-0.0328

[a] $\underline{V}$ = 0.16 ml.

[b] See footnote p. 77.

Time, hr.	G, Glucose, mg./100 λ neutralized reaction mixture	X, equiv. mmoles[d] per ml. reacted cellobiose	$\log \frac{C_o - X}{C_o}$
Run 128-7-10-62			
Ferric ion concentration: 0.01 g. ion/liter Initial pH at 90°C. = 1.98 Ionic strength: 0.08M			
1.17	0.114[a]	0.0037	-0.0068
2.17	0.168	0.0054	-0.0101
3.00	0.210	0.0067	-0.0127
4.00	0.290	0.0093	-0.0176
5.00	0.356	0.0114	-0.0221
6.00	0.440	0.0141	-0.0271
6.75	0.498	0.0160	-0.0308
7.50	0.540	0.0173	-0.0334
Run 129-7-12-62			
Ferric ion concentration: 0.00 g. ion/liter Initial pH at 90°C. = 2.01 Ionic strength: 0.05M			
1.00	0.070[b]	0.0021	-0.0039
2.00	0.120	0.0037	-0.0069
3.00	0.172	0.0052	-0.0099
4.00	0.242	0.0074	-0.0138
5.00	0.290	0.0088	-0.0167
5.75	0.324	0.0099	-0.0187
7.00	0.414	0.0126	-0.0241
7.58	0.446	0.0136	-0.0260
Run 133-8-2-62			
Zinc ion concentration: 0.01 g. ion/liter Initial pH at 90°C. = 2.62 Ionic strength: 1.5M			
12.75	0.318[c]	0.0099	-0.0187
13.17	0.348	0.0108	-0.0205
14.30	0.360	0.0112	-0.0212
14.58	0.340	0.0105	-0.0200
15.83	0.392	0.0121	-0.0232
17.55	0.448	0.0139	-0.0266
21.48	0.536	0.0166	-0.0320
21.50	0.536	0.0166	-0.0320

[a] V = 0.16 ml.

[b] V = 0.10 ml.

[c] V = 0.12 ml.

[d] See footnote p. 77.

THE REACTION OF GLUCOSE WITH FERRIC ION AT 90 ± 0.1°C.

Run 117-5-7-62

Glucose concentration = 0.0204M
Ferric ion concentration = 0.0102M
Initial pH = 2.59 at 90°C.

Time, hr.	G, glucose in mg./100 λ neutralized reaction mixture	Y, mole/l.[a] glucose remaining in reaction mixture
1.50	0.320	0.0205
3.00	0.312	0.0200
4.66	0.316	0.0203
6.00	0.316	0.0203
7.25	0.316	0.0203
10.25	0.318	0.0204
16.50	0.318	0.0204
20.00	0.318	0.0204

[a]Sample calculation for Y

$$Y = \frac{G \times 10 \times \frac{1.19}{1.03}}{180}$$